Chapter 1

Introduction

1.1 The aromatisation of light alkanes

An energy policy of the world is directed by the need for secure supply and the wish for sustainable growth [1]. This has been further complicated with the added pressure that OPEC puts on a world economy by restricting the crude output and controlling the prices [2]. The high cost of energy has caused inflation in many economies creating a burden on most countries. In the present world energy scenario, the supply of oil and other natural resources are limited and not uniformly distributed. At the current rates of increase in production and use, proven reserves will last only for 40-50 years and in some countries, depletion is predicted sooner [3]. There are continuous efforts to decrease the dependency on oil in view of the limited resources and to increase the use of energy sources other than fossil fuels (solar, wind, biomass) to comply with the Kyoto Protocol on CO_2-emmissions [1]. Natural gas (which is predominantly, methane) represents part of the solution to this problem as illustrated in Figure 1.1.

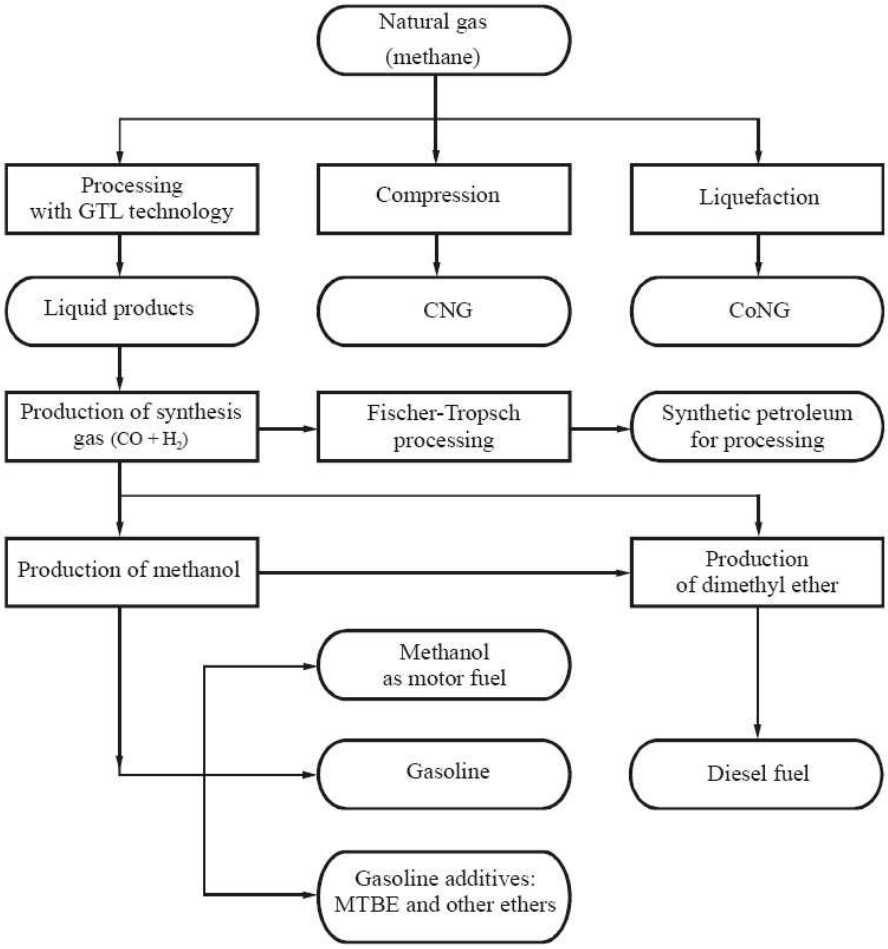

Figure 1.1 Flow chart of processing natural gas into motor fuel [3].

Other possible alternative fuels include, liquefied petroleum gas, methanol, ethanol, dimethyl ether, biofuels and hydrogen [1,3].

On the other hand, aromatic hydrocarbons such as benzene, toluene and xylene (BTX) are commercially used gasoline additives because of their high octane number and as a result they constitute a significant part of the gasoline pool (about 30%) even if due to antipollution legislations their utilization tends to decrease [4]. They

are important raw materials for many intermediates for commodity petrochemicals and valuable fine chemicals, such as monomers for polyesters, engineering plastics, and intermediates for detergents, pharmaceuticals, agricultural-products and explosives [5]. Light alkanes, are an attractive source for the production of aromatics. Light saturated compounds occur in accompanying petroleum gases (liquefied petroleum gas (LPG) contains more than 70% C_2–C_5 alkanes) and in natural gas. Furthermore, refinery and petrochemical processes such as fluid catalytic cracking (FCC), steam cracking and hydrotreating produce huge amounts of these compounds; moreover, low-value C_4–C_5 olefin-rich streams are obtained as by-products from cracking operations [6].

Various commercial processes such as the Cyclar process commissioned by UOP and BP, the M2-forming process by Mobil, the Aroforming process by IFP Salutec, and the Alpha process by Sanyo and Asahi have been developed for the aromatisation of light aromatics [4,6].

It should however, be noted that the commercial processes developed for the aromatisation of light alkanes do not apply for the conversion of methane because of its inert nature. The conversion of methane, which is the major part of this thesis, is discussed in the next section.

1.2 Considerations of methane conversion

1.2.1 Availability and distribution of methane

Natural gas is available in large quantities and the world reserve is not used to the same extent as petroleum crude. There are many potentially rich gas fields which

have not been drilled, because of the need to lay expensive pipes to transport the gas [2]. Despite strong world wide growth in demand for natural gas, more than doubling between 1973-1993, gas reserves continue to grow, but even though discovered they have been left 'in place' for lack of transportation or the gas being less than pipe line quality. The growth in the proven natural gas reserves for two decades from 1985 to 2005 is shown in Figure 1.2.

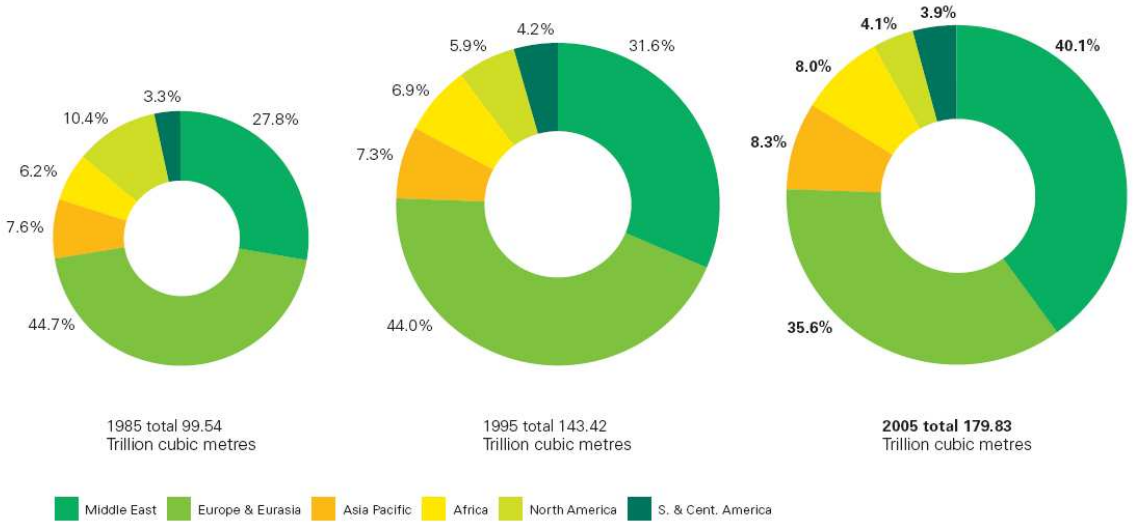

Figure 1.2 Distribution of proven reserves in 1985, 1995 and 2005 [7].

Natural gas has numerous advantages over other energy sources [8]. It is easy to purify and has higher efficiency for electricity, heat and power production. Natural gas burns cleaner and produces fewer pollutants than other fossil fuels. It has the largest heat of combustion relative to the amount of CO_2 formed. It produces 45% less CO_2 than coal for a comparable amount of energy, and also emits considerably less NO_x and SO_x [2,8]. Because methane has a high H/C ratio, natural gas can be used as a clean source of hydrogen for fuel cells.

1.2.2 The properties and conversion of methane

At present, methane is an underutilized resource for chemicals and fuels. This may be due to the fact that methane is the most stable of the alkanes [8]. The structure of the methane molecule with its four C-H covalent bonds of high bond energies (435 kJ mol^{-1}), zero dipole moment, no multiple bonds or functional groups and no asymmetry, is responsible for the extremely low methane reactivity. Thermodynamically, methane is unstable only above 530^{o}C, becoming more unstable than benzene above 1030^{o}C [8]. The methane thermodynamic conversion at 1 atm is low at moderate temperatures (about 5% at 600^{o}C, 11.4% at 700^{o}C and 16.2% at 750^{o}C). The activation of C-H bonds in alkanes, and particularly in the most stable methane, under mild conditions necessary for selective synthesis of derivatives, then became one of the most intriguing and challenging problems in contemporary hydrocarbon chemistry and catalysis studies. The breakage of all C-H bonds in methane is relatively less constrained and that is why only indirect conversion of methane via syngas into higher hydrocarbons or chemicals has been commercialised (see Figure 1.1).

Although the commercialized methane conversion technologies involve indirect pathways via a reforming step, efforts have been made to directly convert methane into valuable products. The activation and direct conversion of methane into hydrocarbons is thermodynamically more favourable with the assistance of oxidants than under non-oxidative conditions. In this regard the oxidative coupling of methane (OCM) and the partial oxidation of methane have been studied for more than two decades [8-10]. However the use of oxygen as an activator usually leads to a poor selectivity caused by simultaneous formation of carbon oxides, favoured thermodynamically. [8]. An alternative direct methane conversion process that has received considerable attention in recent years is the nonoxidative dehydroaromatisation of methane over Mo/H-ZSM-5 catalyst, which was first reported by Wang et al. [11] in 1993.

1.3 Aims and objectives

The overall aim of the study was to investigate the nonoxidative aromatisation of methane over metal loaded ZSM-5-based materials at various levels of percentage XRD crystallinity and to also evaluate their application for the aromatisation of propane. This involved the study of the effect of reaction parameters such as temperature and flow rate on the catalytic properties of Mo/H-ZSM-5 and the effect of variables such as the SiO_2/Al_2O_3 ratio of ZSM-5, the catalyst preparation method, the molybdenum precursor, the presence of dopants and catalyst modification by silanation on the catalytic performance of Mo/H-ZSM-5 catalysts. Various characterisation methods such as X-ray powder diffraction (XRD), surface and pore volume analysis, diffuse reflectance spectroscopy (DRS), temperature programmed (TP) methods, transmission electron microscopy (TEM) and infrared spectroscopy were used in this study.

1.4 Outline of the thesis

A literature review on the various methods of preparation of supported metal catalysts and characterization is given in Chapter 2. A brief description of the synthesis and structure of zeolites is also given.

A literature review on the aromatization of methane in the absence of oxygen over metal-loaded zeolites is presented in Chapter 3. The effects of various parameters on the catalytic nonoxidative conversion of methane as well as the proposed mechanisms of the reaction are discussed. The various methods that have been used in order to improve the stability and activity of the catalysts are also described.

In Chapter 4, a literature review on the aromatisation of propane is given, with more attention given to the aromatisation of propane over Ga-loaded ZSM-5 catalysts. A description of the mechanism of the reaction as well as the parameters that affect the aromatisation reaction is also given. A literature survey on the aromatisation of propane over Mo/H-ZSM-5 catalysts is also presented

The experimental section of the thesis is given in Chapter 5, giving a description of the procedures that were used to prepare and characterise the catalysts.

In Chapter 6, the results obtained in this study on the nonoxidative dehydroaromatisation of methane are given and discussed. The results show the effects of variables such a the type of the support material, percentage XRD crystallinity of H-ZSM-5, the SiO_2/Al_2O_3 ratio of ZSM-5, the reaction temperature, molybdenum loading, the catalyst preparation method and the presence of dopants on the catalytic activity of molybdenum-based catalysts.

The results of the preliminary study of the aromatisation of propane over Mo/H-ZSM-5 catalysts are given in Chapter 7 and the overall conclusions of the study are presented in Chapter 8.

1.5 References

[1] J.R. Rostrup-Nielsen, *Catal. Rev.*, **46** (2004) 247-270.

[2] P. Samuel, *Bull. Catal. Soc. India*, **2** (2003) 82-99.

[3] A.I. Lapidus. I.F. Krylov and B.P. Tonkonogov, *Chem. Technol. Fuel and Oils*, **41** (2005) 165-174.

[4] M. Guisnet and N.S. Gnep, *Appl. Catal.*, *A*, **89** (1992) 1-30.

[5] T.-C. Tsai, S.-B. Liu, I. Wang, *Appl. Catal., A*, **181** (1999) 355-398.

[6] M. Taglibue, A. Carati, C. Flego, R. Millini, C. Perego, P. Pollesel, B. Stocchi and G. Terzoni, *Appl. Catal.*, *A*, **265** (2004) 23-33.

[7] BP Statistical review of world energy June 2006 (www.bp.com/statisticalreview; 12 December 2006).

[8] K. Skutil and M. Taniewski, *Fuel Processing Technol.*, **87** (2006) 511-521.

[9] H.D. Gesser and NR. Hunter, *Catal. Today*, **42** (1998) 183-189.

[10] J.H. Lunsford, *Catal. Today*, **63** (2000) 165-174.

[11] L. Wang, L. Tao, M. Xie, G. Xu, J. Huang and Y. Xu, *Catal. Lett.*, **21** (1993) 35-41.

Chapter 2

Preparation and characterisation of supported-metal catalysts

2.1 Introduction

Homogeneous and heterogeneous catalysis are the two main fields of catalysis, and can be classified according to the phases involved in the process. In homogeneous catalysis, the reactants, the products and the catalysts are in the same phase, usually the liquid phase. In the case of heterogeneous catalysis, the catalysts, the reactants

and the products are in different phases. Usually the catalyst is a solid, and the reactants and products are in the liquid or vapour phase.

In homogeneous catalysis reactions occur through complexation and rearrangements between molecules and ligands of the catalyst [1]. Reactions can be specific, with high yields of desired products and the mechanisms involve readily identified species. These reactions are easily studied in the laboratory using the techniques applied in the field of organometallic chemistry. Liquid phase operation places restrictions on temperature and pressure, so equipment can be complicated. At the end of the reaction the catalyst must be separated from the products, imposing additional difficulties. For these reasons, homogeneous catalysis is found only in limited industrial use, appearing usually in the manufacture of specialty chemicals, drugs and food [1].

Heterogeneous catalysis is widely used in industry [1]. The mechanisms in heterogeneous catalysis are complicated by the fact that the catalyst and the reactants are in different phases. Factors such as diffusion, absorption, and adsorption all play critical roles in establishing the rate. These additional steps become difficult to separate from surface chemistry. Thus, heterogeneous systems are difficult to study in the laboratory. Disappearance of reactant and appearance of products are easily followed, but important features such as the rates and energies of adsorption, structure of the active surface, and the nature of the reactive intermediates require separate experimentation using many characterisation techniques. Often, the sequence of steps can only be deduced from accumulated evidence, with many uncertainties.

Nevertheless heterogeneous catalysts are convenient to use commercially. The transformation of homogeneously catalysed processes (especially acid catalysed reactions) into heterogeneously catalysed systems, by supporting the active species

on solid materials or by developing alternative solid catalysts, is a constant trend in the chemical industry [2]. This is because solid acid and base catalysts are non-corrosive, environmentally benign and present fewer disposal problems than the liquid Brönsted and Lewis acid and base catalysts used in homogeneous catalysis. Solid acids such as alumina and amorphous silica-alumina, heteropolyacids, sulfated zirconia and zeolites, have found numerous applications in heterogeneous catalysis [3].

2.2 Catalyst preparation in heterogeneous catalysis

The catalytic properties of heterogeneous catalysts are strongly affected by the elementary preparation steps together with the quality of the raw materials. The choice of a laboratory method for preparing a given catalyst depends on the physical and chemical characteristics desired in the final composition [4]. The aim of the preparation of catalytic materials that can be used on an industrial scale is to prepare a product with high activity, selectivity and stability [5]. Although some catalytic materials are composed of single substances, most catalysts have different types of easily distinguishable components, active components, a support and, if necessary, the promoter [1]. The active components are responsible for the principal chemical reaction. When the active component is a metal, it must be in a sufficiently dispersed form to give a large specific surface area and consequently in a maximum specific activity [1]. In order to achieve this objective the active metal component is usually deposited on the surface of a support. Promoters on the other hand are added to induce enhancement in the activity, selectivity or lifetime, or to ensure the structural integrity of the catalyst [6].

The support must have a high surface area and suitable mechanical strength to permit dispersion of the metal, also to increase its thermal stability and hence the catalyst

life. The selection of a support is based on it having certain properties, some of which are listed below [4]:

- Inertness. Ideally, support materials should have no catalytic activity leading to undesirable side reactions.
- Desirable mechanical properties, including attrition resistance, hardness and compressive strength.
- Stability under reaction and regeneration conditions.
- Surface area. High specific surface area is usually, but not always, desirable.
- Porosity, including average pore size and pore size distribution. High area implies fine pores, but relatively small pores could become plugged during impregnation, especially if high loading is sought.
- Low cost

Materials with low surface area are generally useful in supporting very active catalytic components in reactions where further side reactions may affect the activity and selectivity, while materials with high surface areas are widely used in precious metal catalysts preparation [4].

The active species in catalysts can be either in the metallic (e.g. iron, copper, platinum, etc.) or metal oxide form or other forms (e.g. sulphides, carbides, etc.). Typical oxides are those of rhenium, chromium, molybdenum, tungsten, vanadium and niobium [7]. In this thesis the phrase "supported-metal catalysts" will be used to collectively mean both supported metallic and oxide active species.

2.2.1 Methodologies of catalysts preparation

In this section, different methods which are usually used to prepare supported catalysts will be discussed.

(i) Impregnation

Impregnation is a procedure whereby a certain volume of solution is contacted with the solid support, which, in a subsequent step, is dried to remove the imbibed solvent. Two methods of impregnation may be distinguished, depending on the volume of solution used: "incipient wetness" or "dry" impregnation and "wet" or "soaking" impregnation [1,4,5,8-11]. In incipient wetness impregnation the volume of the solution of appropriate concentration is equal or slightly less than the pore volume of the support. The volume should be just sufficient to fill the pores and wet the outside of the particles. Although this volume may be determined from measured pore volumes, this is sometimes more reliably determined with preliminary test on aliquot samples [1]. In the simplest way, the impregnating solution is sprayed on the support that is maintained under stirring and that has been previously evacuated. By removing the air trapped in the inner pores, deeper penetration of the solution is allowed and a more uniform distribution of the metal precursor should be attained [1]. The maximum loading is limited by the solubility of the precursor in the solution [5]. When higher loadings are required, this limitation is overcome by carrying out consecutive impregnation steps.

In wet impregnation an excess of solution with respect to the pore volume of the support is used [1,5,8-11]. The system is left to age for a certain period under stirring it is then filtered and dried. This procedure is applied when a precursor-support interaction can be envisaged. Therefore, the concentration of the support will not only depend on the concentration of the solution and on the pore volume of the solution, but also on the type and/or concentration of the adsorbing sites existing at the surface.

Impregnation is often related to ion exchange, specifically, when there are interaction between the support and the ionic species in the solution. In fact, inorganic oxides

such as Al_2O_3, SiO_2, TiO_2, MgO, which are used as support materials tend to polarise and to be surface charged once suspended in an aqueous solution [4,5]. The pH of the solution and the isoelectric point of the solid control this charge. Schematically the reaction involved in the surface polarisation may be written, in acidic medium (pH below the isoelectric point) [5]:

$$S\text{-}OH + H^+A^- \leftrightarrow S\text{-}OH_2^+ A^- \quad (1)$$

While in a basic medium (pH above the isoelectric point) the equilibrium involved is:

$$S\text{-}OH + B^+OH^- \leftrightarrow S\text{-}O^-B^+ + H_2O \quad (2)$$

At pH below the isoelectric point the surface will be positively charged and will be surrounded by anions and will therefore attract and adsorb anions, while at pH above the isoelectric point the surface will be negatively charged and will attract and adsorb cations from the solution. Knowledge of the isoelectric point is very useful in the design of catalysts since it allows foreseeing the adsorption features of the different oxides as a function of the pH of the impregnating solution. To get information on the capacity of ion adsorption, additional information on the evolution of polarisation as a function of pH is necessary [4]. This can be obtained by electrophoretic velocity measurements or by neutralisation experiments at a constant pH.

Depending on their charge in solution, some oxides will mainly adsorb cations (silica, silica-alumina, zeolites), anions (magnesia, lanthana) and both (alumina, chromia, titania, zirconia) [4,5]. The isoelectric points of some oxides that may be used as supports are given in Table 2.1.

Table 2.1 The isoelectric points (IEPS) of various oxides [5]

Oxide	IEPS	Adsorbing species
Sb_2O_5	< 0.4	Cations
WO_3	< 0.5	
SiO_2		
U_3O_8	≈ 4.0	Cations or anions
MnO_2	3.9-4.5	
SnO_2	≈ 5.5	
TiO_2	≈ 6.0	
UO_2	5.7-6.7	
γ-Fe_2O_3	6.5-6.9	
ZrO_2 hydrous	≈ 6.7	
CeO_2 hydrous	≈ 6.75	
Cr_2O_3 hydrous	6.5-7.9	
α-, γ-Al_2O_3	7.0-9.0	
Y_2O_3 hydrous	≈ 8.9	Anions
Fe_2O_3	8.4-9.0	
ZnO	8.7-9.7	
La_2O_3	≈ 10.4	
MgO	12.1-12.7	

The affinity of the functional group for the metal ions will control the strength of the adsorption and will depend on the charge and radius of the cations ($C^{4+} > C^{3+} > C^{2+} > C^{+} \approx H^{+}$), while for anions the strength of the adsorption will increase with the anionic polarizability and ionic charge (e.g. $SO_4^{2-} > I^- > Br^- > Cl^- > F^-$) [5].

The amount of the metal that can be deposited with the method of wet impregnation is limited because multilayer adsorption is not possible, unless intermediate calcination is performed [5]. In general, wet impregnation is used for the preparation

of low-loaded catalysts and in particular expensive precious metal catalysts, where the active metal phase should be highly dispersed in order to obtain high activity. The distribution of the metal precursor will be based on the density of the exchanging sites in the support. With low metal loading and high density of adsorbing sites on supports in granules, pellets, extrudates (where diffusion effects are encountered), the distribution of the precursor will be inhomogeneous [5]. Deposition will mainly take place at the external layers of the particles. By addition of ions capable of competing with the metal precursor for the same adsorbing sites, a better distribution can be obtained.

(ii) Ion exchange

Ion-exchange consists of replacing an ion in an electrostatic interaction with the surface of the support by another ion species [9]. Catalyst systems, which need charge compensation ions are ideal materials for ion exchange (zeolites, cationic clays or layered double hydroxides) [8]. These are ideal ion exchangers because the crystalline lattice bears electric charges. Compensation of electric charges is a prerequisite for stability of the crystalline structure. As a result the lattice charge is compensated for by the oppositely charged ions bound electrostatically in extralattice positions. These ions are readily exchanged by ions bearing an equivalent charge from the aqueous solution [8].

In a typical ion exchange process, the support containing ions A is plunged into an excess volume of the solution containing ions B [9]. Ions B in the solution gradually penetrate into the pore space of the support while ions A are pass into the solution, until equilibrium is established corresponding to a given distribution of the two ions between the solid and solution. For example, the preparation of zeolite supported metals by ion exchange involves the exchange of complex amine cations of Pt or Pd with K^+, Na^+ or NH_4^+ ions at the exchange sites of the zeolite [8]:

$Pt(NH_3)_4^{2+}$ (aq) + $2Cl^-$ (aq) + K^+Zeol^- ↔ $2K^+$ (aq) +$2Cl^-$ (aq) + $Pt(NH_3)_4^{2+}Zeolite^-$ (3)

The co- and counterions in reaction (3) are removed by filtration and washing. On the other hand, if incipient wetness impregnation is used these ions remain in the zeolite. The ammine-coordinated ions in the zeolite channels are decomposed by calcination to produce PtO and Pt^{2+} ions coordinated to the zeolite walls. In contrast, an unknown distribution of Pt^{4+} and Pt^{2+} is obtained by the incipient wetness method.

(iii) Precipitation methods

According to Schwarz et al. [8], a scientific approach to the preparation of catalysts by precipitation routes was introduced by C. Marcily. Precipitation is usually more demanding than several other preparation techniques, due to the necessity of product separation after precipitation and large volumes of salt-containing solutions generated in precipitation processes [12]. Nevertheless, for several catalytically relevant materials, especially for support materials, precipitation is the most frequently applied method of preparation. Supported metal catalysts are usually prepared by either coprecipitation or deposition-precipitation methods.

(a) Coprecipitation

In this procedure the solutions containing the metal salt and a salt of a compound that will be converted into the support are contacted under stirring with a base in order to precipitate as hydroxide and or/carbonates [5]. After washing, these can be transformed to oxides by heating. Typical industrial catalysts prepared by this procedure are Ni/Al_2O_3, used in the steam reforming process, and $CuO-ZnO/Al_2O_3$, used in methanol synthesis. Coprecipitation is suitable for the generation of a

homogeneous distribution of catalyst components or for the creation of precursors with a definite stoichiometry, which can be easily converted to the active catalyst [12]. It is generally desirable to precipitate the desired material in such a form that the counterions of the precursor salts and the precipitating agent, which can be occluded in the precipitate, can easily be removed by the calcination step. The choice of the salts and/or alkali depends on availability at moderate cost, the solubility in the solvent (water), and, most important, on avoiding the introduction of compounds that can cause negative effects in the final catalyst [5]. For example, except in a few cases, chloride ions are known as common poisons and their presence has to be avoided. The same applies to sulphates, which can be reduced to sulphide during activation. Therefore, nitrate salts or organic compounds, such as formate and oxalate are preferred although some problems can arise with them too. In fact, the latter are expensive and during calcination may not completely decompose. Nitrates are inexpensive and are soluble in water, but calcination has to be controlled because of the exothermic evolution of nitrogen oxides. As to the alkali, Na^+, K^+, NH_4^+ hydroxides, carbonates and bicarbonates can be used as precipitating agents, although ammonium hydroxide is often preferred because of the absence of cation residue [5].

Many variables such as an efficient mixing, the order of addition of different solutions, the temperature, the ageing time, the filtering and washing procedure (during washing the precipitate may peptise, i.e. redisperse into a colloidal gel difficult to filter) have to be controlled. Since this is a multicomponent system, the pH has to be carefully controlled in order to avoid precipitation of the component in a different sequence, thus affecting the final structure of the solid. Precipitation is preferred for preparing supported catalysts with a metal loading higher than 10-15%.

(b) Deposition-precipitation

This procedure is in principle similar to the co-precipitation method. It consists of the precipitation of metal hydroxide or carbonate on the particles of a powder support through the reaction of the base with the precursor of the metal [5]. Practical realisation demands that the rate of nucleation is higher at the surface than in the bulk of the solution and that the homogeneity of the bulk solution is preserved [8]. Rapid nucleation and growth in the solution bulk will lead to large crystallites and inhomogeneous distribution, since the large particles will be unable to enter into the pores and will deposit only on the external surface [5]. In order to obtain the best results, an efficient mixing should be used together with a slow addition of the alkali solution in order to avoid the build-up of local concentration gradients. It has been found that the best base is urea, which is usually added at room temperature [4,5,8,9]. By rising the temperature to 70-90 ^{o}C, urea slowly hydrolyses generating ammonium hydroxide homogeneously through the solution. The pH of the solution remains practically constant, as the rate of precipitation is higher than that of hydrolysis. The best results are also obtained when an interaction between the support and the active precursor takes place.

In the electrochemically controlled procedure, the precipitating agent is generated at either the anode or the cathode of an electrochemical cell [8]. The method offers the advantage of fine control of the pH and the valence of the ions to be precipitated. In addition, anodic dissolution of a metal can be combined with its deposition-precipitation onto the suspended support.

After the deposition-precipitation step, the material is filtered, washed, and dried as in the co-precipitation procedure. The only problem is the difficulty of obtaining catalysts with high concentration of metal.

(iv) Other preparation methods

Besides the above-mentioned methods, supported catalysts have also been prepared by grafting [8]. It has also been discovered that metal oxides can be deposited on the surface of supports by physically mixing and heating the resulting mixture to spread the active component. However, this method applies only to active metal oxides that are volatile or have a low melting temperature, such as rhenium oxide, molybdenum oxide, tungsten oxide and vanadium oxide. The disadvantage of this method is the long calcination times required to achieve complete spreading of the active metal oxide over the support surface.

2.2.2 Drying

Drying is an important step in catalyst preparation since it can affect the distribution of the active species. During drying, the solution in the pores will become oversaturated and precipitation takes place [11]. If not done properly, this step can result in irregular and uneven concentration distributions [1]. Different variables such as the heating rate, final temperature and time of treatment and type of atmosphere can influence the drying process and have to be selected according to different systems [5]. In principle, rapid evaporation of the solvent is favourable because it causes rapid supersaturation of the solution in the pores and that is associated with a high dispersion of the active species [11]. However, if the drying rate is too slow evaporation occurs at the meniscus, which retreats down the pore, some salt deposition occurs but most of the solute merely concentrates deeper in the pore [1,5]. When finally crystallised, the salt is located at the bottom of a pore or at the particle centre. When the drying rate is too fast a temperature gradient occurs. Vaporisation deep in the pore forces solution toward the outside, where most of the deposition takes place. The ideal situation is when crystallisation is enough to form

uniform deposits [5]. However, since the support exists with a distribution of pore sizes, it is impossible to satisfy optimum conditions for each.

2.2.3 Calcination and activation

Calcination involves heating the catalysts in an oxidizing atmosphere at a temperature usually as high as or a little higher than encountered during reaction [5]. The purpose of calcination is to decompose the metal precursor with the formation of an oxide and removal of the cations or the anion that have been previously introduced as gaseous products. Besides decomposition, during the calcination sintering of the precursor or of the formed oxide or a reaction of the formed oxide with the support can occur [1,5]. When dealing with bimetallic catalysts, control of calcination temperature is required in order to avoid the formation of two separate oxides or segregation of one of the components.

Other thermal treatments, such as reduction or sulphidation, which are performed in a special atmosphere, are called activation operations [1,4,5]. In some catalyst the reduction, if required, is performed in solution by chemical reagents such as formaldehyde or hydrazine [5]. Variables such as the rate of heating, the final temperature, the temperature of reduction, the concentration of the reducing gas, and the flow rate of the treatment gas have to be carefully chosen depending on the type of metal, catalytic system and reaction type [5]. The quality of the reduction gas or mixture is very important. For example, water vapour pressure has to be as low as possible because it can be detrimental for high dispersion of the metal. Direct reduction of the metal precursor has to be avoided, for instance, metal chlorides are more easily reduced than the corresponding oxides and the hydrochloric acid formed would be corrosive in the presence of small amounts of water vapour [5].

2.3 Synthesis and structure of zeolites

We have noted that supported metal heterogeneous catalysts are composed of the active species, the support and sometimes a promoter. Some of the common supports were listed in table 2.1 together with their isoelectric points. Zeolites may be used as catalysts on their own or as supports for active catalytic species. Because of their unique structure, zeolites can induce shape-selectivity allowing only molecules of certain sizes and shapes to pass through them [13].

Structure

Zeolites are hydrated crystalline, microporous three-dimensional aluminosilicates that are constructed from TO_4 tetrahedra (with T, the tetrahedral atom, being either Si or Al) [4,14,15]. Each apical oxygen is shared between two adjacent tetrahedra giving an O/T framework ratio of two. Because Al^{3+} substitutes some of the Si^{4+}, there is a net negative charge, which is balanced by extra-framework exchangeable cations. Typical cations in natural zeolites are alkali metals and alkaline earth metals. These cations are electrostatically held within the central cavities and are surrounded by water molecules. The water molecules are loosely held in the pores and most zeolites can be reversibly dehydrated, and their cations readily exchanged. The general formula for the composition of zeolites [4,8,15] is:

$$m/y\mathrm{M}^{y+}[(\mathrm{SiO_2})_n(\mathrm{AlO_2})_m]\cdot x\mathrm{H_2O}$$

where the term in the square brackets represents the framework, consisting of SiO_2 and AlO_2 units, M represents the exchangeable cation of valence y, and n, m and x are the variable multipliers. Zeolite-like materials (zeotypes) containing elements other than silicon and aluminium have also been synthesized [17].

Since zeolite frameworks have pore systems with several ring sizes, they have been traditionally classified as small, medium or large pore on the basis of the ring size of the largest pore that limits access to the pore system [16]. Small pore zeolites are limited by eight-membered rings, medium pore by ten-membered rings and large pore by twelve-membered rings or larger.

Zeolites have a wide range of applications, and they constitute a major part of applications involving acid-catalysed reactions [18]. Their acidity character makes them good supports for reactions that require catalysts that exhibit bifunctionality involving the metal active sites and the Brønsted acid sites of the zeolite.

Synthesis of zeolites

Zeolites are normally synthesized from aluminosilicate gels prepared by mixing the alumina and silica sources, metal cations, organic molecules and water in an alkaline solution, and treatment of the resulting gels at elevated temperatures and pressures [19]. The main chemicals used for the synthesis of zeolites are aluminium nitrate, sulfate or hydroxide, sodium aluminate, sodium hydroxide, sodium water glass, colloidal silica sol, fumed silica, precipitated silica, tetramethylorthosilicate and tetraethylorthosilicate [4,19]. One of the most important factors in the synthesis of zeolites is the chemical composition of the gel from which the crystalline products are obtained. In addition to the gross composition of the reaction mixture, time and temperature also play an important role in influencing the structure of the final product.

A typical synthesis involves mixing together alkali, sources of AlO_2^- and SiO_2, water and, if required, other components such as templates, in appropriate proportions [4,19]. Depending on the temperature and the reaction mixture composition, the

crystallization time can range from several hours to several weeks. During this period, the system is in a highly disordered state with higher entropy than more ordered crystallizing product. The formation of the final product is generally governed by the Ostwald's law of successive transformations, which states that in all reactions the most stable state may not be reached at once, but that first a succession of intermediates of less stable states tends to be traversed [4,19]. The course of a crystallization at various times can be followed by stopping the crystallization at various times and sampling the batch.

This SiO_2/Al_2O_3 ratio in the gel places constraints on the framework composition [4,8,19]. The hydroxide concentration influences, among other things the nature of the polymeric species present in the reaction mixture and the rate at which these species interconvert by hydrolysis. Increase in the hydroxide concentration accelerates crystal growth and shortens the induction period preceding crystallization. One explanation for this is that it facilitates transport of the silicate and aluminate species by an enhanced solubility of the reactants at higher pH. The reactants will nucleate and grow faster because of the increase in the collision frequency between the more concentrated precursor species in the solution phase.

In addition to serving as charge compensators, inorganic cations present in the reaction mixture often play a significant role in determining the structure of the zeolite product formed. They can influence the morphology, crystallinity, and yield [4]. The water content of the starting mixture also plays an important role in determining the structure of the zeolitic product. Water has been proposed to interact strongly with cations present in solution and becomes itself a sort of template for structure control.

After synthesis, by the hydrothermal treatment of the synthesis mixture, the solid obtained is filtered, washed with distilled water and dried. In the case where organic

templates have been used the sample is calcined in air at high temperatures (usually around 500 ^{o}C) to remove the template from the zeolite product [4].

2.4 Characterisation of catalysts

After preparing materials purported to be catalysts, it is a norm to characterise them in order to verify if the correct material was produced. Characterisation helps in correlating the catalytic performance of catalysts with their physical and chemical properties. Many techniques and instruments have been developed and have been successfully used to characterise catalysts. Some of the techniques that are commonly applied in the characterisation of catalysts are described below.

2.4.1 X-Ray diffraction

X-ray diffraction analysis is the method most frequently used for the structural analysis of solids [20,21]. The methods range from simple powder diffraction patterns to sophisticated single crystal methods, which allow the localization of all atoms in a unit cell and the calculation of the electron density distribution between these atoms. However, for zeolites, the synthesis of single crystals is difficult and therefore powder diffraction methods are used for identification. Powder diffraction data are most commonly used as a "fingerprint" in the identification of a material [22]. Different features of a powder diffraction pattern can be exploited in the characterization of materials. Analysis of a diffraction pattern allows for the determination of the quantities of the XRD detectable phases, unit cell parameters, degree of structural order, size and shape of crystallites and composition of solid solutions [21,22]. The broadening of diffraction peaks versus crystallite size effects

can be exploited to determine the average sizes of zeolites or the metal crystallites on various supports. The relationship of crystallite size to X-ray line-broadening is given by the Scherrer equation (Equation 2.1) [23]:

$$d_p = K\lambda/\beta\cos\theta \tag{2.1}$$

where d_p is the particle diameter, λ is the wavelength and θ is the Bragg angle. The variable β is the pure diffraction line width, which is corrected for Kα X-ray doublet separation and instrumental broadening, and is expressed in radians in terms of 2θ. In its simplest application, β is the full line-width at half-maximum intensity. The constant K depends on the particle shape and the line indices and its value ranges from 0.7 to 1.7, but is often taken as 0.9.

The intensity or the integral area of the diffraction peaks can be used to determine the crystallinity of zeolites. According to Adnajević *et al*. [24], during crystallization the degree of crystallinity (or percentage crystallinity) of a certain type of zeolite can be defined as the relative content of the zeolite phase in the total solids obtained from the reaction system. The determination of percentage crystallinity is done by comparing the sum of the intensities (or integral peak areas) of a number of peaks (or one peak) of the sample with the sum of the intensities of the same peaks (or peak) of a reference sample using Equation 2.2 [24].

$$\%\text{XRD crystallinity} = \frac{\sum I_{sample}}{\sum I_{reference}} \times 100 \tag{2.2}$$

where I_{sample} is the intensity (or integral peak area) of the chosen peaks characteristic of the investigated sample, and $I_{reference}$ is the intensity (or integral peak area) of the same peaks of the reference sample. The peaks chosen are selected specifically in order to obtain peaks which are the least affected by the degree of hydration of the sample and by other factors.

However, the percentage crystallinity is influenced by some particular properties of the samples, such as the size and shape of crystals, dispersion and homogeneity, dominant orientations, etc [24]. The zeolites with very small crystallites present lower crystallinity values mainly because they are below the detection limit [25], and the low crystallinity values obtained for such samples do not always reflect the true crystallinity value.

2.4.2 Surface area determination by nitrogen physisorption

As indicated in Section 2.2, supported metal catalysts are usually prepared using support materials with high surface area to give high metal dispersions. Total surface area is also a crucial criterion for solid catalysts since it determines accessibility of active sites and is thus often related to catalytic activity [26]. The pore architecture of a heterogeneous catalyst controls transport phenomena and governs the selectivity in catalyzed reactions. Therefore, the pore volume and pore size distribution are important parameters in shape-selective catalysis [26,27]. Gas adsorption methods are important in the determination of the surface area and pore size distributions of solid materials. Of the many gases and vapours which are readily available and could be used as adsorbates, nitrogen has remained universally pre-eminent [28]. The starting point of the determination of the surface areas and pore size distributions of solids is the determination of the nitrogen adsorption isotherm at 77 K.

According to the IUPAC classification, six types of isotherms can be distinguished [29] as shown in Figure 2.1. Only four isotherms are usually found during catalyst characterization, viz., Type I, II, IV and VI. Type I isotherms are characteristic for microporous adsorbents, such as zeolites and carbon.

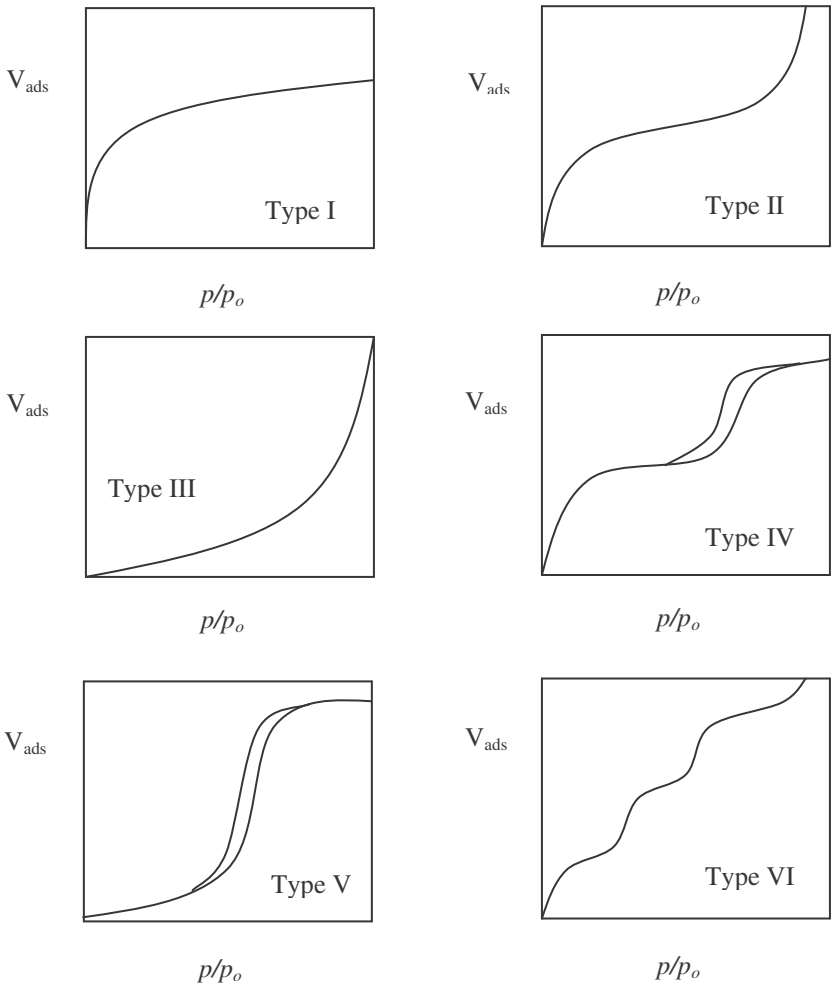

Figure 2.1 The IUPAC classification of adsorption isotherms for gas-adsorption equilibria [29].

Type II isotherms are typical for nonporous or macroporous solids, Type IV isotherms are typical for mesoporous materials and Type VI isotherms are found in uniform ultramicroporous solids.

By analyzing the data with a suitable model, the nitrogen adsorption at 77 K allows the determination of [29]:

- Total surface area of the solid (BET method).
- Total surface and external surface to micropore surface area (*t*-plot or α_s-plot method).
- Mesopore surface distribution versus their size (BJH method).
- Micropore volume (*t*-plot or α_s-plot method).
- Mesopore volume and volume distribution versus their size (Gurvitsch and BJH methods).

The Brunauer-Emmet-Teller (BET) model, which accounts for multilayer adsorption, is the most commonly used model for the determination of the monolayer volume (V_m) of the adsorbate [27]. The isotherm for multilayer adsorption is represented by the BET equation (Equation 2.3) [31]:

$$V = \frac{V_m C x}{(1 - x)[1 + (C - 1)x]} \tag{2.3}$$

where V represents the adsorbed amount of adsorbate at relative pressure x ($x = p/p_o$ with adsorbate pressure, p, and adsorbate saturated vapour pressure at the measuring temperature, p_o), V_m the amount of adsorbate required for monolayer coverage of the adsorbent and C the equilibrium constant of adsorption in the first adsorption layer at the measuring temperature.

The linearised form of Equation 2.3 (Equation 3.4) is usually used for the analysis of adsorption data in the BET range:

$$\frac{x}{V(1-x)} = \frac{1}{V_m C} + \left(\frac{C - 1}{V_m C}\right) x \tag{2.4}$$

By plotting the experimental data in the form of $x/V(1-x)$ versus x, a straight line is obtained; by linear regression the straight line intercept, $1/V_mC$, and slope, $(C-1)/V_mC$, can be easily evaluated. From the two equations for slope and intercept, the values of V_m and C are obtained separately. Then the specific surface area of the sample, S_g, is evaluated from V_m by the use of the area which one molecule of adsorbate covers on the adsorbent surface, σ (for nitrogen adsorption at the normal boiling point of nitrogen a value of 0.162 nm^2 is commonly applied), as given in Equation 2.5.

$$S_g = \frac{V_m N_A \sigma}{22414\ m} \quad m^2 g^{-1} \tag{2.5}$$

where V_m is the monolayer volume, N_A is Avogradro's number, σ is the area covered by one molecule of the adsorbate and m is the mass of the catalyst.

Volumetric characteristics of porous adsorbents may be assessed by determination of the pore size distribution and description of the pore shapes [21]. It is usual to classify pores according to their width as ultramicropores (less than 7 Å), micropores (less than 20 Å), mesoporous (between 2 Å and 500 Å) and macropores (exceeding 500 Å). The total pore volume is usually derived from the amount of gas adsorbed at a relative pressure close to unity, by assuming that the pores are then filled with condensed adsorbate in the normal liquid state. The micropore volume is usually determined by using either a *t*-plot or a α_s-plot method.

The *t*-plot method, developed by de Boer, is based on the comparison of adsorption isotherm data of a porous sample and of a nonporous sample of identical chemical composition and surface character (reference isotherm, type II) [26]. The *t*-plot is considered to be the graph of adsorbed volume (V_{ads}) versus the statistical thickness (*t*) of the adsorbed layer. If both the reference and sample isotherm are identical, as

is the case for nonporous solids, a straight line passing through or close to the origin, should result (Figure 2.2(a)).

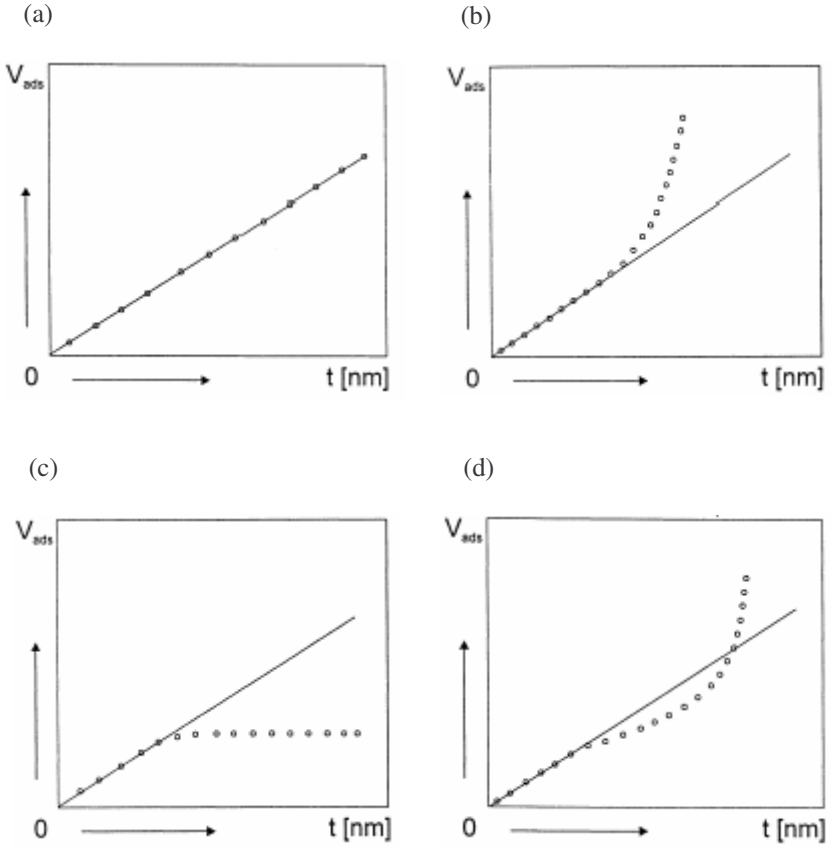

Figure 2.2 *t*-Plots of (a) nonporous, (b) mesoporous, (c) microporous and (d) micro- and mesoporous solids [27].

The slope of this line (m) is directly proportional to the surface area of the solid (A_s) according to Equation 2.6 [27].

$$A_s = (m/22414)tN_a\sigma, \tag{2.6}$$

where N_a is the Avogadro number and σ the area covered by one nitrogen molecule.

Vertical departures from the straight line indicate the presence of mesopores (Figure 2.2(b) while horizontal departures reveal micropores (Figure 2.2(c)). The micropore volume present is obtained from a straight line extrapolated to a positive intercept on the ordinate. Although the method could be used quantitatively to determine the micropore surface area, for routine analysis it is, however, difficult to obtain reference isotherms of nonporous solids and thereby ensure a precise analysis [26]. The α_s-plots, proposed by Sing [28], take a similar approach to the assessment of micropores. The method uses the quantity α_s, that is the ratio between the adsorbed volume and the adsorbed volume at p/p_o = 0.4 [26]. Equation 2.7 can directly be used to calculate the surface area of the sample under consideration from the surface area of the reference material:

$$A_s = \frac{A_s \text{ (reference) } V_{ads} \text{ (sample at } p/p_o = 0.4)}{V_{ads} \text{ (reference at } p/p_o = 0.4)} \tag{2.7}$$

The pore volume can be calculated as in the *t*-plot method.

The BJH (Barret, Joyner, Halenda) method is the most widely used method to describe the adsorption-capillary condensation process that takes place in mesopores [26,27]. The model is simple. In the capillary condensation region (p/p_o> 0.4), each pressure increase causes an increase of the thickness of the layer adsorbed on the pore walls and capillary condensation in the pores having a core (which is the empty space in the pores after the adsorption of the monolayer) size r_c defined by Equation 2.8 (the Kelvin equation)

$$\ln(p/p_o) = \frac{-(2\gamma w_m \cos\varphi)}{RTr_c} \tag{2.8}$$

where r_c represents the radius for cylindrical pores or the distance between walls for slit shaped pores, γ is the surface tension, w_m the molar volume and φ the contact angle. The assumption of a geometric model (usually cylindrical or slit) allows the calculation of the contribution of the adsorbed film to the total adsorption and then the core volume [27]. From these results and from the assumed pore geometry it is possible to transform the core volume into the pore volume and core sizes into pore size.

In such a way, by examining step by step the isotherm in the range $0.42<p/p_o<0.98$, the mesopore volume and the distribution of the mesopores can be obtained.

2.4.2.2 Selective Chemisorption

Chemisorption unlike physisorption is based on the formation of a strong chemical bond between the adsorbate molecules and the exposed surface on the catalysts. Selective chemisorption is an important characterisation method for studying the catalysts, especially supported-metal catalysts. With this method it is possible to determine metal surface area, dispersion and average crystallite size [23,31-33]. Dispersion is expressed as the ratio of the total number of accessible metal atoms on the surface to the total number of metal atoms in the sample [31]. Before carrying out the actual chemisorption experiment, it is important to carefully choose a suitable gas molecule and operating conditions (temperature and pressure). Ideally, for a given catalyst, the gas (and operating conditions) should be chosen to minimise adsorption on the support and to have an irreversible (or weakly reversible) chemisorption on the metal [33]. The most frequently used gas is hydrogen, and when problems are anticipated with the use of hydrogen, carbon monoxide and oxygen may also be used.

The amount of the gas chemisorbed at the monolayer can be measured either by static (volumetric or gravimetric) or dynamic techniques [23,31-33]. Static methods are performed at reduced pressures and involve allowing the system to reach equilibrium between the adsorbed and gaseous states. A previously pretreated and evacuated catalyst is dosed with a known quantity of the adsorbate gas and allowed to reach equilibrium. Equilibration times may range from five minutes to an hour [23]. The amount of adsorbed gas is determined by measuring the pressure after the adsorption equilibrium is reached. The dosing-and-equilibration process is repeated as a function of increasing pressure of the adsorbate. The volume of the adsorbed gas at each pressure is then plotted against the equilibrium pressure to give an isotherm (usually a Langmuir-type of isotherm) [23,33]. The volume of the chemisorbed monolayer (V_m) is determined by extrapolation of the linear region of the isotherm to zero equilibrium pressure.

The evaluation of the total adsorbate uptake (V_m) at the monolayer coverage is subject to some uncertainties, if using the volumetric system. In fact, a slow chemisorption with increasing pressure is sometimes observed and has been ascribed to (i) impurities in the support or on the surface of the metal particles, (ii) contributions from physical adsorption on the support, (iii) spillover of the gas adsorbed to the support [5,23,33]. In order to distinguish between adsorption due to these factors and the chemisorption on the metal, two isotherms are usually required [5,23]. The first isotherm measures both chemisorbed and physisorbed gas and after pumping using proper conditions the second measurement is made to determine the physisorbed gas. From the difference of the two isotherms the volume of the chemisorbed gas can be determined.

In the dynamic or “pulse-flow” methods, the pretreated catalyst is flushed by an inert gas at a temperature sufficient to remove all adsorbed species [5,23,31-33]. After cooling to the required temperature under an inert carrier gas, pulses of a known amount of the adsorbate are introduced into the stream. The amount of the adsorbing

gas that remains from the pulse is measured by a TCD detector. The first few pulses may be completely consumed, while only small fractions of the subsequent peaks would be taken up by the sample [31]. The area of the peaks detected eventually reaches a constant level indicating that the sample has reached monolayer capacity. The amount of the gas adsorbed at the monolayer is obtained by summing the injected volumes. This method is generally faster and less expensive than the static method.

An alternative, dynamic method of determining the amount of chemisorbed molecules/atoms, involves the use of temperature-programmed desorption procedures [23,31-33]. The adsorbate gas is allowed to flow through the pretreated catalyst at the required temperature until the TCD detector shows a constant area. This is followed by purging with an inert gas to remove weakly adsorbed gases, and then the temperature is raised at a controlled rate. This method has the advantage of providing details of the heterogeneity of the surface as indicated by the shape of desorption profiles and the proportions of the molecules desorbed at a particular temperature [23,33].

Once the monolayer volume has been determined, the chemisorption stoichiometry has to be known. The chemisorption stoichiometry (n) is defined as the average number of surface metal atoms associated with the adsorption of each adsorbate molecule. The chemisorption stoichiometries are determined most directly by measuring the adsorption on an unsupported metal with a known surface area [32]. The validity of the extrapolation of the supported metals is tested by comparing the adsorption uptake by the supported-metal catalysts to the metal surface area, which is estimated by X-ray diffraction, electron microscopy or any other method [32]. For hydrogen, the stoichiometry is usually 2 since hydrogen adsorbs dissociatively on metals and each hydrogen atom is adsorbed on one metal atom [5]. Carbon monoxide stoichiometry can change from 2 to 1 since an associative chemisorption in a bridge or a linear from can occur, i.e. covering two or one metal atom

respectively. With oxygen, values from 2 to 1 or even lower (0.75) can be found depending on the type of metal. In addition to the chemisorption stoichiometry, the number of metal atoms per unit area of surface (a_m) has to be known [5]. From the volume of chemisorbed gas required to form a monolayer, V_m, the specific metal surface area is given by Equation 2.9 [33]:

$$A = \frac{V_m}{22414} N_A n \quad \frac{1}{m} a_m \quad \frac{100}{(wt\%)} \; m^2 g^{-1} \text{ metal} \tag{2.9}$$

where V_m is expressed in cm^3 (STP), N_A is the Avogadro number, n is the chemisorption stoichiometry, m the mass of the sample (g), a_m the surface area (m^2) occupied by the metal atom, and (*wt.*) the metal loading.

The average metal dispersion is directly obtained from equation 2.10 [33]:

$$D = \frac{V_m n \; 100M}{22414 \; m \; (wt\%)} \tag{2.10}$$

where M is the atomic mass of metal.

From a knowledge of the free-metal area (A), the mean particle diameter (d_v) can be obtained. For spherical particles the particle diameter can be determined using Equation 2.11 [5]:

$$d_v = 6V/A \tag{2.11}$$

where the volume (V) is usually calculated from a knowledge of the mass of the metal and its density.

2.4.3 Temperature-programmed analysis

Temperature-programmed analysis is a well established technique for characterising heterogeneous catalysts. Differential thermal analysis (DTA), thermogravimetry (TG), and differential scanning calorimetry (DSC) are standard techniques in solid state chemistry [34]. However, the main concern in the field of heterogeneous catalysis is an understanding of gas-solid interactions and of surface reactivities. Hence techniques such as temperature-programmed desorption (TPD), reduction (TPR), oxidation (TPO), and surface reaction (TPSR) have been developed. These methods involve monitoring surface (or bulk) processes between the solid catalyst and its gaseous environment via continuous analysis of the gas phase composition as the temperature is raised [33]. The position and shape of the peak from the analysis profiles is sensitive to parameters such as the catalyst particle size, catalyst depth, carriers flow rate and the composition of the carrier gas [35].

Temperature-programmed desorption

Temperature-programmed desorption is commonly used to study the bonding energy of adsorbates on catalytic surfaces. The temperature of the desorption peak maximum is indicative of the strength with which the adsorbate is bound to the surface [34]. The higher the temperature of the desorption peak the stronger the bond between the adsorbate and the surface. Temperature-programmed desorption uses probe molecules to examine the interactions between the surface with gases or liquid-phase molecules [34]. The probe molecules are chosen with respect to the nature of the adsorbed species believed to be important for the catalytic reaction under study or chosen to provide information about the specific type of surface sites. Analysis of temperature programmed desorption profiles can provide adsorption-desorption mechanisms and their associated kinetics. Kinetic parameters such as heat of adsorption, activation energy of the adsorption and desorption process, order

of desorption can also be determined. Temperature programmed desorption of ammonia has been applied in the study of the acidity of catalytic materials [35, 36].

In a typical TPD experiment, the catalyst is pretreated and then saturated with an adsorbing gas under well-defined conditions [34]. The excess gas is purged out of the reactor with an inert gas and then the sample is subjected to a linear temperature ramp. The effluent gas composition is continuously monitored by a detector placed at the exit of the reactor. The experiment permits the total determination of gas that was adsorbed, and kinetic parameters of the desorption process, particularly its activation energy [34]. Temperature-programmed desorption of ammonia has been mostly used to measure the surface acidity of solid catalysts.

Temperature-programmed reduction and oxidation

In a typical TPR experiment, a defined mass of catalyst powder is placed in a quartz reactor and if applicable pretreated in flowing oxygen to ensure a well-defined oxidation state of the catalyst precursor at the start of the reduction experiment [34]. The sample is then cooled to the start temperature and the gas flow is changed from inert gas flow to a reducing gas mixture. A reducible catalyst or catalyst precursor is exposed to a flow of a reducing gas mixture (typically argon containing a small percentage of hydrogen) while the temperature is raised linearly. The rate of reduction is followed by measuring the composition of the reducing gas mixture at the outlet of the reactor. The experiment allows the determination of the total amount of hydrogen consumed, from which the degree of reduction and thus, the average oxidation state can be calculated. The kinetic parameters of reduction can also be determined provided good models are available [34,35].

Temperature-programmed oxidation (TPO) is commonly applied in the study of the kinetics of coking, evaluation of catalysts carbon burn-off, determination of the

different forms of carbonaceous deposits present on the catalysts [35,37]. The sample is heated at a uniform rate as the reactant gas, typically 2-5% oxygen in helium, is applied to the sample in pulses or as a steady stream. The oxidation reaction occurs at a specific temperature resulting in the uptake of oxygen. The amount of oxygen consumed is related to the quantity of carbonaceous species on the surface of the catalyst.

2.4.4 Electron microscopy

Electron microscopy is one of the most important tools for characterising heterogeneous catalysts. The technique has been widely applied in the study of zeolites and supported-metal catalysts [32,38]. With regard to the determination of the crystallite sizes, electron microscopic techniques have an advantage over X-ray diffraction techniques. With electron microscopy, the individual particles can be observed and measured, while X-ray diffraction estimates the average crystallite size.

Transmission electron microscopy (TEM), which involves the passage of electrons through a sample, is a powerful and routinely used technique for the analysis of particle size and morphology in supported metal catalysts [25]. One major limitation of TEM imaging is that we observe two-dimensional images from samples that are three-dimensional. Image contrast cannot be directly interpreted in terms of sample thickness [25,38]. Scanning transmission electron microscopy (STEM) is the best technique for directly determining a wide range of metal particle sizes. It is routinely used to image metal clusters with diameters below 1 nm while conventional transmission electron microscopy (TEM) can image particles larger than 1 nm and identify the composition and structure of larger clusters [32]. Furthermore, the scanning transmission electron microscopy technique is capable of resolving the

atomic scale structure of surfaces with atomic resolution [39]. Scanning electron microscopy (SEM) is good for characterizing macroscopic features, especially crystal morphology and surface steps [38]. SEM is sensitive to metal particles on the surface of the support and even particles located in the interior can be imaged using back scattered imaging.

2.4.5 Vibrational spectroscopy

Vibrational spectroscopies are among the most important widely used methods for catalyst characterisation [40,41,42]. In situations where X-ray diffraction is not applicable, vibrational spectroscopies can often provide information on phase transitions and changes in composition of bulk catalyst materials, their crystallinity, and on the nature of the surface functional groups. Because of their relative simplicity and wide applicability, infrared transmission-absorption spectroscopy and diffuse reflectance spectroscopy are most frequently used in catalysis research, whereas Laser Raman spectroscopy is increasingly finding more applications [40]. Vibrational spectroscopies are suitable for the determination of [41]:

- the bond strength in molecular units, in particular in hydrogen bond research,
- intermolecular bonding features,
- distortion of molecular units at various lattice sites,
- the structure of molecular units in solids,
- the coordination polyhedra of metal ions,
- space group symmetries,
- determination of isotypism, and
- many other physical properties, such as free carrier concentrations, etc.

Infrared spectroscopy has also been used to the probe the acidity of oxides and molecular sieves [43]. As the type of probe molecule chosen will influence the

obtained characteristics of the probed solid and, hence, will also affect the structure-activity relationship derived, the choice of the appropriate probe molecule is very important [43]. The most important criteria for choosing a probe molecule has been summarised by Lercher et al. [41] as follows:

- The probe molecule should have dominating base rather than weak acidic properties.
- The IR spectrum of the sorbed probe molecule should allow distinguishing between sorption on protonic (Brønsted) and aprotic (Lewis) acid sites.
- The probe molecule should allow differentiating acid sites of the same type, but of different strength.
- The size of the probe molecule should be comparable to the size of the reactant used to probe the concentration of acid sites relevant for a particular reaction.

The applicability of the transmission technique is determined by the properties of the sample under study [40]. Samples that exhibit only weak bulk absorption and in which the average particle size (d) is smaller than the wavelength of the infrared radiation in the region of interest will be best suited for the transmission mode. The particle size condition ($\lambda > d$) which determines the wavelength range of suitably low scattering losses is usually met in the mid and far infrared regions, whereas scattering losses become strongly involved in the near infrared region. However, most samples show strong bulk absorption in the low wavenumber region (roughly < 1000 cm^{-1}). As a result, the low frequency range, in which the vibration modes of interest for structural characterisation of the solid powder material are frequently located, is often not accessible to *in situ* studies using the pressed wafer technique in transmission mode. The sample is prepared by grinding a small amount of the sample (usually 1-3 mg) with about 400 mg of powdered KBr [41]. However, for *in situ* investigations this technique is not applicable and self-supporting wafers have to

be prepared. Sample preparation is usually difficult and hence, the disadvantage of the use of transmission-absorption IR spectroscopy [42]

In situations where the transmission techniques fails due to scattering, diffuse reflectance can be used, provided the solid material does not absorb too strongly in the frequency range to be studied [40]. In diffuse reflectance spectroscopy (DRS) the ratio of the light scattered from an infinitely thick layer and the scattered light from an ideal non-adsorbing reference sample is measured as a function of the wavelength (λ) [44]. The illumination of powdered samples by incident radiation leads to diffuse illumination of the samples. The incident light is partially absorbed and partially scattered. The scattered radiation emanating from the sample is collected in an integration sphere and then detected. If the sample is infinitely thick, the diffuse reflection of the sample (R_∞) is related to the apparent absorption (K) and apparent scattering coefficient (S) via the Kubelka-Munk (K-M) function [40,44,45]:

$$R_\infty = \frac{(1-R_\infty)^2}{2R_\infty.} = \frac{K}{S} \qquad (2.12)$$

This function is valid under the conditions: (i) diffuse monochromatic irradiation of the powder sample, (ii) isotropic light scattering, (iii) an infinite layer thickness and (iii) absence of fluorescence [44].

Diffuse reflectance infrared spectroscopy (DRIFTS) offers the advantage of simpler sample preparation, the capacity to analyse non-transparent samples, irregular surfaces and coatings, exposure of the sample to simulated reaction conditions while analysing the changes in the species at the material surface, recording the sample at elevated temperature and/or under pressure [45]. The main drawback of this technique is the difficulty of quantitative measurements. Another limitation concerns the reproducibility of the measurements. Since the diffusion coefficient

varies with each preparation, it is difficult to compare two spectra of the same material recorded in two different experiments.

Many other techniques such as X-ray absorption spectroscopy (XAS), X-ray photoelectron spectroscopy (XPS), Electron spin resonance (ESR), Nuclear magnetic resonance (NMR), etc. have also been widely applied for the characterisation of catalysts.

2.5 References

[1] J.T. Richardson, Principles of Catalyst Development, Plenum Press (1989) p6-7

[2] F. Cavani and F. Trifiro, *Catal. Today*, **34** (1997) 269-279.

[3] E. Brunner, *Catal. Today*, **38** (1997) 361-376.

[4] C. Perego and P. Villa, *Catal. Today*, **34** (1997) 281-305.

[5] F. Pinna, *Catal. Today*, **41** (1998) 129-137.

[6] G.J. Hutchings, *Catal. Lett.*, **75** (2001) 1-12.

[7] I.E. Wachs and K. Segawa, in Characterization of Catalytic Materials, I.E. Wachs, ed., Butterwort-Heinemann, 1992, Boston, p69-88.

[8] J.A. Schwarz, C. Contescu and A. Contescu, *Chem. Rev.*, **95** (1995) 477-510.

[9] M. Campanati, G. Fornasari, A. Vaccari, *Catal. Today*, **77** (2003) 299-314.

[10] G. Leofanti, G. Tozzola, M. Padovan, G. Petrini, S. Bordiga and A. Zecchina**,** *Catal. Today*, **34** (1997) 307-327.

[11] G. Mul and J.A. Moulijn, in J.A. Anderson, M.F. García, eds., Supported Metals in Catalysis, Imperial College Press, 2005, London, p1-32.

[12] F. Schüth and K. Unger in Handbook of Heterogeneous Catalysis, G. Ertl, H. Knözinger and J. Weitkamp, eds, Vol. 2, Wiley-VCH, 1997, Weinheim, p72-86.

[13] F. Ramôa Ribeiro, F. Alvarez, C. Henriques, F. Lemos, J.M. Lopes and M.F. Ribeiro, *J. Mol. Catal. A: Chem.*, **96** (1995) 245-270.

[14] M.E. Davis and R.F. Lobo, *Chem. Mater.*, **4** (1992) 756-768.

[15] Y. Huang, R.M. Paroli, A.H. Delgado and T.A. Richardson, *Spectrochim. Acta Part A*, **54** (1998) 1347-1354.

[16] J.B. Higgins, Large pore zeolite frameworks and materials. *Catalysis Today*, **19** (1994) 7-26.

[17] C.S. Cundy and P.A. Cox, *Chem. Rev.*, **103** (2003) 663-701.

[18] Ref

[19] E.J.P. Feijen, J.A. Martens and P.A. Jacobs, in Zeolites and related microporous materials: State of the art 1994. Studies in surface science and catalysis, J. Weitkamp, H.G. Karge, H. Pfifer and W. Hölderich, (Eds.), Volume 84, Elsevier, 1994, Amsterdam, p3-21.

[20] G. Perego, *Catal. Today*, **41** (1998) 251-259.

[21] E.M. Serwicka, *Catal. Today*, **56** (2000) 335-346.

[22] L.B. McCusker, *Microporous and Mesoporous Mater.*, **22** (1998) 527-529.

[23] J.A. Anderson, M. Fernadez-Garcia and A. Martínez-Arias in J.A. Anderson, M.F. García, eds., Supported Metals in Catalysis, Imperial College Press, 2005, London, p123-154.

[24] B. Adnadjević, J. Vukićević, Z. Filipović-Rojka and V. Marković, *Zeolites*, **10** (1990) 699-702.

[25] E.F. Sousa-Aguiar, A. Liebsch, B.C. Chaves and A.F. Costa, *Microporous and Mesoporous Mater.*, **25** (1998) 185-192.

[26] S. Storck, H. Bretinger and W.F. Maier, *Appl. Catal.*, *A*, **174** (1998) 137-146.

[27] G. Leofanti, M. Padovan, G. Tozzola and B. Venturelli, *Catal. Today*, **41** (1998) 207-219.

[28] K. Sing, *Colloids Surf., A*, **187-188** (2001) 3-9.

[29] C. Sangwichien, G.L. Aranovich and M.D. Donahue, *Colloids Surf., A*, **206** (2002) 313-320.

[30] P. Schneider, *Appl. Catal., A*, **129** (1995) 157-165.

[31] F. Eigenmann, M. Maciejewski and A. Baker, *Thermochim. Acta*, **359** (2000) 131-141.

[32] G. Meitzner, in Characterization of Catalytic Materials, I.E. Wachs, ed., Butterwort-Heinemann, 1992, Boston, p17-45.

[33] G. Bertgeret and P. Gallezot in Handbook of Heterogeneous Catalysis, G. Ertl, H. Knözinger and J. Weitkamp, eds, Vol. 2, Wiley-VCH, 1997, Weinheim, p439-464.

[34] H. Knözinger in Handbook of Heterogeneous Catalysis, G. Ertl, H. Knözinger and J. Weitkamp, eds, Vol. 2, Wiley-VCH, 1997, Weinheim, p676-689.

[35] S. Bhatia, J. Beltramini and D.D. Do, *Catal. Today,* **7** (1990) 309-438.

[36] H. Wang, Z. Liu, J. Shen and H. Liu, *Catal. Commun.*, **5** (2004)

[37] C.A. Querini and S.C. Fung, *Catal. Today*, **37** (1997) 277-283

[38] A.K. Datye, *J. Catal.*, **216** (2003) 144-154.

[39] J.V. Lauristen, R.T. Vang and F. Basenbacher, *Catal. Today*, **111** (2006) 34-43.

[40] G. Mestl and H. Knözinger in Handbook of Heterogeneous Catalysis, G. Ertl, H. Knözinger and J. Weitkamp, eds, Vol. 2, Wiley-VCH, 1997, Weinheim, p539-574.

[41] J. Ryczkowoski, *Catal. Today*, **68** (2001) 263-381.

[42] G. Busca, *Catal. Today*, **27** (1996) 323-352.

[43] J.A. Lercher, C. Gründling and G. Eder-Mirth, *Catal. Today*, **27** (1996) 353-376.

[44] BM Weckuysena and RA Schoonheydt, *Catal. Today*, **49** (1999) 441-451.

[45] T. Armaroli, T Bécue and S. Gautier, *Oil Gas Sci. Tech.* **59** (2004) 215-237.

Chapter 3

The nonoxidative dehydroaromatisation of methane

The conversion of methane in the absence of oxygen (nonoxidative conversion) to higher hydrocarbons provides a number of benefits compared to the oxidative conversion, including the possibility to produce hydrogen, which can be used for fuel cells. The direct conversion of methane into aromatics in the absence of oxygen was first reported in 1993 by Wang and co-workers [1]. This pioneering work was later followed by a large number of publications on the subject, indicating the importance of this reaction. Some excellent reviews on the subject were also published [2-5].

This chapter is also a form of a review of the literature dealing with methane aromatisation.

3.1 Catalysts used in the nonoxidative dehydroaromatisation of methane

The conversion of methane remains a challenge for scientists and engineers around the world. Wang et al. [1] showed that the conversion of methane to aromatics was possible over a Mo/H-ZSM-5 catalyst without the presence of oxygen. With this catalyst they obtained high activity for the dehydroaromatisation of methane, without any loss in activity and selectivity under the reaction conditions used for the study. Subsequent studies on different transition metal ions (TMI) revealed that the activities of TMI/H-ZSM-5 catalysts for methane conversion followed the trend Mo>W>Fe>V>Cr [6]. A lot of interest has arisen on the use of molybdenum as the active metal for the methane dehydroaromatisation catalysts. However, other studies have also demonstrated that zeolite-supported rhenium exhibits a catalytic performances similar to that of molybdenum for the dehydroaromatisation of methane [7,8]. In addition, higher catalytic activities were also reported for acidified tungsten-based catalysts [9,10]. The tungsten-based catalyst systems are also said to offer better resistance to high-temperature sublimation that usually occurs with Mo-based catalysts. Hence, Mo, W and Re are regarded as the most promising catalytic components as nonoxidative methane dehydroaromatisation catalysts.

When identifying the best support for the active metal it was established that zeolites with a two-dimensional structure and with a pore size near to the dynamic diameter of benzene, notably ZSM-5, ZSM-8 and ZSM-11, are the best supports for Mo-based catalysts for methane dehydroaromatisation [11]. The good catalytic activities observed on the catalysts prepared using these zeolites have been attributed to the unique pore systems possessed by these zeolites. Molybdenum supported on

materials such as MCM-22 [12], MCM-49 [13], ITQ-2 [14], MCM-36 [15], HZRP-1 [16,17] and Al-FSM-16 [18] also showed good catalytic performances.

Mo/H-MCM-22 catalysts were compared with Mo/H-ZSM-5 and it was found that Mo/H-MCM-22 catalysts were more active and stable for the dehydroaromatisation reaction than Mo/H-ZSM-5 catalysts [19]. Higher selectivities to benzene and lower selectivities to naphthalene were also observed over the Mo/H-MCM-22 catalysts. Similar observations were made with Re/MCM-22 [20]. The better efficiency of MCM-22-supported catalysts was attributed to its open topology allowing a better dispersion of the molybdenum species and a more rapid diffusion of the reaction species [19]. MCM-22 has a topological structure composed of the interconnected $\{4^3 5^6 6^3 [4^3]\}$ building unit, forming two independent pore systems which are accessible through the ten-membered rings (with dimensions 0.41 nm × 0.55 nm). One of these pore systems is defined by two-dimensional sinusoidal channels, which maintain an effective ten-membered ring diameter (with dimensions 0.40 nm × 0.55 nm) throughout the structure, while the other consists of large supercages (with dimensions 0.71 × 0.71 × 1 .82 nm × 0.7 nm) defined by twelve-membered rings [20-22]. ZSM-5 on the other hand posses a two-dimensional channel system which belongs to the orthogonal or monoclinic crystal systems. The pore structure consists of an elliptical straight channels running parallel to [010], having ten-membered rings of dimensions 0.53 × 0.56 nm free diameter, as well as sinusoidal channels running parallel to [100], having ten-membered rings of free diameter 0.51 × 0.55 nm [23]. Therefore, MCM-22-supported catalysts could supply more space for the carbonaceous deposition which occurs during the reaction of methane because of the presence of large cavities and could allow for the fast diffusion of the less bulky products because of the presence of more elliptic or more slit-like pore openings than found for H-ZSM-5 [19]. As a result, better stability and higher selectivity to benzene may be achieved on the H-MCM-22 supported systems.

3.2 The preparation of catalysts for the nonoxidative dehydro-aromatisation of methane

Preparation procedures are known to affect the catalytic performance of the resulting catalysts. In this section the methods which are usually used in the preparation of Mo/zeolite catalysts used for methane dehydroaromatisation are discussed.

3.2.1 Preparation methods which are commonly used

The preparation of Mo/H-ZSM-5 and Mo/H-MCM-22 catalysts is usually carried out by incipient wetness impregnation of H-ZSM-5 with aqueous solutions of ammonium heptamolybdate ($(NH_4)_6Mo_7O_{24}$) followed by calcination in air at 400-700^oC for 4 to 6 hrs [1,6,12,23-27] or by grinding MoO_3 and H-ZSM-5 powders followed by calcination in air [28-31]. It has been reported that during the incipient wetness impregnation the large aqueous molybdate ions do not exchange directly onto H-ZSM-5 cation exchange sites [32]. Bulk-like ammonium heptamolybdate (AHM) entities were observed when the impregnated mixtures were calcined 110^oC [32] or 130^oC [25]. During calcination in air (at temperatures between 227 and 337^oC), the AHM decomposed into MoO_3 on the outer surface of the zeolite [6,32,33]. The MoO_3 crystallites dispersed on the external surface of the zeolite and then migrated as $(MoO_3)_n$ oligomers into the zeolite channels at a calcination temperature of 500^oC [6,33]. As the isolated MoO_x species migrate into the zeolite channels via gas-phase or surface diffusion, they react with H^+ atoms at exchange sites to form $(MoO_2(OH))^+$ species, which can condense with another one to form a $(Mo_2O_5)^{2+}$ dimer and H_2O as shown in Scheme 1 below [28]:

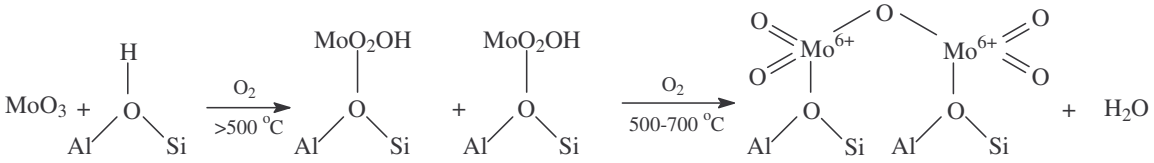

Scheme 1 The reaction of Brønsted acid sites with Mo species to form a coordinated $(Mo_2O_5)^{2+}$ dimer [28].

$(MoO_2(OH))^+$ species can also react with a zeolite OH group to form water and a $(MoO_2)^{2+}$ cation bridging two acid sites as illustrated in Scheme 2:

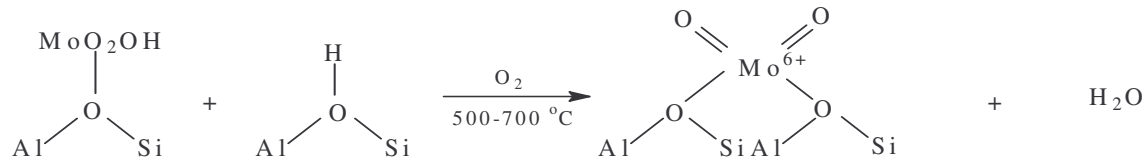

Scheme 2 Reaction of Brønsted acid sites with Mo species to form a $(MoO_2)^{2+}$ cation bridging two acid sites [28].

Recently, Tessonier et al. [34] showed that the above anchoring modes depend on the Si/Al ratio of H-ZSM-5. They concluded that the dimeric monodentate species (Scheme 1) were more likely to form on H-ZSM-5 with high Si/Al ratio whereas the monomeric species (Scheme 2) form at low Si/Al ratios**.** Furthermore, Ma et al. [35] suggested that for Mo/H-MCM-22 catalysts, the monomer Mo species is formed when Mo species are exchanged with Brønsted acid sites of H-MCM-22.

In the case of the preparation by physical mixing of MoO_3 and H-ZSM-5, Iglesia and co-workers [28] suggested that the mechanism of interaction involves the initial formation of an external MoO_3 monolayer on the zeolite via surface migration at temperatures from 360 to 500°C. When the molybdenum content exceeds that required to from a monolayer, MoO_x species are lost as $(MoO_3)_n$ oligomers via sublimation or as unreducible and inactive $Al_2(MoO_4)_3$ domains via reactions with framework Al atoms. Between 500 and 700°C, surface and gas-phase transport paths lead to migration of MoO_x species into the zeolite channels and reaction with OH groups to form MoO_2-$(OH)^+$ species that condense quickly to form H_2O and a strong Mo-O-Al anchoring bond. The Mo species existed as $(Mo_2O_5)^{2+}$ ditetrahedra interacting with two zeolite exchange sites as shown in Scheme 1. The exchanged $(Mo_2O_5)^{2+}$ species are the precursors to the methane activation sites in Mo/H-ZSM-5 catalysts [28].

3.2.1 Calcination temperature and time

It has been shown that ammonium heptamolybdate decomposes to form MoO_3 on the external surface of the zeolite at 300°C and the MoO_3 species migrate into the zeolite channels at high calcination temperatures (500-700°C) [25,33,36]. This indicates that the interactions between the molybdenum species and the zeolite are to some extent influenced by the calcination parameters (temperature and time). Indeed, it has been shown that the higher the calcination temperature ($\geq$ 750°C), the stronger the interaction between MoO_3 and the H-ZSM-5 zeolite in Mo/H-ZSM-5 catalysts [33]. With increasing molybdenum loading and calcination temperature, the interaction can be so strong that all the aluminium in the framework can be extracted by molybdenum species to form an $Al_2(MoO_4)_3$ crystalline phase, as detected by XRD and ^{27}Al MAS-NMR techniques [37]. This extraction causes the ZSM-5 zeolite framework to collapse and as a result the activity of the Mo/H-ZSM-5 catalysts for methane dehydroaromatisation drops dramatically. A recent study

showed that prolonging the calcination duration at 500^{o}C favours the diffusion and migration of molybdenum species from the external surface of Mo/H-ZSM-5 into the channels of H-ZSM-5 [38]. Wang et al. [25] have also noted that the concentration of molybdenum in the channels of the zeolite increases as the temperature and the duration of calcination increases. The influence of the calcination temperature and duration on the catalytic conversion of methane will be discussed in the following section.

3.3 Factors that influence the catalytic performance of methane dehydroaromatisation catalyst

The factors which were found to affect the performance of methane dehydroaromatisation catalysts are discussed. The discussion is based mainly on the results obtained for Mo/ZSM-5 catalysts because they have been studied in more detail than other catalysts.

3.3.1 The effect of Mo loading

Wang and co-workers [1] showed that the conversion of methane was maximal at molybdenum loadings of about 2-3 wt%. Further increments in the molybdenum loading above these values substantially decreased the conversion of methane and reached the lowest level at 6 wt% Mo loading. The selectivity to C_2 hydrocarbons increased with Mo loading reaching a maximum at 6 wt% Mo loading, while the reverse scenario was observed for the selectivity to aromatics. Chen et al. [39] also concluded that optimum activity for the dehydroaromatisation of methane was obtained for the catalysts with Mo loading of 2-3 wt%. Shu et al. [27] observed that methane conversion increased with molybdenum content in the range 0.1-2 wt%.

The 2 wt% Mo catalyst was found to be the most active and selective toward methane aromatisation. However, an increase in Mo loading above 2 wt% up to 5 wt% resulted in a decrease in the methane conversion. The observed decrease was attributed to the partial blockage of the zeolite channels by agglomerated molybdenum oxide species. It has also been shown that an increasing the Mo loading higher than a monolayer coverage, the interaction between the framework aluminium becomes so strong that the framework aluminium is extracted by Mo to form $Al_2(MoO_4)_3$ [37]. This extraction has also been reported for both nanosized and microsized H-ZSM-5 catalysts [26]. The formation of $Al_2(MoO_4)_3$ is said to be the main detrimental factor for methane dehydroaromatisation [26,29,37,40]. Lu et al. [41] on the other hand observed that the conversion and the selectivity to aromatics increased rapidly with increasing Mo loading up to 4 wt%, while the selectivity to coke and ethylene decreased sharply with increasing Mo loading. When the molybdenum loading was further increased above 4 wt% the activity and product selectivities remained almost unchanged with increasing Mo loading. They concluded that the high Mo loading is not a crucial factor for the destruction of the zeolite lattice, but the valence state of the Mo is.

3.3.2 Calcination temperature and duration

Although the calcination duration and temperature were discussed in the preparation of Mo/zeolite catalysts, these factors also influence the catalytic performance of the resultant catalyst. Wang and co-workers [8] showed that the conversion of methane and the aromatics selectivity decreased with increasing calcination temperature, while on the other hand the selectivity to C_2 hydrocarbons increased with an increase in the calcination temperature. It was believed that since the migration of Mo species into the channels of the zeolite was easier with increasing calcination temperature, the concentration of Mo species located in the channels may be increased by the high calcination temperature, eventually blocking the zeolite

channels. Xu et al. [33] concluded that a strong interaction between MoO_3 and the zeolite at high calcination temperatures (700^oC) caused the formation of MoO_4^{2-} species, produced from the lattice oxygen of the zeolite and Mo species leading to a sharp decrease in the catalytic performance. Tan et al. [36] concluded that calcination at 500 or 700^oC would cause the Mo species to disperse on the external surface and diffuse into the zeolite channels, whereas above 750^oC there was dealumination of the zeolite coupled with the decrease in the crystallinity. This partial destruction of the zeolite led to lower methane aromatisation activities. It has also been shown that with increasing calcination temperatures, the interaction between framework aluminium and Mo species became sufficiently strong such that all the aluminium in the framework could be extracted by Mo species to from a crystalline $Al_2(MoO_4)_3$ phase [37]. This resulted in the collapse of the zeolite framework and dramatic decrease in the catalytic activity for methane dehydroaromatisation. As already mentioned prolonging the calcination duration increased the degree of diffusion of Mo species into the zeolite channels [25,38] and the Brønsted acidity was also decreased [38]. The amount of Mo species associated with Brønsted acid sites increased with increasing calcination duration and, as a result, improved catalytic activities and stabilities were observed.

3.3.3 The effect of the pretreatment atmosphere and temperature

Wang et al. [40] observed that treatment of the Mo-Zr/H-ZSM-5 catalyst under an air atmosphere at 600^oC enhanced the catalytic activity of the catalyst. The catalysts were pretreated under air or helium stream in the temperature range of 500 to 700^oC for 30 min and then methane was introduced and the temperature increased to the required reaction temperature (700^oC). However, pretreatment of the catalysts in air at high temperatures (700^oC) led to an increase in the pore size of the catalysts and a decrease in the conversion of methane and catalyst stability. The catalytic activity and stability of Mo-Zr/H-ZSM-5 catalysts also decreased with increasing pre-

treatment temperature. Using a similar pretreatment procedure but performed only at 500°C, Lu et al. [41] also reported that better catalytic performance was obtained as compared with that resulting from a pretreatment procedure in air for 1 h at 700°C.

Zhang et al. [42,43] observed that the conversion of methane and selectivity to benzene were very low when the catalyst was pretreated in air, with a conversion of 4.7% and an aromatics selectivity of 47.5%. Pretreatment of the catalysts in hydrogen led to medium activity (8.5%) and relatively high selectivity to benzene (88.9%). When the pretreatment atmosphere was changed to methane the conversion was 9.3% and the benzene selectivity was 81.3%. The highest activity and benzene selectivity were obtained using nitrogen; the activity and benzene selectivity were dramatically enhanced from 4.9% to 10.9% and 47.5% to 90.0%, respectively, when compared with the treatment in air.

3.3.4 The effect of promoters

The activity and stability of Mo/H-ZSM-5 can also be influenced by the addition of other elements, mostly transition metal elements, though some work has also been reported on the effects of some non-transition metals [2]. Wang and co-workers [49,44] showed that the addition of tungsten into the Mo/H-ZSM-5 improved the activity and stability of the catalyst. The promotional effect was correlated with the formation of Mo-W mixed oxides [43]. Ruthenium was also found to enhance the catalytic activity and stability of Mo/H-ZSM-5 [45-47]. Shu et al. [45] suggested that ruthenium improved the performance of Mo/HZSM-5 by promoting the reducibility of Mo species in the catalyst. On the contrary, Sily et al. [46] observed a decrease in the reducibility of Mo species, and they suggested that Ru decreased the formation of heavier coke deposits, thus protecting the Mo_2C active sites.

Gallium was said to enhance the activity of Mo/H-ZSM-5 catalyst by promoting the reduction of MoO_3 particles on the surface and/or in the zeolite channels [48], while Cu acted by suppressing the reduction of Mo species and the dealumination of H-ZSM-5 support, thus maintaining the zeolite framework [49]. Zhang and co-workers showed that chromium increased the acidity of the catalyst [42], while Zn had an acidity decreasing effect [43].

Promotional effects of Al, Co, Cu, Fe, Pt, Zn and Zr have also been reported [39,50-54]. The introduction of V, Li and P on the other hand decreased the catalysts reactivity [39,53,54]. Although cobalt was shown to promote aromatisation of methane [50,52] over Mo/HZSM-5 catalysts, Burns et al. [53] did not observe such promotional effects. The addition of platinum in Mo/HZSM-5 slightly decreased the conversion of methane but improved the durability of the catalyst compared to undoped Mo/HZSM-5 [55]. Strangely, the selectivity to coke, which is believed to be the main cause of deactivation, was slightly increased in the presence of Pt. Palladium on the other hand was found to be detrimental to both activity and stability [46].

3.3.5 The effect of the reaction temperature

Xu et al. [8] observed an increase in the conversion of methane and the selectivity to aromatics increased with an increase in reaction temperature. The selectivity to C_2 hydrocarbons decreased with increasing temperature. Thermodynamic predictions suggest that the high reaction temperature is favourable for the aromatisation reaction of methane [25], which is in line with observations reported by Xu and co-workers [8]. However, Chen et al. [39] observed that if the reaction temperature was too high serious carbon deposition occurred and as a result the conversion and the selectivity to benzene both decreased.

3.3.6 Space velocity

Xu et al. [8] observed that the conversion of methane and the selectivity to aromatics decreased with increasing space velocity of methane. The selectivity to C_2 hydrocarbons and the ratio of ethylene to ethane increased with increasing space velocity. This suggested that ethylene was the initial product of the reaction and aromatics were secondary products. Similar conclusions were reached by other authors [29,39]. Ha et al. [19] on the other hand noticed that acetylene was also formed during the dehydroaromatisation reaction of methane. Upon varying the space velocity of the feed they observed that the pressure of acetylene increased with increasing space velocity, while that for ethylene and benzene decreased. From these observations they suggested that acetylene instead of ethylene was the primary product for the formation of benzene. The space velocity of methane affects the induction period of the dehydroaromatisation reaction. The lower the methane hourly space velocity, the longer was the induction period [47,56].

3.4 The active sites and the proposed mechanisms

As far as the active sites and/or reaction mechanism are concerned there are some discrepancies among the work of various researchers. In this section the processes that occurs during the induction period, the nature of the active species and the reaction mechanisms will be discussed.

3.4.1 The induction period and the formation of active sites

Wang and co-workers initially believed that MoO_3 [1] and later $MoO_{(3-x)}$ [45] were the active species involved in activating methane. Later studies indicated that there

is an induction period which exists before the initial formation of benzene [21,24,25,40]. During this induction period virtually no hydrocarbon products were formed, and the principal gas-phase products were H_2, CO, CO_2 and H_2O. Wang et al. [40] suggested that a Mo phase transformation took place at the first step of methane reaction on the catalyst, which is a prerequisite for aromatics and C_2 hydrocarbons formation and the new Mo phase formed was probably molybdenum carbide. X-ray photoelectron spectroscopy (XPS) [21,25] and X-ray absorption spectroscopy (XAS) [57] studies confirmed that during the initial induction period, methane reduced the original Mo^{6+} ions in the zeolite to Mo_2C and this was accompanied by the formation of carbonaceous deposits [25]. Jiang et al. [58] studied the induction period of methane aromatization over Mo/H-ZSM-5 using temperature programmed surface reaction (TPSR), UV laser Raman, and ^{13}C CP MAS NMR spectroscopy. They suggested that the induction period before the initial formation of benzene closely relates to the gradual reduction of Mo species and it is the Mo species in the lower valence state which may be responsible for the conversion of methane to ethylene and benzene.

Ma et al. [21] observed three regions in the TPSR of methane over Mo/H-MCM-22. The first one is from about 547 to 687 ^oC. In this region, the main products were CO_2 and H_2O, and there was no apparent formation of H_2 and CO. After that, a sharp consumption of methane accompanied by a sharp formation of CO and H_2 occurred (the second region). Benzene could only be formed at almost the end of CO_2 production stage (the third region). The first two stages were taken as the induction period of the reaction. The authors believed that these stages corresponded to the formation of MoO_2 (the first stage) and molybdenum carbide (the second stage). These two steps can be illustrated as follows:

First stage: $MoO_3 + CH_4 = MoO_2 + CO_2 + H_2O$

Second stage: $MO_2 + CH_4 = Mo_2C + CO + H_2 + CO_2 + H_2O$

The second step is said to be more rapid as compared with the first one.

Kim et al. [29] also suggested that reduction of molybdenum species occurs in two steps. The first step involves the reduction of Mo^{6+} to Mo^{4+} with the formation of sites that activate methane but which do not desorb hydrocarbon fragments, but instead retain carbon atoms from CH_4 and release hydrogen atoms as H_2. The second step is slower and it leads directly to the formation of active sites for methane conversion, but these sites form sequentially along the catalyst bed, because of inhibition of reduction/carburisation processes by the oxygen containing products of this reaction

It is generally believed that the benzene does not form until the end of the induction period. But some studies involving the use of resonance-enhanced 2-photon ionisation spectroscopy suggested that small amounts of benzene were produced during the induction period [59,60]. Although the amounts of benzene formed are negligible compared with the amount formed after the induction period, this observation may have some implications on the mechanism of reaction.

3.4.2 The nature of the active phase

As mentioned in Section 3.2.1, the exchanged $(Mo_2O_5)^{2+}$ species are the precursors to the methane activation sites in Mo/H-ZSM-5 catalysts. These species are reduced and carburised by methane during the induction period to form small MoC_x clusters (0.6-1 nm in size) [61]. Although it is generally agreed that molybdenum carbide is formed during the induction period little is known about the actual type of the carbide species that is formed. According to Bouchy et al. [62] there exist two thermodynamically stable molybdenum carbide phases, the hexagonally close

packed (hcp) β-Mo_2C and the face-centered cubic (fcc), metastable α-MoC_{1-x}. The α-MoC_{1-x} can be formed from bulk MoO_3 by activation under either hydrogen or hydrogen/butane mixture followed by carburization under methane, whereas direct carburization of MoO_3 leads to stable β-Mo_2C. In the case of supported MoO_3, carburization of the sample activated under hydrogen only yields β-Mo_2C, while the carburization of the sample activated under hydrogen/butane mixture gave α-MoC_{1-x}.

When these carbide phases are supported on H-ZSM-5 different catalytic activities were observed [62]. The fcc α-MoC_{1-x}/H-ZSM-5 gave higher conversions and better stability than the hcp β-Mo_2C/H-ZSM-5. Higher selectivities to benzene were also observed on the former catalyst. On the other hand Nagai et al. [18] suggested that η–Mo_3C_2 is the active carbide species for activating methane. The possibility of the involvement of molybdenum oxycarbides (MoO_xC_y) as the activating species has also been mentioned [12,63-66]. It has been shown that Mo^{6+} species associated with the Brønsted acid, which reside primarily inside the channels, can only be partially reduced in methane MoO_xC_y, play crucial roles in methane dehydroaromatisation [31,38,64-66]. The fcc-MoO_xC_y structure was found to be more active and stable than the hcp-MoO_xC_y [66], which is in agreement with the observations made by Bouchy et al. [62].

3.4.3 Proposed reaction mechanisms

As already mentioned earlier reports by Wang and co-workers [1,45] suggested that methane was activated by MoO_3 species and $MoO_{(3-x)}$. The mechanism proposed at the time suggested that both heterolytic splitting of methane, (via polarisation of methane by the active species) and reaction of the polarised molecule with Brønsted acid sites, and formation of carbene intermediates. These molybdenum carbene-like species then dimerised to form ethylene as the primary products. Later, they noticed that there was an induction period before the formation of benzene and they

suggested that Mo phase transformation took place at the first step of methane reaction on the catalyst and that the new molybdenum phase was probably molybdenum carbide [41]. This molybdenum carbide phase was suggested to be the active species for the activation of methane [25,40,57]. Molybdenum oxycarbides were also suggested to be the active species for methane activation [63-66]

A bifunctional mechanism was suggested [57] in which, methane aromatisation proceed at the interface of molybdenum carbide (or oxycarbide) sites to form CH_x and C_2 species which may migrate at the interface of the H-ZSM-5 acidic support, followed by dehydroaromatisation of C_2 intermediates to benzene and naphthalene, as illustrated in Scheme 3.

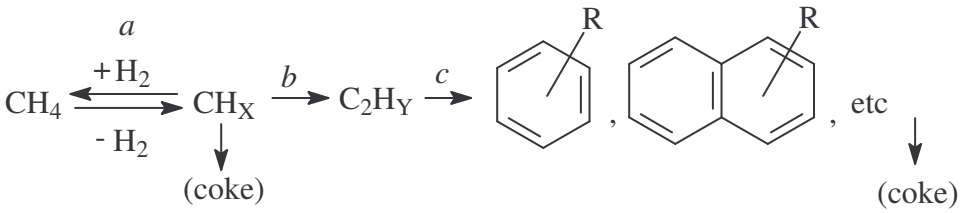

Scheme 3 A representation of the bifucntional mechanism for the dehydro-aromatisation of methane over Mo/Zeolite catalysts. *a* and *b* occur on Mo sites of carbide or oxycarbide and *c* occurs on H-ZSM-5 acid sites [57].

On the other hand Ha et al. [19] claimed that the bifunctional mechanism was less important and the primary product of the reaction was acetylene. They proposed that the reaction mechanism for the production of aromatics proceeds via either a monofunctional mechanism where acetylene, the primary product, is oligomerised on Mo_2C into polyene such as hexadiene or cyclised thermally into aromatics, or acetylene (ethylene to a less extent) is forming higher-molecular weight polyenes via a vinyl cation intermediate on Brønsted acid sites. It should be noted that acetylene

was also observed during the purging of a carburised Mo/Al-FSM16 catalyst with helium [18]. Nagai et al. [18], concluded that benzene was formed from methane through the intermediate formation of butane species while methane was converted to ethylene and propene with hydrogen formation. Consequently, methane was responsible for the pyrolytic carbons becoming conjugated to form η–Mo_3C_2 on the surface form hydrogen and benzene as illustrated in Figure 3.1:

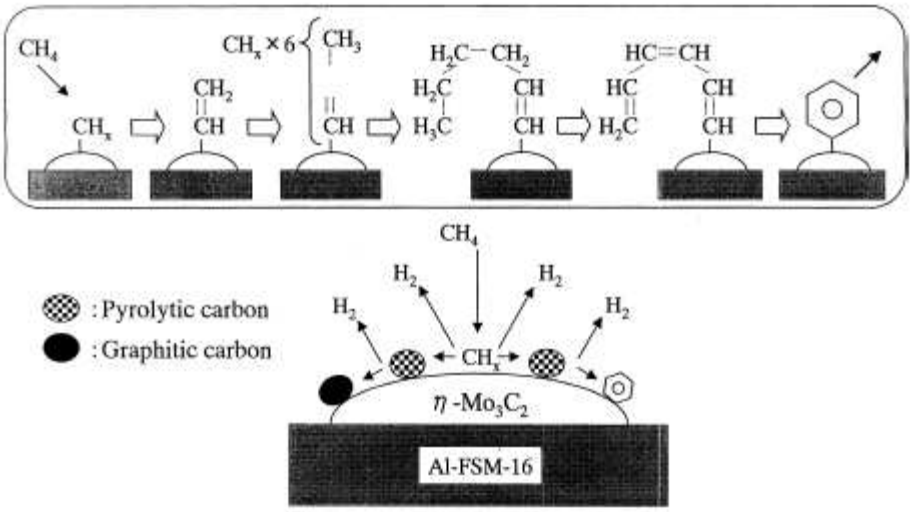

Scheme 4 Reaction scheme of benzene formation from methane overMo/Al-FSM16 at 700°C [18].

Another reaction mechanism, proposed by Chen et al. [39], suggested that methane conversion was catalysed by the molybdenum species inside the H-ZSM-5 channels together with the strong acid sites of the zeolite. This process would form $CH_3\cdot$ free radicals, which could dimerise to form ethane and ethylene easily. Then ethylene would be aromatised to benzene with the aid of protons of H-ZSM-5 zeolite as shown in Scheme 5. This mechanism was later supported by Shu and co-workers [27].

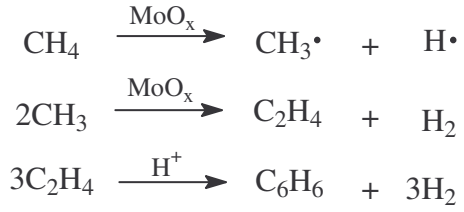

Scheme 5 A reaction mechanism for the nonoxidative dehydroaromatisation of methane over Mo/Zeolite catalyst activated via homolytic cleavage of the C-H bond [39].

Illiuta et al. [56] studied the kinetics of the nonoxidative aromatisation of methane over Ru-Mo/HZSM-5 and concluded that that the rate-determining step of the reaction was the surface dehydrogenation reaction of adsorbed methane. The activation energy was calculated to be 88.2 kJ/mol and the calculated enthalpy and entropy of methane adsorption on Mo active sites were -73.4 kJ/mol and -75.3 J/mol.K, respectively. Hassan and Sayari obtained and activation energy of about 71.8 kJ/mol over Ru-Mo/HZSM-5 catalysts [47].

Although, there are a number of mechanisms that have been suggested [2], the bifunctional mechanism involving the molybdenum carbide (or oxycarbide) species and the Brønsted and is generally more acknowledged than the other mechanisms.

3.5 The role of Brønsted acidity in methane aromatisation

The generally accepted mechanism of the methane dehydroaromatisation suggests the importance of Brønsted acidity in methane aromatisation. However, it is interesting to note that the formation of aromatic products also occurs over Mo/SiO_2 catalysts [19,63], which are not expected to have Brønsted acid sites. Furthermore, it

was also pointed out that the presence of Brønsted acid sites is not the only condition for the aromatisation of ethylene [67]. Óvári and Solymosi [68] suggested that on Mo_2C/SiO_2 catalysts, methane activation occurs on the carbide, and oligomerisation aromatization of intermediate species occurs on the Lewis acid sites. On the contrary, Liu et al. [57] showed that only the Brønsted acid sites of Mo/H-ZSM-5 were involved in the aromatisation of methane while the Lewis acid sites were not involved. Shu et al. [27] also concluded that aromatisation is promoted by Brønsted acidity and not by Lewis acid sites after observing that aromatisation could not occur when 2%Mo/Cs-ZSM-5.

Although, it is suggested that Lewis acid sites may be involved in the case of Mo/SiO_2 catalysts, Brønsted acidity is more important for zeolite supported molybdenum catalyst systems. Su et al. [64] concluded that the Brønsted acid sites are important for the dehydroaromatisation of methane over Mo/HZSM-5 catalysts under nonoxidative conditions. They also suggested Brønsted acid sites are necessary for driving Mo species into and for anchoring Mo species onto the zeolite channels. It has also been shown that the coordination mode of impregnated Mo species is also affected by the density of the Brønsted acid sites [34]. Monomeric bidentate species are formed at low Si/Al ratios and dimeric monodentate species are formed at high Si/Al ratio. Liu et al [38] showed that the MoC_x species formed from MoO_x species associated with Brønsted acid sites are more active and stable than those formed from MoO_x species non-associated with the Brønsted acid sites under the methane dehydroaromatisation reaction conditions.

One other aspect which requires attention is the question of how much Brønsted acidity is necessary in the reaction. Liu and Xu [69] concluded that about 60% of the original Brønsted acid sites on H-ZSM-5 may need to be kept free on the surface of the catalyst for good catalytic performance in methane dehydroaromatisation. Su et al. [64] concluded that there is an optimum value of the Mo(in the channels)/$[H^+]$ ratio which is equal to about 1 for H-ZSM-5 zeolites impregnated with Mo, implying

that about half of the free Brønsted acid sites will be taken up by Mo species diffusing into the channels. Only the catalysts possessing this optimum value of Mo/[H^+] can catalyse the reaction effectively and smoothly. Liu et al. [57] found that the catalysts with a SiO_2,/Al_2O_3 ratio between 20 and 70 showed maximum Brønsted acidity and the highest benzene formation rates were observed for Mo/H-ZSM-5 catalyst having a SiO_2/Al_2O_3 ratio of 40. Some studies have suggested that only a small amount of Brønsted acidity is required for the nonoxidative dehydroaromatisation of methane [67,70,71], while excessive amounts of free Brønsted acid sites caused severe deposition of carbonaceous species which deactivate the catalyst [70,71]. Regarding the strength of the Brønsted acid sites required for the methane dehydroaromatisation, Li et al. [72] concluded that the nonoxidative aromatisation of methane can proceed in the presence of only weak Brønsted acid sites. Dong et al. [52] on the other hand concluded that strong acid sites are the centre of methane aromatisation.

3.6 The nature of carbon deposited on the catalysts

Beside the gaseous products formed during the dehydroaromatisation of methane, some solid carbonaceous deposits (coke) are also produced. At 700 ^oC, about 20-40% of the converted methane is deposited on the catalysts surface as coke [73]. Since the formation of these carbonaceous deposits is said to be responsible for the deactivation of catalysts it is important to understand the nature of these carbon species. This information could be useful in developing regeneration protocols and perhaps also the methods that could minimise the formation of these species.

Weckuysen et al. [74] identified three types of surface carbonaceous species formed during the aromatisation of methane over Mo/H-ZSM-5 catalyst using XPS. With the characteristic C1s binding energies (BE), the carbon species were identified as,

the graphitic-like carbon (BE = 284.6 eV), the carbide-like carbon (BE = 282.7 eV) and the hydrogen-poor sp type or pre-graphitic carbon (BE = 283.2 eV). The graphitic-like carbon was mainly present in the zeolite channel system and the carbide-like carbon Mo_2C was mainly located at the outer surface of the zeolite, while the pre-graphitic type was also located on the outer surface of the zeolite. Since the amount of the pre-graphitic carbon increased with increasing time on stream, the authors believed that this type of carbon species gradually covers both the zeolite and the Mo_2C phase during methane reaction and is responsible for the deactivation of Mo/H-ZSM-5 catalyst. Jiang et al. [58] concluded from solid state nuclear magnetic resonance (NMR) studies, that there were two kind of carbonaceous deposits; one is located on the acid sites and the other is located on partially reduced Mo species. The latter form of carbon may be responsible for methane activation and effectively transform from carbene-like species and/or carbide species to ethylene. By using UV-Raman spectroscopy, Yuan et al. [75] concluded that the coke species deposited on Mo/HZSM-5 were moderately polymerised aromatic species. Ma et al. [76] also reported, from UV-Raman and NMR studies, that that the coke deposited on Mo/MCM-22 was hydrogen-deficient and it deposited on Brønsted acid sites. Honda et al. [77] also showed that coke accumulation predominantly occurred on the Brønsted acid sites. Very recently, Zheng et al [78] showed that the coke species were mainly aromatic carbonaceous species deposited on the Brønsted acid sites and carbidic carbon in molybdenum carbide.

Liu et al. [79] used temperature programmed methods and thermogravimetry (TG) to study the nature of carbonaceous deposits formed during methane dehydroaromatisation. Temperature programmed oxidation (TPO) profiles revealed two temperature peaks, one at about 503^{o}C and the other one at about 582^{o}C. Temperature programmed experiments revealed that H_2 could only react with the coke which is burnt of at high temperatures, while CO_2 could eliminate coke burnt-

off at both low and high temperatures. Temperature programmed reactions in CO_2 followed by H_2 were more effective in reducing the amount of coke.

3.7 Methods used for the suppression of poisonous carbonaceous species production

As already indicated, some of the carbonaceous species deposits are poisons for the catalyst used for the dehydroaromatisation of methane. In the literature, two approaches have been used to tackle the problem of catalyst deactivation during the nonoxidative methane conversion. One approach involves co-feeding methane with other components such as carbon oxides, hydrogen, steam and oxygen, while the second involves the treatment of the catalyst or the zeolite component by steam, or external surface modifications with bulky organosilane compounds.

3.7.1 The effect of feed additives

3.7.1.1 CO and CO_2

Liu et al. [80,81] were the first to report the promotional effect of CO and CO_2 in methane dehydroaromatisation over Mo/HZSM-5 catalysts. They observed that by adding CO (1.8-12%) in the feed gas, the stability of the catalyst was improved for all concentrations of CO used. In addition, the formation rates of benzene and naphthalene were almost constant during prolonged reaction of more than 50 hours. Similar promotional effects of CO on methane conversion were also reported by Osawa et al. [82] for CO concentrations from 5 to 30%. However, in this case the amount of benzene and naphthalene produced significantly increased on addition of

5 to 10% CO and it decreased at concentrations from 20 to 30%. Tan et al. [83] also indicated that the yield of aromatics increased with time on stream even when the CO concentration was 18.6% and also noticed that although deactivation occurred at a later time, it was less severe. On the other hand Bradford et al. [84] reported that CO did not influence the rates of catalyst deactivation and it remained unreacted. By using ^{13}CO and CH_4 mixture as the feed to conduct the reaction, Liu et al. [80,81] observed that carbon derived from CO dissociation was efficiently incorporated into benzene. First, CO dissociates on Mo sites to form the active carbon species which are hydrogenated to form CH_x and C_2 species (reactions (2) and (3)). This is followed by the oligomerisation of C_2 species to form higher hydrocarbons such as benzene and naphthalene on the catalyst (reaction (1)). The dissociated oxygen species [O] from CO may react with the surface inert carbon species to regenerate CO, resulting in the suppression of the coke formation on the catalyst (reactions (4) and (5)).

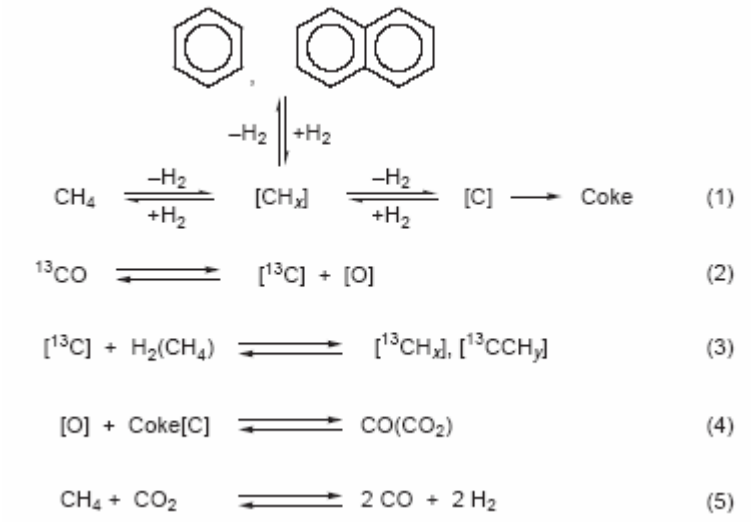

Scheme 6 Proposed mechanism for promotion by CO addition to a methane feed to improve catalyst stability and reduce coke formation on Mo/HZSM-5 [80].

The stability of the catalyst was also improved by adding a few percent CO_2 into the feed gas. Addition of 1.6% CO_2 gave higher methane conversion but benzene formation was suppressed in comparison with CO addition [80,81]. The benzene formation rates were stable during prolonged reaction. However, addition of larger amounts of CO_2 (> 10%) in the methane feed largely inhibited the formation of aromatics.

When the partial pressure of CO_2 in the feed gas was low (< 4%), twice the amount of CO was detected relative to the added CO_2 on a carbon basis, while no CO_2 was observed in the outlet stream [81]. This was attributed to the possibility of a reforming reaction occurring between methane and CO_2 ($CO_2 + CH_4 \rightarrow 2CO + 2H_2$). The formed CO was said to be responsible for the observed promotional effects. Liu et al. [85], on the other hand suggested that CO_2 increased the catalyst stability and decreased product molecular weight by scavenging CH_x species formed in methane activation steps by forming hydrogen, which inhibits deactivation and hydrocarbon synthesis rates. Osawa et al. [82] reported that the conversion of methane increased from 5 to 10% by the addition of up to 0.66% CO_2 and then decreased at greater CO_2 concentrations. The amounts of benzene were almost constant with the addition of CO_2 up to 1.4%. The addition of 5% CO_2 significantly decreased the production of benzene, while CO formation increased with an increasing amount of CO_2. Tan et al. [83] observed a decrease in the initial aromatics yield upon addition of 5.3% CO_2, but the yield later increased with time on stream and the catalyst deactivated moderately at longer time in stream. The deactivation was less drastic than that for the reaction with pure methane. Increasing the CO_2 concentration to 12.8% gave about a 40% loss in aromatics yield and when the CO_2 became excessive (18.6%), the formation rate of aromatics was completely inhibited.

From XPS studies on the used catalyst, Tan et al. [83] showed that there were two different zones in the reactor bed when CO_2 was co-fed with methane. The authors suggested the sequential existence of two reaction regions in the catalyst bed,

namely, the reforming and the aromatisation zone. The reforming zone extended over the entire catalyst at high CO_2 concentrations (18.6%), thus suppressing the formation of molybdenum carbide so that aromatisation is completely inhibited. The increased stability observed in the presence of CO_2 was attributed to the hydrogen that is produced during aromatisation.

3.7.1.2 Oxygen

Yuan et al. [75] have also shown that the addition of suitable amounts of oxygen in the methane feed is beneficial to the stability of the activity for aromatisation of methane over Mo/H-ZSM-5. However, there is a critical concentration of oxygen. This critical amount increased with the rising reaction temperature. The critical concentrations were about 0.7%, 3% and 7% at 700, 750 and 850^{o}C, respectively. If the oxygen concentration is below the critical value, the aromatisation reaction proceeds, and when the concentration is higher than the critical value, total oxidation and oxidative coupling of methane become predominant. The authors suggested that the added oxygen acts by maintaining the active phase, (possibly as MoO_xC_y/H-ZSM-5) and by removing part of the coke species, hence improving the lifetime of the catalyst. Tan et al. [83] also studied the effect of O_2 and NO on the aromatisation of methane over Mo/HZSM-5 catalysts. From this study they concluded that with a suitable amount of oxygen (< 5.3%) or nitric oxide (> 9.1%) in the feed, the catalyst stability was improved (could last for more than 6 hours). Since at a concentration of lower than 5.3% there was complete oxygen conversion, the improved stability was attributed to H_2 and CO generated during the reaction.

In the presence of these oxidants, three regions were formed in the catalyst bed, namely, the methane oxidation, methane reforming, and methane aromatisation region [83]. However, with a rise in oxygen or oxygen concentration above the critical values, the aromatisation region disappeared and CO and CO_2 were the

predominant carbon-containing products. Osawa et al. [82] reported that the addition of small amounts of oxygen (0.49%) increased the amount of benzene produced. The addition of more than 0.49% of oxygen decreased the conversion of methane, while increasing the amount of CO produced.

3.7.1.3 Hydrogen and water

Ma and co-workers [86] studied the effect of adding small amounts of hydrogen to the methane feed. Their results indicated that in the presence of small amounts (3-6%) of hydrogen in the feed the catalyst stability was greatly increased. It was concluded that adding hydrogen in the feed was an effective method for suppressing coke formation on the catalyst, especially coke formed on the Brønsted acid sites.

Osawa et al. [82] observed that the addition of hydrogen did not affect the conversion of methane and the aromatic compounds produced, but improved the lifetime of the catalyst. It was postulated that the addition of hydrogen prevented catalyst deactivation by reducing the surface carbon. Liu et al. [85] observed that the conversion of methane and the benzene formation rates decreased when 3% hydrogen was present. The product selectivity was, however, not strongly influenced by the addition of hydrogen in the feed. This inhibition of methane aromatisation reaction by hydrogen is consistent with the expected thermodynamic effects of hydrogen on the reaction: $6CH_4 \rightarrow C_6H_6 + 9H_2$.

Liu et al. [87] studied the effect of water in the catalytic performance of Mo/HZSM-5 catalysts in methane dehydroaromatisation. They observed that the addition of small amounts of water to the methane feed promotes benzene and hydrogen production, and significantly improved the stability of the catalyst. It was suggested that in the presence of water, a reforming type of reaction was proceeding to remove coke to form extra CO and H_2, which in turn reacted with the coke. Although the

amount of coke decreased with increasing water concentration, this was followed by a sudden drop in catalytic activity after several hours on stream when the water concentration in the feed was high (at about 2.6%). This was attributed to the migration of aluminium out of the framework to extraframework positions at a water concentration of 2.6%. Ma et al. [88] recently studied the effect of co-addition of hydrogen and water into the methane feed, and they observed that coke was suppressed more effectively than in the reaction with the individual additives. Much more stable methane dehydroaromatisation performance was obtained and higher hydrogen formation rates were also obtained. Furthermore, the destruction of the catalyst by steam dealumination during the reaction was also suppressed by hydrogen. Tan et al. [83] observed that the addition of hydrogen in the feed suppressed methane conversion and the aromatics yield, but increased the selectivity to C_2-hydrocarbons and the C_2H_4/C_2H_6 ratio. On the other hand, the stability of the catalyst improved although the results were not as good as in the case with the use of CO.

3.7.2 Catalyst modifying methods

In the previous section the promotional effects of co-feeding methane with CO, CO_2 O_2 and H_2 were discussed. However, using oxidative co-fed material increases the complexity of the reaction requirements and at the same time enhances the cost of commercialisation of the reaction [73]. Other methods that could improve the stability of the catalyst are discussed below.

3.7.2.1 Steam treatment

Lu et al. [70,73] have shown that dealuminating H-ZSM-5, by steam-treatment, before impregnation with ammonium heptamolybdate solutions improved the

catalytic performance of the resulting Mo/H-ZSM-5 catalysts. Higher benzene yields and lower coke selectivities were obtained over the dealuminated samples as compared with the parent catalyst systems. It was concluded that suitable dealumination of the zeolite will benefit aromatics formation and coke suppression and, as a result, will benefit the stability of the catalysts. Furthermore, it was suggested that only a relatively small amount of Brønsted sites is necessary for Mo/H-ZSM-5 to be effective in methane aromatisation, while superfluous Brønsted acid sites facilitated the holding of coking precursors for a longer time on the surface, which allows for the further polymerisation reactions of these precursors, thus largely increasing the aromatic-type carbonaceous deposition. Removal of these unnecessary Brønsted acid sites by steam dealumination leads to an efficient and effective suppression of aromatic coke in the reaction. Therefore, a much higher benzene yield and much longer durability of the catalysts are obtained when compared with conventional Mo/H-ZSM-5 catalysts [70]. On the other hand Wang et al. [44,89] studied the effect of the post-steam treatment of Mo/H-ZSM-5 catalyst on their catalytic properties. The results obtained indicated that post-steam treatment did not change the chemical composition of the catalyst but assisted in the migration of Mo species into the channels of H-ZSM-5 zeolite, leading to fewer free Brönsted acid sites per unit cell. The treated catalyst showed higher aromatics selectivities as compared to the untreated catalyst. Moreover, the catalyst durability was enhanced by post-steam treatment. It should be noted that a portion of the aluminium species in the framework were extracted after the steam treatment of Mo/H-ZSM-5.

Dong et al. [90] showed that the thermal treatment of H-ZSM-5 in nitrogen improved the benzene yield of Mo/H-ZSM-5 and inhibited coke formation during methane dehydroaromatisation. This improvement was due to the fact that thermal treatment in nitrogen could eliminate excess strong acid sites, usually responsible for the formation of coke during methane dehydroaromatisation. It should be noted that although the authors referred to the treatment as a N_2 thermal treatment, the actual

treatment involved the calcination of NH_4-ZSM-5 in 2%H_2O/steam at 500^oC for 6 hours followed by calcination in dry nitrogen at 600^oC for another 6 hours.

3.7.2.2 Selective poisoning of the external Brønsted acid sites

An alternative approach to these steam treatment methods is selective poisoning of the external acid sites, which are not restricted by the zeolite pore structure, by silanation using bulky organosilane compounds. Ding et al. [91] studied the effect of silanation of the external acid sites, using the chemical liquid deposition method, on the catalytic behaviour of Mo/H-ZSM-5 catalysts. They observed that silanation decreased the density of the external acid sites, as expected. The selective removal of external OH groups improved the efficiency and completeness of the MoO_x exchange onto the intrachannel acid sites and therefore the resulting MoC_x of the carburisation reaction of exchanged MoO_x species were located in the zeolite channels. Higher methane conversion levels and selectivities to benzene were obtained over the silanated Mo/H-ZSM-5 catalyst. Furthermore, lower selectivities to naphthalene and heavier products were obtained on this catalyst. X-ray absorption studies showed that silanation of external OH groups does not influence the structure of the active MoC_x species formed during methane reactions. Liu et al. [71] used the method of chemical vapour deposition of tetraethylsilane to passivate the external acid site of H-ZSM-5 used in preparing Mo/H-ZSM-5 catalysts. The results obtained indicated that the catalytic performance of the silanated Mo/H-ZSM-5 catalyst was much better than that over the conventional Mo/H-ZSM-5 catalyst. The deactivation rate constant was smaller on the silanated Mo/H-ZSM-5 catalyst than on the untreated catalyst. The number of Brønsted acid sites per unit cell of the treated catalyst was lower than that of the untreated catalyst suggesting that the concentration of Brønsted acid sites per unit cell needed in the oligomerisation, cyclisation and aromatisation of the active intermediates is quite small. Kikuchi et al. [92] also showed that the silanation greatly improved the selectivity to benzene

and the stability of the catalyst due to the effective suppression of naphthalene formation. The silanation treatment was only effective when the Brønsted acid sites on H-ZSM-5 were reacted with a limited amount of the bulky compounds that have a base group (e.g., and amino group) and an imidazole group in their molecules. Furthermore, the surface of the zeolite can be modified with a small amount of the silyl compounds, but excess doping of the silyl compounds by 0.75-2.5% SiO_2 may form thicker films of silica, which block the external pore of H-ZSM-5, reducing the external aperture size.

Wu et al. [93] reported the effects of modifying the external surface of the zeolite by large organometallic complexes on the catalytic activities of Mo/H-ZSM-5 catalysts for methane aromatisation. Their results showed that modifying the external surface of H-ZSM-5 increased the yield of benzene while that of naphthalene was decreased. In addition the selectivity to coke was also decreased by this modification. These observations were ascribed to the fact that upon modification of the external surface of the zeolite, the acid site density on the external surface of H-ZSM-5 is reduced as is the number of MoO_x species deposited at such surfaces. As a result, in the case of the modified H-ZSM-5, MoO_x species are mostly formed in the channels of the zeolite due to lack of external acid sites. Hence, the formation rates of coke and naphthalene are low, and the selectivity to benzene is higher.

3.8 Methane dehydroaromatisation over W/H-ZSM-5 catalysts

As already indicated in Section 3.1, tungsten is one of the promising active components of catalyst for the dehydroaromatisation of methane in the absence of oxygen. The fact that thermodynamics favours benzene formation with increasing temperature and the fact that tungsten is thermally stable at high temperatures makes tungsten the element of choice. Therefore, in this section the results that have been

reported on the use of W/H-ZSM-5 catalysts will be summarised. Zeng and co-workers [9] showed that W-H_2SO_4/H-ZSM-5 prepared from a H_2SO_4-acidified solution of ammonium tungstate (pH = 2-3) exhibited high methane dehydro-aromatisation activities. On the other hand, W/H-ZSM-5 catalyst prepared from alkaline or neutral solutions of ammonium tungstate showed a much lesser activity for the dehydroaromatisation reaction. The better activity observed for the acidified W/H-ZSM-5 was attributed to the formation of $(WO_6)^{n-}$ groups with an octahedral coordination as the precursor of the catalytically active species. These $(WO_6)^{n-}$ species are more reducible than the tetrahedrally coordinated $(WO_4)^{2-}$ ions formed with neutral or alkaline impregnation solutions.

The addition of Zn, Mn, Zr, Li or La, was found to markedly improve the activity and stability of the W-H_2SO_4/H-ZSM-5 catalyst for the nonoxidative aromatisation of methane [9,10]. These catalysts were also able to operate under a reaction temperature of 800^oC and gain about twice the activity obtained over Mo/H-ZSM-5 catalyst operating at 700^oC. At 700^oC, these catalysts are capable of showing activities similar to that of Mo/H-ZSM-5. Furthermore, the high reaction temperatures did not lead to the loss of the W component by sublimation, while this was the case with Mo/HZSM-5 catalysts. It was found that doping with Zn or Li resulted in elimination of a large amount of strong surface Brønsted acid sites, which tended to lead to coke formation, and simultaneous generation of new medium-strong acid sites [10]. The reducibility of the W^{n+} species was also improved.

Ding et al. [98] studied the structure of W/H-ZSM-5 catalysts prepared by sublimation of WCl_6 at 400^oC followed by hydrolysis at 250^oC. Their isotopic exchange studies showed that each W^{6+} replaced two Brønsted acid sites to form $(WO_2)^{2+}$ cations interacting with two exchange sites as illustrated by Scheme 2 for Mo species. These species were carburised during the early stages of the induction period to form WC_x clusters (~ 0.6 nm diameter). The formed WC_x species activated the C-H bond in methane to form initial C-C bonds in products, and oligomerisation,

cracking, and cyclisation of alkene then occurred on the Brønsted acid sites aided by WC_x species that removed H-atoms. The induction periods of the reaction are significantly longer than on Mo/HZSM-5 as a result of the slower reduction and carburisation of isolated WO_x species, compared with $(Mo_2O_5)^{2+}$ dimers during methane reactions. This is in line with the suggestion by Zeng and co-workers [10] who indicated that high temperatures were required for the reductive activation of the catalyst precursor. On the contrary Yang et al. [95] concluded that in the case of a W/H-ZSM-5 catalyst prepared by impregnation, then W^{4+} oxide was probably the active site for the activation of methane.

3.9 An overview of the nonoxidative conversion of methane

Methane has been successfully activated and aromatised on molybdenum-zeolite catalysts. Zeolites with a two-dimensional structure and pore sizes near the kinetic diameter of benzene are the best supports for the active metal species. Mo, Re and W are said to be the most active metal species for the catalysts used for nonoxidative methane dehydroaromatisation. The preferred zeolites for this purpose were found to be ZSM-5 and MCM-22. The MCM-22-based catalysts are attractive because of the high selectivity to benzene, low selectivity to naphthalene and the better catalytic stability for longer periods of time as compared to the ZSM-5-based catalysts. The better catalytic stability and selectivity in MCM-22-based catalysts is attributed to the unique channel system found in this zeolite, as described in Section 3.1.

Two main methods for the preparing of Mo-Zeolite catalyst were described in Section 3.2. The factors affecting the catalytic performance of Mo/ZSM-5 have been established and they are that low Mo loading between 2-3 wt% gives the best catalytic performance while calcination temperatures between 500 and 600^{o}C are recommended. There is no clear consensus on which is the best atmosphere for pre-

treating the catalyst before the reaction. The best catalytic activities were obtained in nitrogen. Promotional effects were observed with the addition of Al, Co, Cu, Fe, Ga Ru Pt, W, Zn and Zr, while V, Li, P, Pt and Pd decreased the catalytic activity of the catalyst. The conversion tends to increase with increasing reaction temperature as expected but very high temperatures favour the formation of carbonaceous coke which deactivates the catalyst.

The mechanisms of reaction have also been studied and it is generally accepted that methane is activated via a bifunctional mechanism. In this mechanism, methane is activated on molybdenum carbide (or oxycarbide) to form ethylene (the primary product) which is subsequently aromatised on the Brønsted acid sites of the zeolite to benzene as described in Section 3.4. In the process of reaction carbonaceous coke is formed and it is one of the main factors that contribute to deactivation. Three forms of carbon species were identified on used catalyst. They are the carbidic carbon, graphitic carbon and the hydrogen-poor sp-type carbon. It has also been established that the poisonous carbonaceous coke is mainly aromatic in nature (Section 3.6). This coke predominantly accumulated on the Brønsted acid sites.

It was found that co-feeding methane with small amounts of gases such as CO, CO_2, O_2 and H_2 was effective in reducing the deactivating effects of coke, thus improving the catalytic stabilities. Pretreatment of the catalysts with steam or bulky organosilanes also improved the activity and stability of the catalysts.

As an alternative for using molybdenum, tungsten-based catalysts have also been considered. The tungsten-based catalysts have the advantage of being immune to sublimation at high temperatures as opposed to molybdenum-based catalysts. This advantage gives more room for increasing the conversion of methane by operating at higher temperatures.

3.10 References

[46] L. Wang, L. Tao, M. Xie, G. Xu, J. Huang and Y. Xu, *Catal. Lett.*, **21** (1993) 35-41.

[47] Y. Xu and L. Lin, *Appl. Catal.*, **188** (1999) 53-67.

[48] Y. Xu, X. Bao and L. Lin, *J. Catal.*, **216** (2003) 386-395.

[49] Y. Shu and M. Ichikawa, *Catal. Today*, **71** (2001) 55-67.

[50] T.V. Choudhary, E. Aksoylu and D.W. Goodman, *Catal. Rev.*, **45** (2003) 151-203.

[51] B.M. Weckuysen, D. Wang, M.P. Rosynek and J.H. Lunsford, *J. Catal.*, **175** (1998) 338-346.

[52] L. Wang, R. Ohnishi and M. Ichikawa, *Catal. Lett.*, **62** (1999) 29-33.

[53] L. Wang, R. Ohnishi and M. Ichikawa, *J. Catal.*, **190** (2000) 276-283.

[54] J.-L. Zeng, Z.-T. Xiong, H.-B. Zhang, G.-D. Lin and K.R. Tsai, *Catal. Lett.*, **53** (1998) 119-124.

[55] Z.-T. Xiong, L.-L. Chen, H.-B. Zhang, J.-L. Zeng and G.-D. Lin, *Catal. Lett.*, **74** (2001) 227-239.

[56] C.-L. Zhang, S. Li, Y. Yuan, W.-X. Zhang, T.-H. Wu and L.-W. Lin, *Catal. Lett.*, **56** (1998) 207-213.

[57] Y. Shu, D. Ma, L. Xu, Y. Xu and X. Bao, *Catal. Lett.*, **70** (2000) 67-73.

[58] D.Y. Wang, Q.B. Kan, N. Xu, P. Wu and T.H. Wu, *Catal. Today*, **93-95** (2004) 75-80.

[59] A. Martínez, E. Peris and G. Sastre, *Catal. Today*, **107-108** (2005) 676-684.

[60] P. Wu, Q. Kan, D. Wang, H. Xing, M. Jia and T. Wu, *Catal. Commun.*, **6** (2005) 449-454.

[61] Y. Shu, D. Ma, X. Liu, X. Han, Y. Xu and X. Bao, *J. Phys. Chem. B*, **104** (2000) 8245-8249.

[62] Y. Shu, D. Ma, X. Bao and Y. Xu, *Catal. Lett.*, **66** (2000) 161-167.

[63] M. Nagai, T. Nishibayashi and S. Omi, *Appl. Catal., A*, **253** (2003) 101-112.

[64] V.T.T. Ha, L.V. Meriaudeau and C. Naccache, *J. Mol. Catal. A: Chem.*, **181** (2002) 283-290.

[65] Y. Shu, R. Ohnishi and M. Ichikawa, *Appl. Catal., A*, **252** (2003) 315-329.

[66] D. Ma, Y. Shu, M. Cheng, Y. Xu and X. Bao., *J. Catal.*, **194** (2000) 105-114.

[67] J. Bai, S. Liu, S. Xie, L. Xu and L. Lin, *Catal. Lett.*, **90** (2003) 123-130.

[68] W. Liu, Y. Xu, S.-T. Wong J. Qiu and N. Yang, *J. Mol. Catal. A: Chem*, **120** (1997) 257-265.

[69] F. Solymosi, J. Cserényi, T. Bánsági and A. Oszkó, *J. Catal.*, **165** (1997) 150-161.

[70] D. Wang, J.H. Lunsford and M.P. Rosynek, *J. Catal.*, **169** (1997) 347-358.

[71] W. Zhang, D. Ma, X. Han, X Bao, X. Guo, X. Wang, *J. Catal.*, **188** (1999) 393-402.

[72] J. Shu, A. Adnot and B.P.A. Grandjean, *Ind. Eng. Chem. Res.*, **38** (1999) 3860-3867.

[73] R.W. Borry III, Y.H. Kim, A. Huffsmith, J.A. Reimer and E. Iglesia, *J. Phys. Chem. B*, **103** (1999) 5787-5796.

[74] Y.-H. Kim, R.W. Borry III and E. Iglesia, *Microporous and Mesoporous Mater.*, **35-36** (2000) 495-509.

[75] L. Chen, J. Jin, H.C. Zeng and K.L. Tan, *Catal. Commun.*, **2** (2001) 201-206.

[76] B. Li, S. Li, N. Li, H. Chen, W. Zhang, X. Bao and B. Lin, *Microporous and Microporous Mater.*, **88** (2006) 244-253.

[77] A.L. Agudo, A. Benitez, J.L.G. Fierro, J.M. Palacios, J. Neira and R. Cid, *J. Chem. Soc. Faraday Trans.*, **88** (1992) 385-390.

[78] Y. Xu, Y. Shu, S. Liu, J. Huang and X. Guo, *Catal. Lett.*, **35** (1995) 233-243.

[79] J.-P. Tessonnier, B. Louis, S. Walspurger, J. Sommer, M.-J. Ledoux and C. Pham-Huu, *J. Phys. Chem. B*, **110** (2006) 10390-10395.

[80] D. Ma, Q. Zhu, Z. Wu, D. Zhou, Y. Shu, Q. Xin, Y. Xu and X. Bao, *Phys. Chem. Chem. Phys.*, **7** (2005) 3102-3109.

[81] P.L. Tan, Y.L. Leung, S.Y. Lai and C.T. Au, *Appl. Catal., A*, **228** (2002) 115-125.

[82] W. Liu, Y. Xu, S.-T. Wong, L. Wang, J. Qiu and N. Yang, *J. Mol. Catal. A: Chem.*, **120** (1997) 257-265.

[83] H. Liu, W. Shen, X. Bao and Y. Xu, *Appl. Catal., A*, **295** (2005) 79-88.

[84] L. Chen, L. Lin, Z. Xu, X. Li and T. Zhang, *J. Catal.*, **157** (1995) 190-200.

[85] L. Wang, Y. Xu, S.-T. Wong, W. Cui, X. Guo, *Appl. Catal., A*, **152** (1997) 173-182.

[86] Y. Lu, Z. Xu, Z. Tian, T. Zhang and L. Lin, *Catal. Lett.*, **62** (1999) 215-220.

[87] Y. Zhang, D. Wang, J. Fei and X. Zheng, *Aust. J. Chem.,* **55** (2002) 531-531.

[88] Y Zhang, D. Wang, J. Fei and X. Zheng, *React. Kinet. Catal. Lett*., **74** (2001) 151-161.

[89] H. Wang, L. Su, J. Zhuang, D. Tan, Y. Xu and X. Bao, *J. Phys. Chem. B*, **107** (2003) 12964-12972.

[90] Y. Shu, Y. Xu, S.-T. Wong, L. Wang and X. Guo, *J. Catal.*, **170** (1997) 11-19.

[91] P.D. Sily, F.B. Noronha, F.B. Passos, *J. Nat. Gas Chem.*, **15** (2006) 82-86.

[92] H. Hassan and A. Sayari, *Appl. Catal., A,* **297** (2006) 159-164.

[93] S. Tang, H. Chen, J. Lin and K.L. Tan, *Catal. Commun.*, **2** (2001) 31-35.

[94] S. Li, C. Zhang, Q. Kan, D. Wang, T. Wu, and L. Lin, *Appl. Catal., A*, **187** (1999) 199-206.

[95] S. Liu, Q. Dong, R. Ohnishi and M. Ichikawa, *Chem. Commun*., (1997) 1455-1456.

[96] B. Liu, Y. Yang and A Sayari, *Appl. Catal., A*, **214** (2001) 95-102.

[97] Q. Dong, X. Zhao, J. Wang, M. Ichikawa, *J. Nat. Gas Chem.*, **13** (2004) 36-40.

[98] S. Burns, J.S.J. Hargreaves, P. Pal, K.M. Parida and S. Parija, *Catal. Today,* **114** (2006) 383-387.

[99] S. Burns, J.S.J. Hargreaves, P. Pal, K.M. Parida and S. Parija, *J. Mol. Catal. A: Chem.*, **245** (2006) 141-146.

[100] T. Pinglian, X. Zhusheng, Z. Tao, C. Laiyuan and L. Liwu, *React. Kinet. Catal. Lett.*, **61** (1997) 391-396.

[101] M.C. Illiuta, I. Illiuta, B.P.A. Grandjean and F. Larachi, *Ind. Eng. Chem. Res.*, **42** (2003) 3203-3209.

[102] S. Liu, L. Wang, R. Ohnishi and M. Ichikawa, *J. Catal.*, **181** (1999) 175-188.

[103] H. Jiang, L. Wang, W. Cui and Y. Xu, *Catal. Lett.*, **57** (1999) 95-102.

[104] L. Men, L. Zhang, Y. Xie, Z. Liu, J. Bai, G. Sha and J. Xie, *Chem. Commun.*, **18** (2001) 1750-1751.

[105] Y. Xie, B. Wang, L. Wang and J. Bai, *React. Kinet. Catal. Lett.*, **83** (2004) 99-103.

[106] W. Ding, S. Li, G.D. Meitzner and E. Iglesia, *J. Phys. Chem. B*, **105** (2002) 506-513.

[107] C. Bouchy, I. Schmidt, J.R. Anderson, C.J.H. Jacobsen, E.G. Derouane and S.B. Derouane-Abd Hamid, *J. Mol. Catal. A: Chem.*, **163** (2000) 283-296.

[108] F. Solymosi, A. Szöke and J. Scerenyi, *Catal. Lett.*, **39** (1996) 157-161.

[109] L. Su, Y. Xu and X. Bao, *J. Nat. Gas Chem.*, **11** (2002) 18-27.

[110] H. Liu, W. Shen, X. Bao and Y. Xu, *J. Mol. Catal. A: Chem.*, **244** (2006) 229-236.

[111] H. Liu, X. Bao and Y. Xu, *J. Catal.*, **239** (2006) 441-450.

[112] P. Mériaudeau, V.T.T. Ha and L. Van Tiep, *Catal. Lett*., **64** (2000) 49-51.

[113] L. Óvári and F. Solymosi, *J. Mol. Catal. A: Chem.*, 207 (2004) 35-40

[114] W. Liu and Y. Xu, *J. Catal.*, **185** (1999) 386-392.

[115] D. Ma, Y. Lu, L. Su, Z. Xu, Z. Tian, Y. Xu, L. Lin and X. Bao, *J. Phys. Chem. B*, **106** (2002) 8524-8530.

[116] H. Liu, Y. Li, W. Shen, X. Bao, Y. Xu, *Catal. Today*, **93-95** (2004) 65-73.

[117] S. Li, D. Ma, Q. Kan, P. Wu, Y. Peng, C. Zhang, M. Li, Y. Fu, J. Shen, T. Wu and X. Bao, *React. Kinet. Catal. Lett.*, **70** (2000) 349-356.

[118] Y. Lu D. Ma, Z. Xu, Z. Tian, X. Bao and L. Lin, *Chem. Commun*., (2001) 2048-2049.

[119] B.M. Weckuysen, M.P. Rosynek and J.H. Lunsford, *Catal. Lett*., **52** (1998) 31-36.

[120] S. Yuan, J. Li, Z. Hao, Z. Feng, Q. Xin, P. Ying and C. Li, *Catal. Lett.*, **63** (1999) 73-77.

[121] D. Ma, Y. Shu, X. Han, X. Liu, Y. Xu and X. Bao, *J. Phys. Chem. B*, **105** (2001) 1786-1793.

[122] K. Honda, X. Chen and Z.-G Zhang, *Catal. Commun.,* **5** (2004) 557-561.

[123] H. Zheng, D. Ma, X. Liu, W. Zhang, X. Han, Y. Xu and X. Bao, *Catal. Lett.*, **111** (2006) 111-114.

[124] H. Liu, T. Li, B. Tian and Y. Xu, *Appl. Catal., A*, **213** (2001) 103-112.

[125] S. Liu, Q. Dong, R. Ohnishi and M. Ichikawa, *Chem. Commun.*, (1998) 1217-1218.

[126] R. Ohnishi, S. Liu, Q. Dong, L. Wang and M. Ichikawa, *J. Catal.*, **182** (1999) 92-103.

[127] T. Osawa, I. Nakamo and O. Takayasu, *Catal. Lett.*, **86** (2003) 57-62.

[128] P.L. Tan, Y.L. Leung, S.Y. Lai and C.T. Au, *Catal. Lett.*, **78** (2002) 251-258.

[129] M.C.J. Bradford, M. Te, M. Konduru and D.X. Fuentes, *Appl. Catal., A*, **266** (2004) 55-66.

[130] Z. Liu, M.A. Nutt and E. Iglesia, *Catal. Lett.*, **81** (2002) 271-279.

[131] H. Ma, R. Ohnishi and M. Ichikawa, *Catal. Lett.*, **89** (2003) 143-146.

[132] S. Liu, R. Ohnishi and M. Ichikawa, *J. Catal.*, **220** (2003)57-65.

[133] H. Ma, R. Kojima, S. Kikuchi and M. Ichikawa, *Catal. Lett.*, **104** (2005) 63-66.

[134] H. Wang, G. Hu, H. Lei, Y. Xu, and X. Bao, *Catal. Lett.*, **89** (2003) 75-79

[135] X. Dong, Y. Song and W. Lin, *Catal. Commun.*, **7** (2006) 741-744.

[136] W. Ding, G.D. Meitzner and E. Iglesia*, J. Catal.*, **206** (2002) 14-22.

[137] K. Kikuchi, R. Kojima, H. Ma, J. Bai and M. Ichikawa, *J. Catal.*, **242** (2006) 349-356.

[138] P. Wu, Q. Kan, X. Wang, D. Wang, H. Xing, P. Yang and T. Wu, *Appl. Catal.*, A, **282** (2005) 39-44.

[139] W. Ding, G.D. Meitzner, D.O. Marler and E. Iglesia, *J. Phys. Chem. B*, **105** (2001) 3928-3936.

[140] Y. Yang, F. Deng, M. Zhang, Q. Luo and C. Ye, *J. Mol. Catal. A: Chem*, **202** (2003) 239-246.

Chapter 4

The aromatisation of propane

As mentioned in Chapter 1, there is a need for alternative sources of energy and chemical feed stocks as a measure against a possible drought in crude oil reserves. Since light alkanes such as methane, ethane, propane and butane are available in natural gas (NG) and liquefied petroleum gas (LPG) and their production exceeds their use, these light alkanes are potential feedstocks for the production of fuel and useful chemical products. A foundation for the production of aromatics from light alkanes was laid out by the early works of Csicsery in 1970, using Pt/Al_2O_3 catalysts [1-4]. However, the Pt/Al_2O_3 catalyst also exhibited high activity for hydrogenolysis and unrestricted condensation reactions leading to coke. These problems were

circumvented by using H-ZSM-5, which is applied in the M2-forming process (by Mobil) [5]. Unfortunately, the substantial cracking activity of unmodified H-ZSM-5 leads to a large selectivity for C_1 and C_2 products. This problem is overcome by adding additional dehydrogenation functions in the form of extra-framework species like Ga, Zn and Pt [6]. The elevated hydrogenolysis activity of Pt-based catalysts and the volatility of Zn species in H_2 at higher temperatures, has led to the identification of Ga/H-ZSM-5 catalysts as a commercially viable choice and this led to the development of the Cyclar process (by BP and UOP).

The aromatisation of propane has received considerable attention and has been comprehensively reviewed [7-11]. This chapter summarises some of the important observations from the aromatisation of propane over Ga/ZSM-5 catalysts. A brief summary of the results of the aromatisation of propane over Mo-based catalysts is also included since the Mo/H-ZSM-5 catalysts are used in this thesis.

4.1 Propane aromatisation over Ga-based ZSM-5 type zeolites

The introduction of gallium species into the ZSM-5 zeolite has been achieved using various methods. These methods include the hydrothermal synthesis of gallosilicates [12-15] with a ZSM-5 topology, chemical vapour deposition (CVD) using $GaCl_3$ or $Ga(CH_3)_3$ [16-21], solid-state ion exchange with physical mixtures of Ga_2O_3 [22-26], impregnation and ion exchange with solutions of gallium salts [23,25,27-29]. During solid-state ion exchange, gallium cations can be transferred to ion exchange positions in a zeolite, while solution ion exchange and impregnation of the gallium species are mostly deposited on the external surface of the zeolite crystallites [15,19,29]. This is because the hydrated gallium cations are too large and cannot enter the channels of the ZSM-5 zeolite during impregnation or ion exchange.

Whatever the mode of introduction, gallium can have a beneficial effect on the rate and selectivity of alkane aromatisation [11]. All these modes of introduction yield practically always the same type of Ga species after calcination. Bayense and van Hooff [23] also showed that the introduction of gallium into H-ZSM-5 by impregnation, ion-exchange, physical mixing or partial isomorphous substitution has a small effect on the effect on the activity of aluminosilicates in propane conversion and in all cases resulted in strongly enhanced aromatics selectivity.

4.1.1 The effect of hydrogen pretreatment

Kanazirev et al. [30] have demonstrated that pretreatment of the Ga/H-ZSM-5 catalysts (prepared by mechanical mixing of H-ZSM-5 and Mo_2O_3) in hydrogen at elevated temperatures resulted in a significant improvement in the catalytic aromatisation of propane. Similar observations were also reported in other studies [26,31]. Price and Kanazirev [22] established that the intimacy of a Ga_2O_3/H-ZSM-5 mixture, the partial pressure of hydrogen, temperature and heating rate along with zeolite acidity are all important factors which influence reduction of the catalysts. Price and Kanazirev [22] suggested the following reaction equation represents the migration of the gallium into the exchange sites of the zeolite during reduction.

$$Ga_2O_3 + 2H^+Z^- \rightarrow 2Ga^+Z^- + 3H_2O \qquad (1)$$

where Z^- represents the anionic zeolite framework

In the case of the catalysts prepared by impregnation and solution ion-exchange, the gallium species migrate from the external surface of the zeolite crystallites into the channels during the reduction treatment where reaction (1) occurs [24,26,28,31].

The reduction reaction (1) can also occur in propane, since the conversion of propane produces hydrogen [25,31].

Although it is acknowledged that during the reduction pretreatment step the gallium species migrate to the exchange sites of the zeolite, the exact nature of the gallium species remains a matter of debate. Kanarirev and co-workers [22,32,33] concluded that the active state of Ga formed through hydrogen reduction of Ga/H-ZSM-5 catalysts is probably Ga^{+} stabilised in the interior of the zeolite crystallite. Similar conclusions were reached by Abdul Hamid et al. [29]. It was also indicated [29] that Ga^{+} species are reoxidised to Ga^{3+} during regeneration. However, Kazansky et al. [32] noted that cooling of a reduced sample in molecular hydrogen leads to the formation of gallium hydride species that compensates the negative charge of the framework and also proposed that oxidation of the Ga^{+} ions does not proceed via traces of water but by the oxidative addition of hydrogen giving tervalent gallium hydride species. Southward et al. [25] concluded, from DRIFTS studies, that the activation of Ga_2O_3-based aromatisation catalysts is achieved by reduction of Ga_2O_3, leading to the formation of Ga_2O which migrates into the zeolite pores to react with Brønsted acid sites. Kwak and Sachtler [17] concluded that at high loading of Ga, the formation of gallyl ions, $(GaO)^{+}$, prevails and each $(GaO)^{+}$ replaces one zeolite proton, which results in a linear decrease in acidity with Ga loading.

On the other hand, *in-situ* X-ray absorption studies showed that the reduced Ga species consisted of monomeric Ga^{+} compounds and that the reoxidation of reduced species to Ga^{3+} species occurred upon cooling to room temperature even in H_2 or propane [34]. However, this reoxidation cannot occur when all the protonic sites are exchanged by Ga^{+}. Biscardi and Iglesia [35] suggested that the steady-state-product of the reduced gallium is neutral [GaOH] species is stabilised by interaction with basic oxygens within ZSM-5 channels. They then suggested, a reduction-oxidation mechanism for the desorption of H-atoms as H_2 during catalytic reactions of propane on Ga/HZSM-5, as shown in Scheme 1:

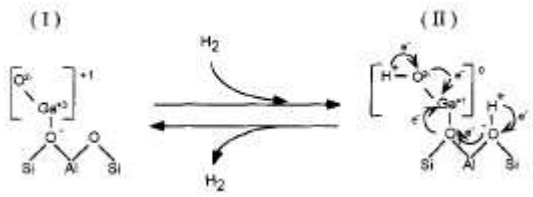

Scheme 1 The reduction-oxidation mechanism for the desorption of H-atoms during propane reactions over Ga/H-ZSM-5 catalysts.

4.1.2 The effect of co-feeding propane with other gases

Buckles and Hutchings [36] studied the effect of co-feeding propane with nitric oxide, oxygen, and hydrogen on the catalytic performance of H-ZSM-5 and Ga/H-ZSM-5 catalysts. They observed that NO co-feeding either continuously or as a pulse led to a rapid decrease in conversion together with an increase in propene selectivity. They suggested that NO was acting as a catalyst poison. The introduction of oxygen in the presence of H-ZSM-5 led to an immediate increase in the yield of propene and a decrease in the yield of H_2. Oxygen co-feeding also caused significant deactivation and the yield of methane and aromatic products to decrease. This effect is similar to the effects observed when nitric oxide (NO) was co-fed and indicates that both NO and O_2 interfere with the acid-catalysed cracking, oligomerisation, and aromatisation reactions. While NO does not effect the selective activation of propane to propene, O_2 enhances this reaction by removing H_2. On the contrary, Halász et al. [37] reported an increase in the lifetime of the catalysts when oxygen was present. They attributed this improvement of the catalyst stability to the removal of a surface coke layer as CO_x. The effects of co-feeding H_2 showed that the addition of H_2 leads to a very small decrease in the conversion of propane over H-ZSM-5 whereas a significant decrease was observed for Ga_2O_3/H-ZSM-5 [36].

The effect is mainly due to the decrease in the formation of aromatic products. The formation of propene was not significantly affected.

4.1.3 The effect of the calcination, hydrothermal treatment, and factors affecting zeolitic acidity

Studies have shown that the treatment of gallosillicate and galloaluminosilicates isostuctural with ZSM-5 at high temperatures causes extraction of gallium from the framework [38-44]. This resulted in a decrease in the strong acidity of the catalysts and a large decrease in the propane conversion activity. In contrast to the unstable framework Ga, the framework Al was more stable to thermal treatments [42], and no change in the Si/Al ratio was observed even after the most severe treatment. The decrease in the acidity due to degalliation of the framework Ga indicates the importance of framework Ga (or acidity) in the aromatisation of propane. The importance of acidity was also demonstrated by the fact that the conversion of propane and the selectivity for aromatics increases with the degree of H^+ exchange [41].

Choudhary et al. [39] showed that the initial conversion of propane and aromatisation activity decreased sharply on increasing the Si/Ga ratio. The propane conversion activity and the aromatics selectivity as well the dehydrogenation/cracking (D/C) ratio were found to increase sharply with increasing density of the acid sites and non-framework gallium of the gallosilicate catalysts. In determining the influence of Si/Al ratio on the activity of Ga/H-ZSM-5 catalysts, Choudhary et al. [41] observed that both the total conversion of propane and the selectivity for aromatics decreased markedly with increasing Si/Al ratio, as a result of decreasing zeolitic acidity, but the selectivity for propene was markedly increased. However, at isoconversion levels of propane, an increase in the Si/Al ratio resulted in

a decrease in the selectivity for aromatics and propene, but an increase in the selectivity for methane, ethane and ethylene, and therefore, a decrease in the D/C ratio.

One other important parameter which directly influences the acidity of the zeolites is the percentage XRD crystallinity. It has been shown that the number of strong Brønsted acid sites increases with increasing percentage XRD crystallinity of ZSM-5 zeolites [45]. This may be due to the fact that the incorporation of aluminium atoms in ZSM-5 zeolites is enhanced at higher crystallinities [46]. The effect of varying the crystallinity of gallium modified ZSM-5 zeolite-based materials on their catalytic performance in the aromatisation of propane has been studied [47,48]. The conversion of propane over the gallium modified samples exhibited a dependence on crystallinity that was similar to that seen with H-ZSM-5 and the activities of the two series were also similar. The catalytic activity and aromatics selectivity for all the catalysts increased with increasing %XRD crystallinity up to 60%, beyond which a decrease was observed. It should, however, be noted that the selectivity for aromatics was much higher in the case of the gallium modified samples.

4.1.4 The effect of the reaction temperature

During the aromatisation of propane, reactions such as cracking, dehydrogenation, and aromatisation occur, as shown below [49]:

$$\text{Dehydrogenation: } C_3H_8 \rightarrow C_2H_6 + H_2 \quad (1)$$

$$\text{Cracking: } C_3H_8 \rightarrow C_2H_4 + CH_4 \quad (2)$$

$$\text{Aromatisation: } 2C_3H_8 \rightarrow C_6H_6 + 5H_2 \quad (3)$$

Derouane et al. [49] evaluated the thermodynamic feasibility of these reactions, in the temperature range of 400 to 550^{o}C, by considering the three scenarios, viz., the occurrence of all three reactions by themselves; aromatisation, dehydrogenation, and dehydrogenation. Their results obtained indicated that propane dehydrogenation is the least thermodynamically favoured reaction at all temperatures. Propane cracking is the most thermodynamically preferred reaction over aromatisation for temperatures below 502^{o}C. When all three reactions are allowed in the considered temperature range of 400 to 550^{o}C, the major product is methane and the equilibrium selectivities to C_1-C_2 hydrocarbons and C_6H_6 are 54 and 46%, respectively.

In a study of the effect of temperature on propane aromatisation over H-GaMFI it was observed that the conversion of propane increased almost linearly on increasing the temperature [50]. As it was established that the product selectivity was influenced by conversion, comparisons were done at isoconversions and the following observations were made. The aromatics selectivity decreased with increasing temperature. The propylene selectivity increased as the temperature increased, but such an effect is small when comparisons are done at higher conversions. The selectivity for methane and C_4 hydrocarbons is also influenced strongly but its variation with temperature is gradually changed at higher conversions, showing a strong dependence on the conversion. The ethylene selectivity increased markedly but the ethane selectivity decreased.

It was also interesting to note that the selectivity to aromatics decreased markedly with increasing temperature. This was contrary to predictions from thermodynamic calculations, suggesting that the reaction was kinetically controlled rather than thermodynamically controlled. Similar observations were later made over GaAlMFI [51]. However, unlike with the H-GaMFI where a significantly pronounced effect was observed with increasing reaction temperatures no such effect was observed on H-GaAlMFI, at lower propane conversion levels (< 10%).

4.1.5 The effect of space velocity

Choudhary and co-workers studied the effect of space velocity on the product selectivity and distribution of aromatics and xylenes in propane aromatisation over H-[Ga]ZSM-5 [52] and H-[Ga,Al]ZSM-5 [53] catalysts, at different reaction temperatures. The results obtained showed a strong dependence of the product selectivity on the conversion of propane. For both catalyst systems the authors observed that when the space velocity is decreased (or the conversion is increased) the selectivity to aromatics is increased markedly, whereas the selectivity for propene, ethylene and C_4 hydrocarbons decreased.

It was observed that, with increasing aromatic yield (at decreasing space velocity) the selectivity for toluene increased. The selectivity for C_8 and C_9 aromatic products passed through a maximum with decreasing space velocity and the concentration of the C_8 species is significantly higher at the lower propane aromatisation temperatures. The *p*-xylene selectivity decreased with increasing aromatic yields, while the selectivity for *m*-xylene increased.

The authors proposed a reaction pathway shown in Figure 4.1 based on the observed product distribution [53]. They concluded that propene is the primary product for the aromatisation of propane, and that ethene is formed by the primary cracking of propane as well as from the cracking of higher olefins. Benzene, ethyl benzene and *p*-xylene are formed by direct aromatisation, but the other aromatics result from the secondary aromatic transformations. Toluene is formed as a primary product and from secondary transformations. The discussion of the mechanism of propane aromatisation is presented in the next section.

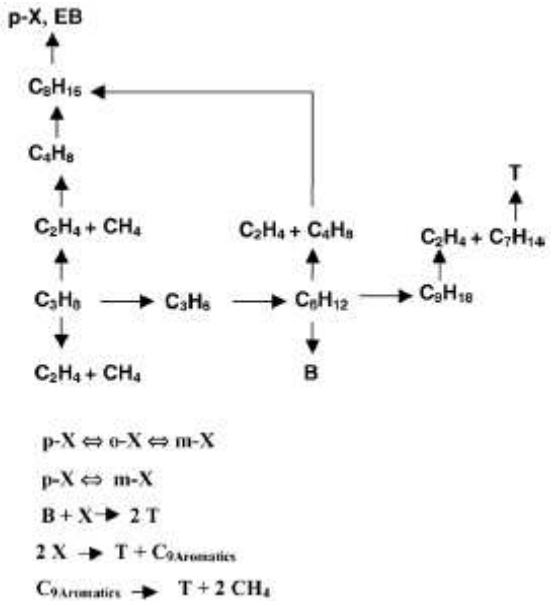

Figure 4.1 Reaction path for the formation of different aromatics in the aromatisation of propane (B = benzene, T = toluene, X = xylene, TMB = trimethylbenzene) [53].

4.2 Mechanism of propane aromatisation over Ga-loaded zeolites

As shown in the pathway in Figure 4.1, the reactions of propane on modified H-ZSM-5 leads to the formation of a broad range of aromatics, alkane, and alkenes, suggesting the involvement of a complex reaction sequence [35]. Aromatic products consist of a mixture of benzene, toluene, xylenes (BTX) and larger aromatics and the formation of these products requires several chain growth (oligomerisation) and cracking events before aromatisation. H-ZSM-5 zeolites without gallium additives are able to catalyse propane aromatisation following a reaction scheme given in Figure 4.2 [11].

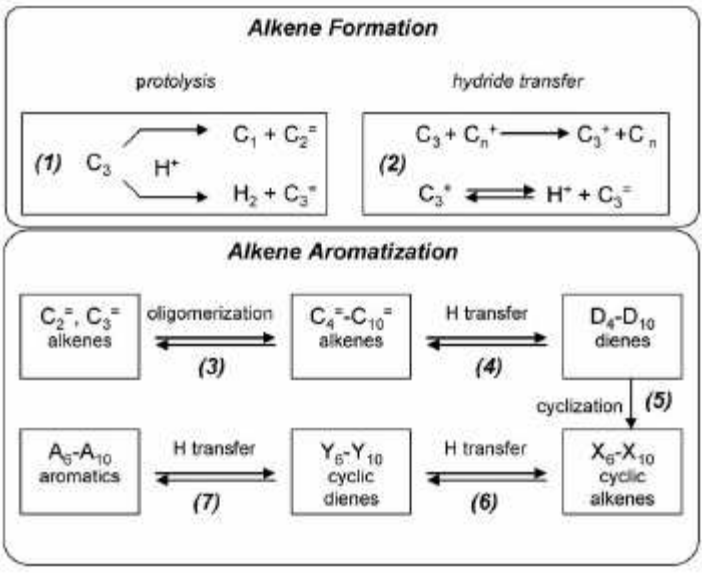

Figure 4.2 Pathway of propane aromatisation over H-ZSM-5 and Ga/H-ZM-5 catalysts [11].

The first step is the dehydrogenation and the cracking of the reactant through carbonium ion intermediates (reaction 1). However propane can also dehydrogenate through another path: hydride transfer from propane to carbonium ions resulting from the adsorption of product alkene followed by propene desorption (reaction 2). Propene and ethylene resulting from reactions 1 and 2 undergo rapid successive reactions via carbenium ion intermediates: oligomerisation, cyclisation, hydrogen transfer leading to C_6-C_{10} aromatics. Unfortunately, hydrogen transfer reactions (reactions 4, 6 and 7 in Figure 4.2) also lead to the undesired short chain alkanes (from olefins) whose transformation requires, as a first step, the slow reactions 1 and 2. Nguyen et al. [54] recently reported the results from their experimental and kinetic modelling studies of the pathways for the aromatisation of light alkane over H-ZSM-5. From these studies they concluded that propane conversion occurs via the protolytic cracking (PC) and hydride transfer (HT) routes. Cracking of C-C bonds is favoured over cracking of C-H bonds. The contribution of the HT route increased with increasing conversion. Analysis of the hydride transfer reaction steps has shown that at low conversions of propane, ethane is formed in the HT steps

involving propane and adsorbed ethene molecules, and not in the steps of ethane hydrogenation. Alkene oligomerisation and cracking steps control the distribution of the product alkenes during alkane aromatisation reactions.

It is now known that the addition of gallium species to the H-ZSM-5 zeolites using the various methods increases the rate of propane aromatisation as well as the rate of hydrogen production. There is also a general agreement that the aromatisation of propane proceeds through a bifunctional mechanism over Ga/HZSM-5. Following the scheme shown in Figure 4.2, during the aromatisation of propane, the gallium species (working synergistically with the Brønsted sites of the zeolite) are responsible for the dehydrogenation of: propane (reaction 1), oligomers (reaction 4) and cyclic olefins and diolefins (reactions 6 and 7) [9,11,27, 55].

Although there is no doubt that the gallium species play an important role in the aromatisation of propane, there is not consensus on the actual state of the gallium species at work during reaction. Guisnet and Gnep [9] suggested that the active gallium species was Ga_2O_3 rather than GaO [9]. Abdul Hamid et al. [56] concluded that the most active gallium species are in the oxidation state of 3+ and that dehydrogenation processes and H-adatom recombination most probably involves the Ga(III)/Ga(I) redox couple. Rane et al. [21] concluded that the Ga^+ species are more active than the GaH_2^+ species in dehydrogenation of propane and the GaO^+ cations are the most active. They also concluded that paraffinic C-H bond activation is preferred.

Regarding the first step of the of propane, Derouane et al [49] proposed that propane interacts heterolytically with the (Ga^{3+},O^{2-}) ion pair via a positive and a negative charged hydrogen atom, and that it is converted to a pseudo cyclopropane entity which can be protonated by a neighbouring Brønsted site as shown in Figure 4.3.

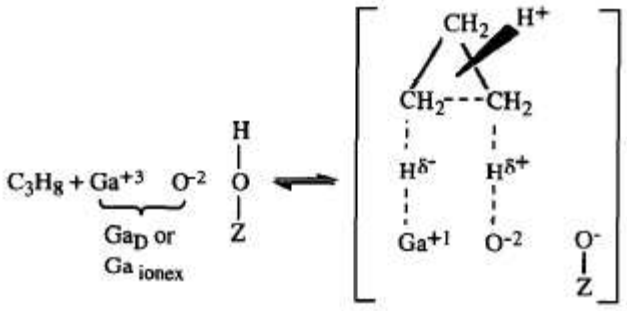

Figure 4.3 Mechanism for the bifunctional activation of propane on Ga-containing H-ZSM-5 catalysts [49].

On the other hand Meriaudeau and Naccache [27] concluded propane is activated over Ga/H-ZSM-5 through a bifunctional mechanism in analogy with the activation of propane over Ga_2O_3 as shown in Figure 4.4.

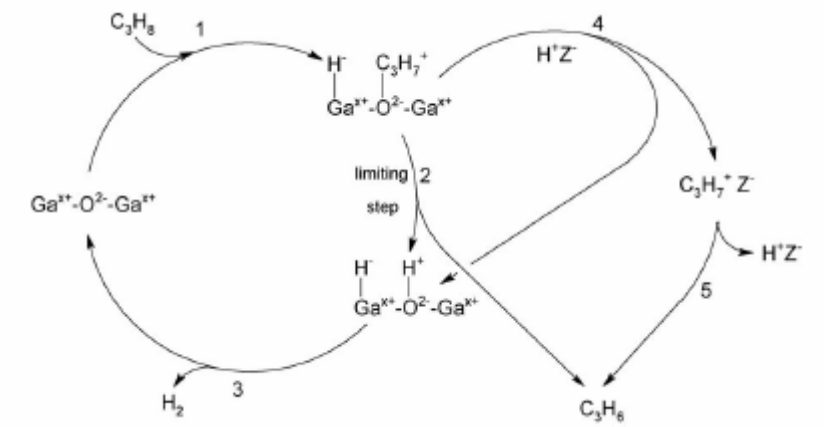

Figure 4.4 Ga-acid bifunctional mechanism of propane dehydrogenation over Ga/H-ZSM-5 catalysts [11].

In the first step, the Ga^{x+} ions abstract the hydride from propane to form $C_3H_7^+$ adsorbed on the oxygen of Ga_2O_3 or the zeolite. This $C_3H_7^+$ species is then decomposed into H^+ and C_3H_6 on the zeolite and in the last step H_2 is released by a recombinative desorption reaction.

As already mentioned, considering the nature of the products formed the aromatisation of propane involves reaction sequences. A comprehensive representation of the mechanism of the aromatisation of propane over gallium-modified zeolites is shown in Figure 4.5.

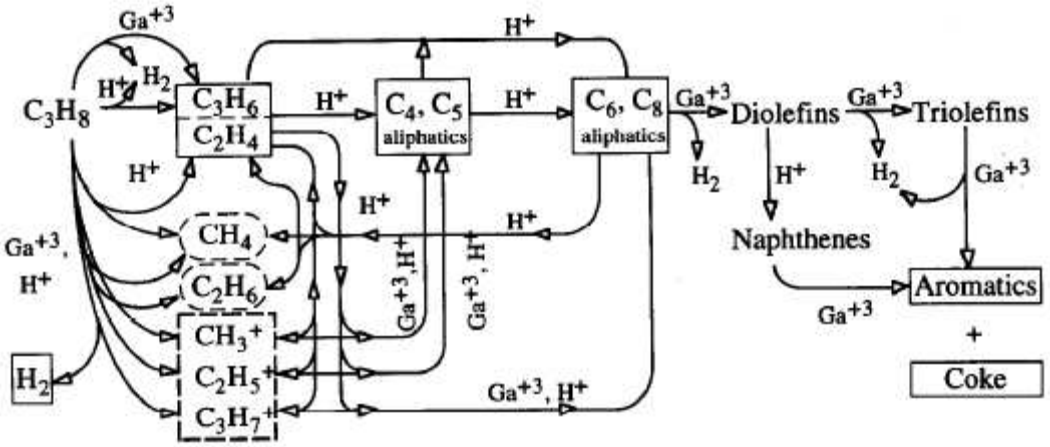

Figure 4.5 The overall mechanism for the formation of propane over Ga-containing H-ZSM-5 zeolite catalysts [49]

4.3 Deactivation and regeneration of the catalysts

Although it is known that the presence of gallium species in ZSM-5 zeolites improved their catalytic activity for the aromatisation of propane, the deactivation of the catalysts remains a problem. The deactivation of the catalysts is mainly attributed to the deposition of carbonaceous coke on the catalysts [40,57-59]. Studies have revealed that the deposition of coke on the catalysts for propane aromatisation also alters the product selectivity of the catalysts [56-59]. Choudhary et al. [56] concluded that the selectivity for aromatics decreased while the selectivity for propene increased with increased level of deactivation, while the distribution of

the aromatic products was not significantly affected. The shape selectivity of the catalysts was improved by the deactivation as a result of the increased diffusion resistance imposed by the presence of bulky coke molecules at the intersections of the channel of the zeolite. Later, Choudhary and co-workers [57] observed that the deactivation of the catalysts by coking decreased both the internal and external acid sites as well as the nitrogen sorption capacity of the zeolites.

The studies of the temperature programmed oxidation of coked H-gallosilicates for propane aromatisation revealed that the oxidation of coke is strongly influenced by the composition of the zeolite as well as the conditions used during pretreatment [59]. The influence of the zeolite composition and pretreatment parameters was attributed to the changes in the zeolite acidity and the non-framework gallium oxide species. It was also pointed out that properties of the zeolite not only influenced the oxidation of coke directly but also controlled the nature of the coke formed indirectly

Guisnet and Gnep [9] established the mode of coke formation from the composition of coke formed during the aromatisation of propene over Ga/H-ZSM-5 at 250 and 350^{o}C. They concluded that the presence of gallium does not affect the composition of coke and the formation of coke occurs via a succession of alkylation, cyclisation and hydrogen transfer steps on acid sites. The dehydrogenative coupling of aromatics was also involved in the formation of coke. Khodakov et al. [14] observed an increase in the conversion of propane and the selectivity for aromatics on increasing the regeneration cycles of the H-gallosilicate zeolites for propane aromatisation. Upon characterising the catalyst by IR spectroscopy and electron spin resonance spectroscopy, the authors concluded that at least two types of non-framework gallium species were present in the gallosilicate zeolite and their concentration increased considerably during regeneration. One type of gallium species was formed in the oxidic form and was located on the outer crystallite surface whereas the second one was found to be a cationic species occupying the lattice cation sites. The non-framework species formed by gallium release from the

framework are involved as catalytic active sites in propane aromatisation (as Lewis acid sites). Choudhary and Devadas [57] studied the regenerability of coked H-gallosilicates and concluded that regeneration resulted in a slow but gradual degalliation of the zeolite, causing continuous decrease in both its internal and external acidity but a large increase in its propane aromatisation activity. The increased activity was attributed to the formation of well-dispersed gallium oxide species in the slow but continuous degalliation. However, regeneration caused a significant decrease in the aromatic selectivity but an increase in the selectivity for ethene, propene and other hydrocarbons. It also caused an appreciable increase in the rate of deactivation due to the increased concentration of non-framework gallium oxide species, which are responsible for the high dehydrogenation activity of the zeolite.

4.4 Propane aromatisation over Mo-based catalysts

Although, as discussed in Chapter 3, Mo/HZSM-5 zeolite catalyst are regarded as the most promising catalysts for the aromatisation of the more unreactive methane, little has been reported about the aromatization of propane using these catalysts. Fu et al. [60] observed that over the Mo/H-ZSM-5 catalyst prepared by solid-state ion-exchange, having a Mo content of 3.5 wt.%, propane mainly underwent cracking to methane and ethane. This was concluded from the fact that compared with H-ZSM-5 which gave aromatics selectivity of 27.1%, Mo/H-ZSM-5 gave an aromatics selectivity of 8.6%, while the total selectivity to cracked products was 28.1% and 88%, respectively. On the contrary, Wang et al. [61] reported that propane cracking was depressed and the selectivity for aromatics was enhanced by the presence of Mo [60]. This difference may be due to the difference in the reaction conditions used by the two groups. Fu and co-workers used a reaction temperature of 500^{o}C and the system used a pulse technique, while the group of Wang did their studies at a

reaction temperature of 550^{o}C and a gas hourly space velocity of 600 h^{-1} (corresponding to a flow rate of 10 ml/min), using a continuous flow system.

The work of Wang and co-workers [61] further showed that the catalytic performance of the Mo/H-ZSM-5 catalysts prepared by the hydrothermal treatment method was much better than that prepared by impregnation and mechanical mixing. This was said to be due to the fact that the hydrothermal treatment method favoured the dispersion of Mo species on H-ZSM-5, which promoted the penetration of Mo into the channels of H-ZSM-5. Solymosi and co-workers [62] studied the reactions of propane over supported Mo_2C catalysts. Their results showed that over H-ZSM-5, propane underwent dehydrogenation and cracking at 600^{o}C, while dehydrogenation was dominant over bulk Mo_2C. It was further observed that the dominant reaction over Mo_2C/SiO_2 at 500-600^{o}C was dehydrogenation to propylene, while aromatization was dominant over Mo_2C/H-ZSM-5.

4.5 Overview of the aromatisation of propane

In general, the aromatisation of propane over Ga-loaded H-ZSM-5 zeolite catalysts is a reaction that has received considerable attention because of its industrial significance. Although the reaction has been studied for over two decades there is still no agreement amongst researchers about the nature of the gallium species in operation during the reaction. The pretreatment of the Ga/H-ZSM-5 catalysts promotes the catalytic conversion of propane. It is acknowledged that this treatment promotes the migration of Ga species to the exchange sites of the zeolites, but there is still no agreement on whether the Ga species exist as Ga^{3+}, Ga^{+}, GaO^{+}, Ga_2O or Ga_2O_3.

Catalysts like Mo/H-ZSM-5 have not received attention with regard to the aromatisation of propane. Since these catalysts are used for the aromatisation of methane which is more stable to activation than propane, more work is needed on the application of these catalysts for propane aromatisation

4.6 References

[1] S.M. Csicsery, *J. Catal.*, **17** (1970) 207-215.

[2] S.M. Csicsery, *J. Catal.*, **17** (1970) 216-218.

[3] S.M. Csicsery, *J. Catal.*, **17** (1970) 315-322.

[4] S.M. Csicsery, *J. Catal.*, **18** (1970) 30-32.

[5] N.Y. Chen and T.Y. Yun, *Ind. Eng. Chem. Process Des. Dev.*, **25** (1986) 151-155.

[6] W.J.H Dehertog and G.F. Froment, *Appl. Catal., A*, **189** (1999) 63.75.

[7] D. Seddon, *Catal. Today*, **6** (1990) 351-372.

[8] M. Guisnet and N.S. Gnep, *Appl. Catal.*, **89** (1992) 1-30

[9] M. Guisnet and N.S. Gnep, *Catal. Today,* **31** (1996) 275-292.

[10] R. Frickle, H. Kosslick, G. Lischke and M. Richter, *Chem. Rev.*, **100** (2000) 2303-2405.

[11] G. Caeiro, R.H. Carhalho, X. Wang, M.A.N.D.A. Lemos, F. Lemos, M. Guisnet and F. Ramôa Ribeiro, *J. Mol. Catal., A: Gen.,* **255** (2006) 131-158.

[12] C.R. Bayense, A.J.H.P. van der Pol and J.H.C. van Hooff, *Appl. Catal., A,* **72** (1991) 81-98.

[13] J. Bandiera and Y. B. Taarit, *Appl. Catal.,* **76** (1995) 199-208.

[14] A.Yu. Khodakov, L.M. Kustov, T.N. Bondarenko, A.A. Dergachev, V.B. Kazansky, Kh.M. Minachev, G. Borbérly and H.K. Beyer, *Zeolites*, **10** (1990) 603-607.

[15] G.L. Price, V.I. Kanazirev and K.M. Dooley, *Zeolites*, **15** (1995) 725-731.

[16] B.S. Kwak and W.M.H. Sachtler, *J. Catal.*, **141** (1994) 729-732.

[17] B.S. Kwak and W.M.H. Sachtler, *J. Catal.*, **145** (1994) 456-463.

[18] El-M. El-Malki, R.A. van Santen and W.M.H. Sachtler, *J. Phys. Chem., B*, **103** (1999) 4611-4622.

[19] V.B. Kazansky, I.R. Subbotina, R.A. van Santen and E.J.M. Hensen, *J. Catal.*, **227** (2004) 263-269.

[20] V.B. Kazansky, I.R. Subbotina, R.A. van Santen and E.J.M. Hensen, *J. Catal.*, **233** (2005) 351-358.

[21] N. Rane, A.R. Overweg, V.B. Kazansky, R.A. van Santen and E.J.M. Hensen, *J. Catal.*, **239** (2006) 478-485.

[22] G.L. Price and V.I. Kanazirev, *J. Catal.*, **126** (1990) 267-278.

[23] C.R. Bayense and J.H.C. van Hooff, *Appl. Catal., A,* **79** (1991) 127-140.

[24] K.M. Dooley, C. Chang and G.L. Price, *Appl. Catal., A,* **84** (1992) 17-30.

[25] B.L.W. Southward, R.J. Nash and C.T. O'Connor, *Appl. Catal., A,* **135** (1996) 177-191.

[26] G.L. Price and V. Kanazirev, *J. Mol. Catal.*, **66** (1991) 115-120.

[27] P. Mériaudeau and C. Naccache, *J. Mol. Catal.*, **59** (1990) L31-L36.

[28] J.F. Joly, H. Ajot, E. Merlen, F. Raatz and F. Alario, *Appl. Catal., A,* **79** (1991) 249-263.

[29] S.B. Abdul Hamid, E.G. Derouane, G. Demortier, J. Riga and M.A. Yarmo, *Appl. Catal., A,* **108** (1994) 85-96.

[30] V. Kanazirev, G.L. Price and K.M. Dooley, *J. Chem. Soc., Chem. Commu.,* (1990) 712-713.

[31] P. Mériaudeau and C. Naccache, *Catal. Today*, **31** (1996) 265-273.

[32] V. Kanazirev, R. Damitrova, G.L. Price, A.Yu. Khodakov, L.M. Kustov and V.B. Kazansky, *J. Mol. Catal.*, **70** (1991) 111-117.

[33] V. Kanarirev, R. Piffer and H. Föster, *J. Mol. Catal.*, **69** (1991) L15-L18.

[34] G.D. Meitzner, E. Iglesia, J.E. Baumgartner and E.S. Huang, *J. Catal.*, **140** (1993) 209-225.

[35] J.A. Biscardi and E. Iglesia, *Catal. Today*, **31** (1996) 207-231.

[36] G.J. Buckles and G.J. Hutchings, *J. Catal.*, **151** (1995) 33-43.

[37] J. Halász, Z. Kónya, Á. Fudala, A. Béres and I. Kiricsi, *Catal. Today*, **31** (1996) 293-304.

[38] G. Gianetto, G. León, J. Papa, R. Monque, R. Galiasso and Z. Gabelica, *Catal. Today,* **31** (1996) 317-326.

[39] V.R. Choudhary, A.K. Kinage, C. Sivadinarayana, P. Devadas, S.D. Sansare and M. Guisnet, *J. Catal*.**, 158** (1996) 34-50.

[40] V.R. Choudhary, A.K. Kinage, C. Sivadinarayana, P. Devadas, S.D. Sansare and M. Guisnet, *Appl. Catal., A,* **136** (1996) 125-142.

[41] V.R. Choudhary, K. Mantri, C. Sivandinarayana, *Microporous and Mesoporous Mater.*, **37** (2000) 1-8.

[42] T.V. Choudhary, A. Kinage, S. Benerjee and V.R. Choudhary, M*icroporous and Mesoporous Mater.*, **87** (2005) 23-32.

[43] T.V. Choudhary, A. Kinage, S. Banerjee and V.R. Choudhary, *Fuels and Energy*, **20** (2006) 919-922.

[44] V.R. Choudhary, P. Devadas, A.K. Kinage, C. Sivadinarayana and M. Guisnet, *J. Catal.,* **158** (1996) 537-550.

[45] C.P. Nicolaides, H.H. Kung, N.P. Makgoba, N.P. Sincadu and M.S. Scurrell, *Appl. Catal., A*, **223** (2002) 29-33.

[46] K.S. Triantafyllides, L. Nalbandian, P.N. Trikalitis, A.K. Ladakos, T. Mavromoustakos and C.P. Nicolaides, *Microporous and Mesoporous Mater.*, **75** (2004) 89-100.

[47] C.P. Nicolaides, N.P. Sincadu and M.S. Scurrell, *Catal. Today*, **71** (2002) 429-435.

[48] N.P. Sincadu, PhD thesis, University of the Witwatersrand, South Africa, 2003.

[49] E.G. Derouane, S.B. Abdul Hamid, I.I. Ivanova, N. Blom and P.-E, Højlund-Nielsen, *J. Mol. Catal.*, **86** (1994) 371-400.

[50] V.R. Choudhary and P. Devadas, *Microporous and Mesoporous Mater.*, **23** (1998) 231-238.

[51] T.V Choudhary T.V. Choudhary, A. Kinage, S. Benerjee and V.R. Choudhary, *Catal. Commun.*, **7** (2006) 166-169.

[52] V.R. Choudhary and P. Devadas, *J. Catal.*, **172** (1997) 475-478.

[53] T.V. Choudhary, A. Kinage, S. Benerjee, V.R. Choudhary, *J. Mol. Catal., A: Chem.*, **146** (2006) 79-84.

[54] D.B. Lukyanov, N.S. Gnep, and M.R. Guisnet, *Ind. Eng. Chem. Res.*, **34** (1995) 516-523.

[55] L.H. Nguyen, T. Vazhnova, S. T. Kolaczkowski and D.B. Lukyanov, *Chem. Eng. Sci.*, **61** (2006) 5881-5894.

[56] S.B. Abdul Hamid, E.G. Derouane, P. Mériaudeau and C. Naccache, *Catal. Today,* **31** (1996) 327-334.

[57] V.R. Choudhary, P. Devadas, A.K. Kinage, C. Sivadinarayana and M. Guisnet, *J. Catal.,* **166** (1997) 380-383.

[58] V.R. Choudhary, P. Devadas, S.D. Sansare and M. Guisnet, *J. Catal.,* **166** (1997) 236-243.

[59] V.R. Choudhary and P. Devadas, *J. Catal.,* **168** (1998) 187-200.

[60] Z. Fu, D. Yin, Y. Yang, X. Guo, *Appl. Catal., A*, **124** (1995) 59-71.

[61] J. Wang, M. Kang, Z. Zhang and X. Wang, *J. Nat. Gas Chem.*, **11** (2002) 43-50.

[62] F. Solymosi, R. Nemeth, L. Ovari and L. Egri, *J. Catal.*, **195** (2000) 316-325.

Chapter 5

Experimental

In this chapter the reagents and their grades, as well as the equipment used to carry out the experiments reported in this study, are discussed. The methodologies used to carry out the study are also presented together with the various techniques used for characterisation of the catalysts and catalyst supports.

5.1 Reagents

A summary of the reagents used in this study together with their purity if known is shown in Table 5.1.

Table 5.1 Reagents used, supplier and their purity or composition

Reagent	Supplier	Purity
Ammonium molybdate	Aldrich	[a]
Ammonium heptamolybdate	Saarchem	[a]
Sodium molybdate	BDH chemicals	> 99
Ammonium paratungstate	Aldrich	99.99%
dodeca-Molybdophosphoric acid	BDH chemicals	[a]
Boric acid	Hopkin & Williams	>99.5%
Lithium nitrate	Merck	[a]
Ethanol	Merck	99%
Potassium carbonate	Saarchem	[a]
Silver nitrate	PAL chemicals	[a]
Molybdenum trioxide	Hopkin & Williams	> 99%
Sodium hydroxide	Saarchem	> 98%
(3-aminopropyl)-triethoxysilane	Aldrich	99%
Ammonium chloride		[a]

[a] *Not available*

The gases were obtained from African oxygen (Afrox) in the ultrahigh purity grade. All the reagents and gases were used without any further purification.

The gases were provided by African Oxygen and were used without purification.

5.2 The preparation of catalysts

5.2.1 The preparation of Mo/H-ZSM-5 catalysts

The ZSM-5-based materials of different crystallinities were synthesised and ion-exchanged as previously reported [1,2]. The variation of the of the %XRD crystallinities of the zeolites was carried out by varying the hydrothermal treatment temperature. The Mo/H-ZSM-5 catalysts were prepared as described by [3]. This was done by impregnating the H-ZSM-5 zeolite with an aqueous solution of ammonium heptamolybdate of appropriate concentration to obtain samples with a metal loading of 2 wt%. The resulting sample was then dried at 120°C overnight and then calcined in air at 500°C for 6 h.

In another experiment the Mo/H-ZSM-5 catalysts was prepared by physically mixing MoO_3 with H-ZSM-5, grinding to obtain a homogeneous mixture and then calcining at 500^{o}C for 6 h.

5.2.2 Addition of dopants

The study of the nonoxidative conversion of methane also involved the addition of dopants during the preparation stage. The dopants of interest included, boron, silver and the alkali metal ions, lithium, sodium, and potassium. The dopants were introduced as follows:

(i) Boron

In the case where boron was required, the zeolite was impregnated with aqueous solutions of HBO_3 dried overnight at 120^{o}C and calcined at 500^{o}C for 6 h prior to the introduction of molybdenum. The amount of boron varied from 0 to 0.2 wt%.

(ii) Silver

Silver was introduced into the already-prepared 2%Mo/H-ZSM-5 by impregnation with a solution of silver nitrate, with the resultant silver content of 0.5 wt%. A sample of 2%Ag/H-ZSM-5 was also prepared as above for comparison.

(iii) Alkali metal ions

The alkali metal ions were introduced in such a way that the molar ratio of molybdenum to the alkali metal ion is 0.5 as in M_2MoO_4, where M represents the alkali metal ion. In all the cases the molybdenum content was kept at 2 wt%. Sodium was introduced as sodium molybdate, while lithium and potassium where co-impregnated with molybdenum as $LiNO_3$ and K_2CO_3, respectively.

5.2.3 Silanation

The silanation of the H-ZSM-5 was done using a procedure reported by Ding et al. [4]. This was done by immersing H-ZSM-5 into an ethanol solution (10 ml/g) containing 3-aminopropyl-triethoxylsilane and subsequently evaporating the ethanol solvent at 120 ^{o}C. The sample was then treated at 550^{o}C for 16 h in air in order to

decompose the organosilane precursors and to form the silica-modified H-ZSM-5 (nominally 4 wt% SiO_2/H-ZSM-5).

5.3 Characterisation of the catalysts

The catalysts were characterised by various methods and the procedures used in carrying out the characterisation are described in the following subsections for each of the methods used.

5.3.1 X-ray powder diffraction (XRD)

Powder X-ray diffraction data were collected using a Brucker AXS D8 equipped with a primary beam Göbel mirror, a radial Soller slit, a VÅntec-1 detector and using Cu-K_α radiation (40kV, 40mA). Data were collected in the 2θ range 5 to 90^o in 0.021^o steps, using a scan speed resulting in an equivalent counting time of 14.7 s per step.

5.3.2 Surface area and porosity analysis

Surface areas and pore volumes were obtained from nitrogen physisorption studies at -195^oC using the Micromeritics Tristar 3000 surface area and porosity analyser. Before analysis the samples were degassed at 350^oC for 6 h in nitrogen.

5.3.3 Temperature programmed reduction (TPR)

Temperature programmed reduction was performed in an in-house constructed apparatus that was equipped with a thermal conductivity detector. Before reduction the sample (about 0.2 g) was pretreated at 700^{o}C for 1 h in nitrogen and then cooled to room temperature. The reduction was performed by using 5% H_2/Ar mixture at a flow rate of 30 ml/min and by heating the sample from room temperature to 800^{o}C at a heating rate of 7.5 ^{o}C/min.

5.3.4 Temperature programmed desorption of ammonia (NH3-TPD)

Temperature programmed desorption of ammonia was performed in an in-house constructed apparatus that was equipped with a thermal conductivity detector. Before adsorption of ammonia the sample (about 0.2 g) was pretreated by heating to 700^{o}C at rate of 10^{o}C/min and held at 700^{o}C for 30 min and then cooled to 100^{o}C. A mixture of ammonia in helium (4% NH_3 balance helium) was passed over the catalyst for 1 h at 100^{o}C and then switched to helium to remove the weakly adsorbed ammonia. Desorption was carried out in helium at a flow rate of 30 ml/min by heating the sample from room 100^{o}C to 700^{o}C at a heating rate of 10 ^{o}C/min.

5.3.5 Temperature programmed oxidation (TPO)

Temperature programmed oxidation was performed in an in-house constructed apparatus that was equipped with a thermal conductivity detector. Before reduction the sample (about 0.05 g) was pretreated at 150^{o}C for 1 h in helium and then cooled to room temperature. The reduction was performed by using 5% O_2/He mixture at a

flow rate of 30 ml/min and heating the sample from room temperature to 900^{o}C at a heating rate of 7.5 ^{o}C/min.

5.3.6 Diffuse reflectance spectroscopy (DRS)

The DRS spectra of the samples were collected by the Varian Cary 500 Scan UV-Vis-NIR spectrophotometer equipped with a diffuse reflectance attachment. The spectra were collected in the UV-Vis region from 200-600 nm at a scan rate of 120 nm/min.

5.3.7 Transmission electron microscopy (TEM)

The samples were suspended in methanol, ultrasonicated for 5 min and then spread over copper grids and allowed to dry at room temperature. Transmission electron micrographs were obtained using the Jeol 100s transmission electron microscope. An acceleration voltage of 80 kV was used for the analysis of the samples.

5.3.8 FT-IR spectroscopy

A Bruker Vector 22 spectrophotometer fitted with AABSPEC #2000-A multi-mode system transmittance cell was used in this study. AABSPEC #2000-A is an all-metal high vacuum cell fitted with KBr windows. This cell is designed to operate at vacuum up to 10^{-8} torr and temperatures of up to 900^{o}C. Opus Version 5.5 software from Bruker is used to operate the spectrophotometer. The instrument is operated in the absorption mode at a resolution of 4 cm^{-1} and collecting 128 scans per spectrum.

A self-supporting wafer is prepared using about 20 mg of a sample and a pressure of 3 tons from a hydraulic press. The wafer was then degassed at 500^{o}C under vacuum (2.3×10^{-5} torr) overnight. A background spectrum of air was collected prior to loading the sample in the cell. Pyridine dried using molecular sieve 3 Å was adsorbed at 100^{o}C and allowed to equilibrate for 12 min. Excess pyridine was evacuated at 100^{o}C for 1h; this also allowed for the removal of the weakly physisorbed pyridine molecule. The sample was then cooled to room temperature prior to collecting the sample spectrum.

5.3.9 Carbon content analysis

The amount of carbon deposited on the catalysts was determined by using the LECO CHNS 932 carbon, hydrogen, nitrogen, sulphur determinator, equipped with the thermal conductivity and infrared detectors. In a typical experiment about 2 mg of the sample was heated in oxygen to 1000^{o}C.

5.4 Catalytic conversion of methane

The methane aromatization reactions were carried out at 750^{o}C in a tubular quartz fixed-bed micro-reactor and the temperature was monitored with a K-type thermocouple located inside a quartz sheath. The reactor was charged with about 1 g of the catalyst. Before the catalytic reaction, the catalyst was pretreated at the reaction temperature (750^{o}C) for 1 h under nitrogen after which a mixture of methane and argon (10% argon, 90% methane), with argon serving as the internal standard, was introduced (at a flow rate of 13 ml/min) into the reactor. The product

stream was analysed using HP5730A and HP5790A gas chromatographs equipped with a Porapack Q and Molecular sieve 5A packed column which were coupled to an FID and the TCD detector, respectively. The outlet pipe line from the end of the reactor was kept at 250^{o}C to minimise condensation and strong adsorption of the higher hydrocarbon products. The first analysis was done after 1 h on-stream. A schematic representation of the catalytic rig setup used in this study is illustrated in Figure 5.1; and that of a typical quartz reactor used is shown in Figure 5.2.

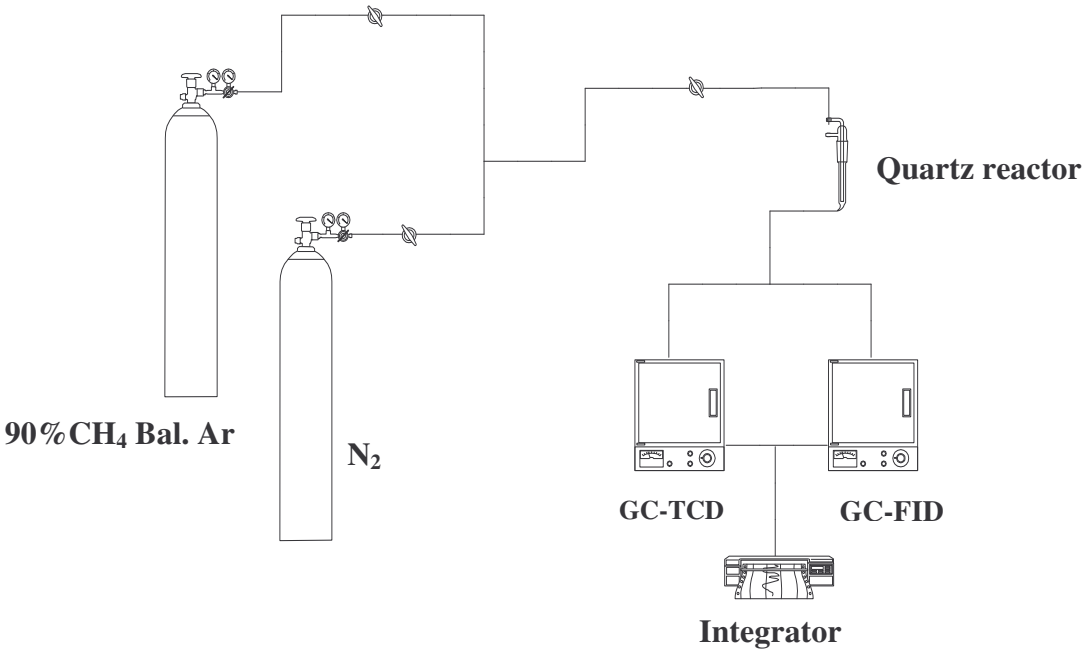

Figure 5.1 Schematic representation of the catalytic rig setup.

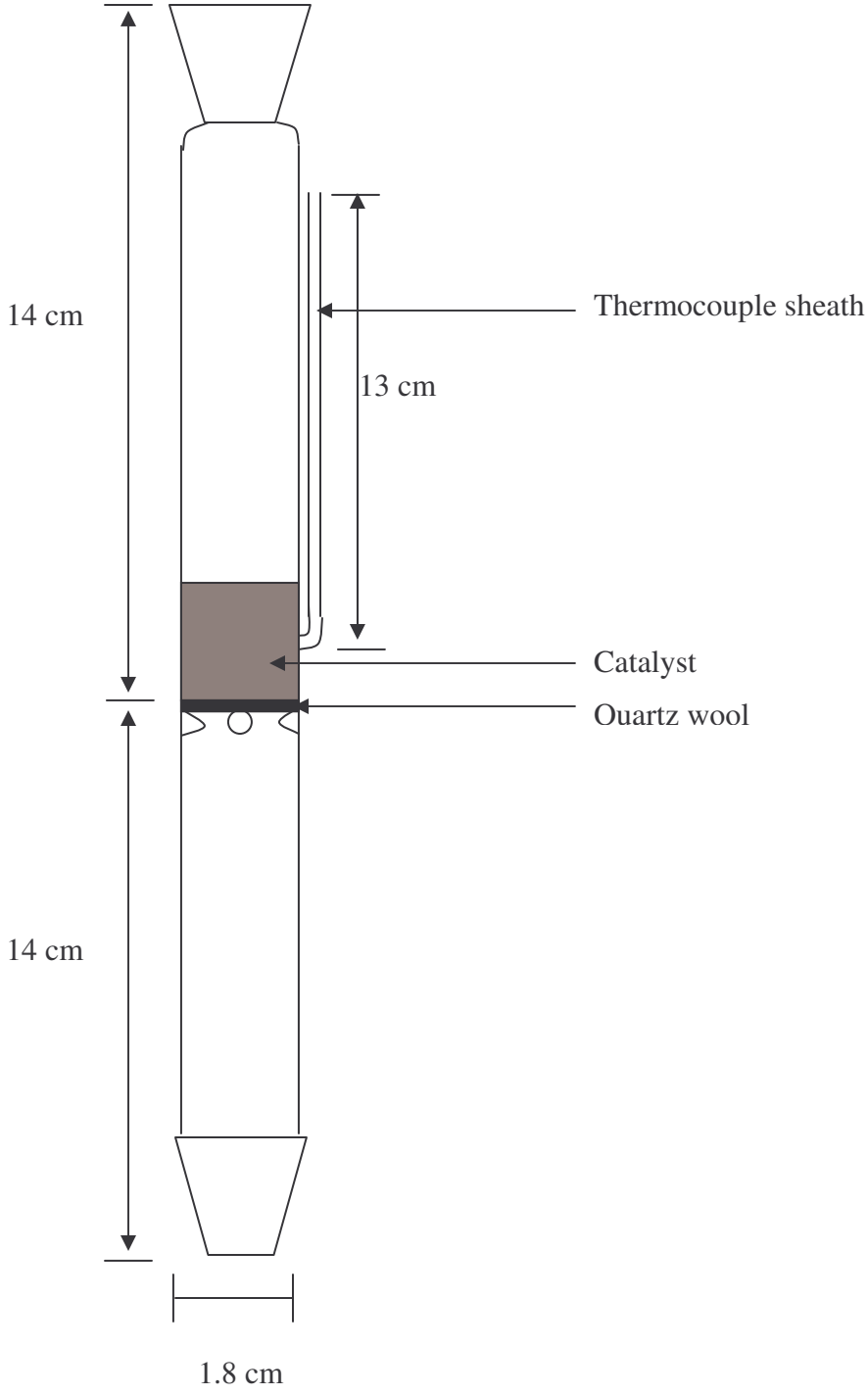

Figure 5.2 Schematic representation of the quartz reactor used in this study.

A typical GC profile for the outlet stream after reaction is shown in Figure 5.3.

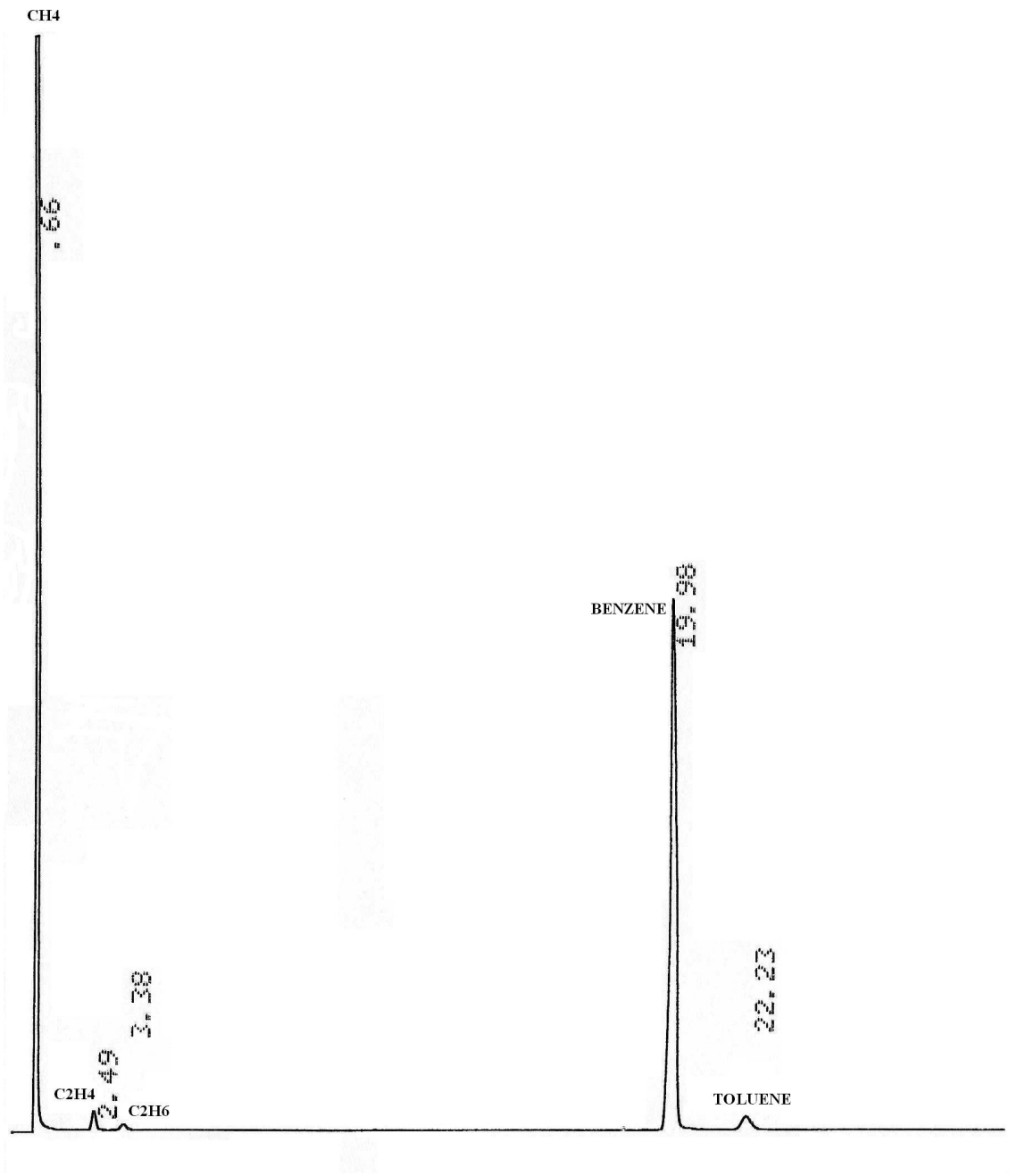

Figure 5.3 A typical GC profile from the catalytic conversion of methane over a Mo/H-ZSM-5 catalyst at 750^{o}C.

(i) Regeneration studies

In order to establish if it is possible to regenerate the catalysts, the regeneration procedure used was as follows: The reaction temperature was lowered to 600^{o}C under nitrogen flow and then air was introduced, to replace the nitrogen, for 1 h. The catalyst was then heated to the reaction temperature (750^{o}C) in nitrogen and then held at this temperature for an hour before methane was introduced into the reactor.

(ii) Calculations

Reported selectivities are defined as the percentage of the methane converted appearing as a given product. The amount of carbon missing within the measured product is reported as coke in the results, but includes carbon consumed to form molybdenum carbides and condensable products remaining in the zeolite channels or in the transfer lines. Although it is commonly reported in the literature [5-7] that naphthalene was also a major product, in our studies it was not determined because of the limitations of the column used and was therefore lumped together with the "coke" produced.

The percentage conversion was calculated using equation 5.1, from the GC trace (TCD detector), with argon as the internal standard:

$$\%\text{Conversion} = \left(1 - \frac{\text{Area\_CH}_{4,\text{in}} \times \text{Area\_Ar}_{\text{out}}}{\text{Area\_CH}_{4,\text{out}} \times \text{Area\_Ar}_{\text{in}}}\right) \times 100 \qquad 5.1$$

The percentage selectivity to product *i*, $\%S_{i,}$ was calculated using equation 5.2.

$$\%S_i = \frac{\%P_i}{\%\text{Conversion}} \qquad 5.2$$

where, $\%P_i$ is the percentage of product *i* in the outlet stream

The percentage selectivity for coke was calculated from equation 5.3

$$\%S_{coke} = 100 - \sum_n \%S_i \qquad 5.3$$

5.5 The aromatisation of propane over Mo/H-ZSM-5 catalysts

The conversion of propane was carried out using a rig setup shown in Figure 5.1, but with propane replacing methane. A sample of about 1 g catalyst was loaded into the quartz reactor and pretreated with nitrogen gas flowing at the rate of 20 ml/min for 2 h at 530°C. The purpose of pretreatment is to remove the absorbed impurities and the moisture in the catalyst. Finally the catalyst was exposed to the mixture of pure propane and nitrogen gas of ratio 1:1, both gases flowing at a rate of 20 ml/min. The products were analyzed using an online HP 5730A Gas Chromatograph and a Varian 4290 integrator. Propane conversion and selectivity of the products were calculated according to the carbon mass balance.

A typical GC profile of the outlet stream obtained from the aromatisation of propane is shown in Figure 5.4.

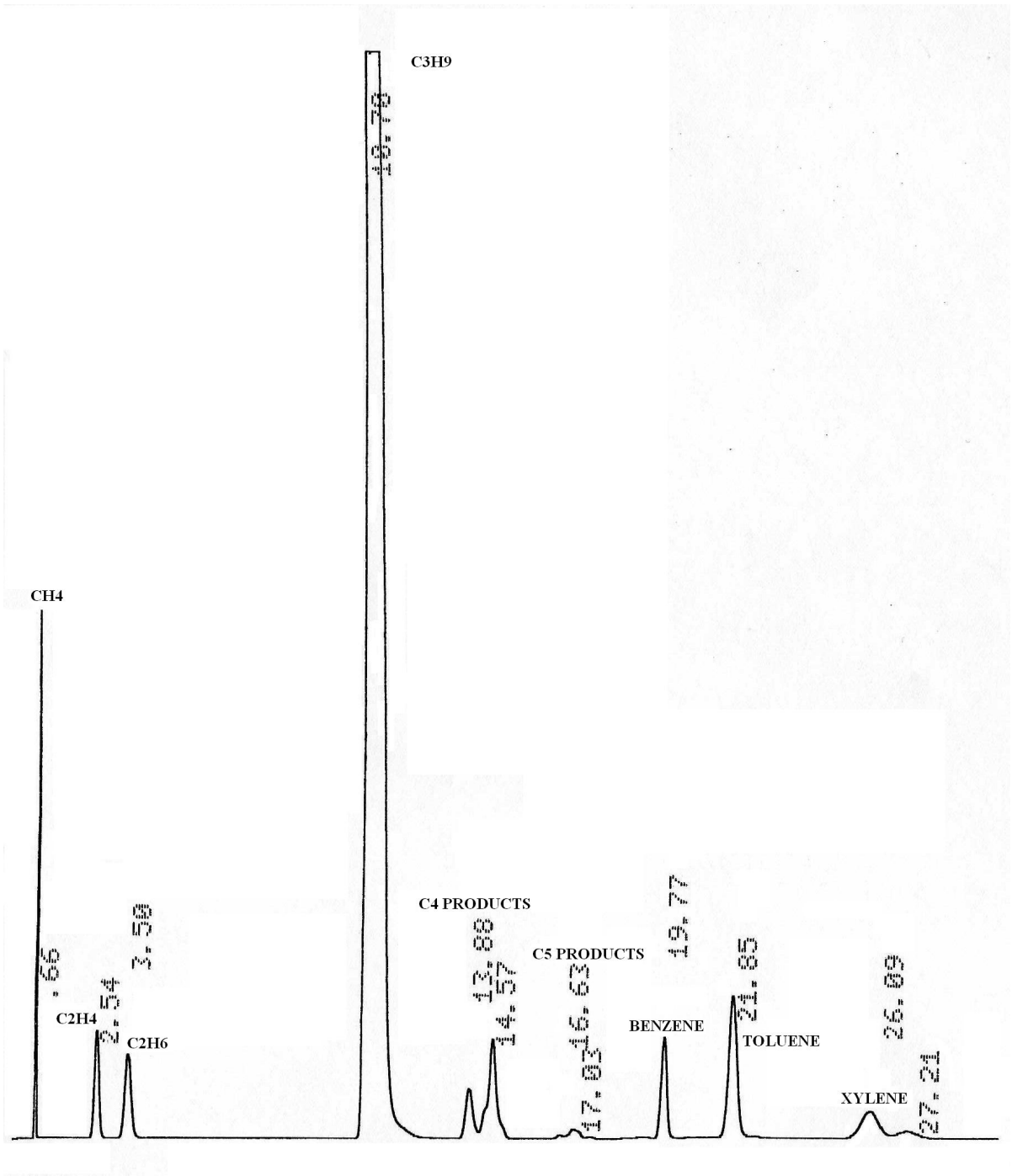

Figure 5.4 A typical GC profile for the conversion of methane over Mo/H-ZSM-5 at 530^{o}C.

(i) Calculations

The percentage conversion was calculated using equation 5.4 and the percentage selectivity as shown in equation 5.4

$$\%\text{Conversion} = \frac{\%\ \text{Propane in feed} - \%\ \text{Propane after reaction}}{\%\ \text{Propane in feed}} \times 100 \qquad 5.4$$

$$\%S_i = \frac{\%\ P_i}{\%\ \text{Conversion}} \times 100 \qquad 5.5$$

5.6 References

[1] C.P. Nicolaides, *Appl. Catal., A*, **185** (1999) 211-217.

[2] NP Sincadu, PhD thesis, University of the Witwatersrand, 2003.

[3] S. Liu, L. Wang, R. Ohnishi and M. Ichikawa, *J. Catal.*, **181** (1999) 175-188.

[4] W. Ding, G.D. Meitzner and E. Iglesia*, J. Catal.*, **206** (2002) 14-22.

[5] Y. Xu and L. Lin, *Appl. Catal.*, **188** (1999) 53-67.

[6] Y. Xu, X. Bao and L. Lin, *J. Catal.*, **216** (2003) 386-395.

[7] Y. Shu and M. Ichikawa, *Catal. Today*, **71** (2001) 55-67.